EUROPEAN COMMISSION
5th EURATOM FRAMEWORK PROGRAMME 1998-2002
KEY ACTION : NUCLEAR FISSION

SPENT FUEL STABILITY UNDER REPOSITORY CONDITIONS – FINAL REPORT OF THE EUROPEAN PROJECT

CONTRACT N° FIKW-CT-2001-00192 SFS

1ST NOVEMBER 2001 –31ST OCTOBER 2004

Edited by **C. POINSSOT (CEA) & C. FERRY (CEA)**

C. POINSSOT[1], C. FERRY[1], M. KELM[5], B. GRAMBOW[2,14], A. MARTINEZ[4], L. JOHNSON[8], Z. ANDRIAMBOLOLONA[3], J. BRUNO[12], C. CACHOIR[9], J.M. CAVEDON[1], H. CHRISTENSEN[13], C. CORBEL[1], C. JEGOU[1], K. LEMMENS[9], A. LOIDA[5], P. LOVERA[1], F. MISERQUE[1], J. DE PABLO[11], A. POULESQUEN[1], J. QUINONES[10], V. RONDINELLA[6], K. SPAHIU[7], D.H. WEGEN[6]

1. CEA
2. ARMINES
3. ANDRA
4. ENRESA
5. FZK
6. ITU
7. SKB
8. NAGRA
9. SCK.CEN
10. CIEMAT
11. UPC
12. ENVIROS
13. STUDSVIK
14. ENSTIMN

Dissemination level :

PU: Public report
S/T: Scientific/Technical reports,

TABLE OF CONTENTS

LIST OF FIGURES

LIST OF TABLES

DISTRIBUTION LIST

European Commission		T. McMenamin
NFPRO coordinators		A. Sneyers B. Neerdael
ANDRA		P. Landais S. Schumacher Z. Andriambololona
CEA	DEN/DDIN	C. Courtois T. Liéven F. Balbaud
	DEN/SAC	JP. Pervès
	DEN/DPC	X. Vitart C. Poinssot P. Lovera C. Ferry A. Poulesquen P. Mauchien F. Miserque
	DEN/DIEC	M. Bordier C. Fillet B. Lorrain J.L. Paul C. Jegou
	DSM/DRECAM	L. Laurent E. Eliot S. Pommeret C. Corbel E. Mendès
CIEMAT		J. Quinones A. Gonzalez de la Huebra
EMN/SUBATECH		B. Grambow C. Landesman
ENRESA		A. Martinez J.A. Gago
ENVIROS		J. Bruno E. Cera J. Merino
ITU		J.P. Glatz D. H.Wegen C. Ronchi V.V. Rondinella J. Cobos T. Wiss D. Serrano
KFZ-INE		M. Kelm A. Loida
NAGRA		L. Johnson

SCK.CEN	K. Lemmens C. Cachoir
SKB	K. Spahiu P.Carbol
STUDSVIK	H. Christensen T. Lundstrom
UPC	J. de Pablo I. Casas J. Gimenez F. Clarens
PSI	JM. Cavedon

EXECUTIVE SUMMARY

The EC 5th Framework Program SFS 'Spent Fuel Stability under repository conditions' (Contract FIKW-CT-2001-00192 SFS) was a collaborative experimental and modelling program dealing with the definition of radionuclide source terms for spent nuclear fuel in geological disposal conditions.

The participants gathered fourteen research institutes and agencies from seven European countries (including EC and Switzerland). Coordination was provided by CEA (France). This program started in November 2001 and was achieved in October 2004. This report synthesises the major findings of this project and try to enlighten their major consequences both for future R&D and spent fuel performance in geological repository.

The overall objective of this project was to bring some **operational answers to the major open questions on spent nuclear fuel stability.** Experiments performed on SNF for more than 30 y. demonstrated that the release of RN from spent nuclear fuel proceeds by two consecutive processes:

(i) A rapid release of radionuclides, often referred to as the **Instant Release Fraction** (IRF), which dominates the short term release. This release is assumed to be related to the radionuclides (RN) which are located within the zones of the rod which have no retention capacity when water arrives at the contact of the fuel in the canister.

(ii) A slow long-term RN release which is often referred to as the **matrix contribution**. This is assumed to correspond to the release of the RN which are embedded within the uranium dioxide matrix. They are therefore released through the dissolution of the matrix. Under the relevant conditions for European repositories, spent fuel matrix has been assumed to be corroded through the radiolytic dissolution linked to the existence of a significant alpha radiolysis at the fuel/water interface.

IRF represents the highest contribution to the final doses arising from direct disposal as shown by any published performance assessment (PA) calculations.

Therefore, the SFS projects focused on both contributions:

(i) by developing a new predictive model of IRF which integrates the potential fuel evolution before the water reaches the fuel, and hence the potential IRF evolution before water access.

(ii) by supporting a large experimental work on the radiolytic dissolution mechanisms and modelling in order to develop a new Matrix Alteration Model liable to predict the fuel alteration rate over time. In particular, the project aimed to relate the spent fuel alteration rate to the known residual α activity and determine whether there is any *time threshold* beyond which spent fuel would alter under the control of the solubility. Furthermore, effort was also focused on the potential strong influence of near-field reducing species as hydrogen produced by container corrosion.

Overall, the project aimed to develop a **global model predicting the radionuclide release rate as a function of time** for the spent fuel in relevant geological disposal conditions.

The Program was subdivided into five Work Packages (WP), along which the report outline the major outcomes during the 4 years of the project.

- **WP1: Evolution of the instant release fraction as a function of time (Coordinator CEA, C. Poinssot).**

Most of the previous works on the IRF mainly aimed to derive empirical correlation between some irradiation-related parameters (like burnup or linear power) and experimental labile fractions measured on short term experiments on relatively fresh fuels. However, recent works enlightened that SNF may evolve before the water ingresses the canister and modify the IRF, in particular due to:

(i) The significant helium production by alpha decay. Helium may contribute to disturb the fuel microstructure by diffusing and precipitating in grain boundaries, reducing therefore their mechanical strength.

(ii) The enhancement of the diffusion process by the continuous alpha self-irradiation (referred to as ASIED) which may lead to a RN redistribution within the rods.

The SFS project developed a new approach which is intrinsically liable to integrate these processes at least as options in order to have a robust and predictive model liable to be used for performance assessment (PA).
The IRF was redefined as the amount of RN which is located in any fuel microstructure for which no confinement properties can be anticipated for the long term. External cladding zirconia layer, gap zone, rim zone for high burnup UOX fuel, fractures and grains boundaries, and Pu-rich cluster in MOX fuels were therefore considered as potential contributors to the IRF. Anyhow, in order to reflect the different national approaches, the choice of the zones to consider as part of the IRF will be let to the end-user of this model. This rational definition on a process-oriented basis is quite different from the former understanding of the IRF which was purely empirical.

The assessment of the RN inventories in each of these zones was based on both post irradiation examinations and leaching data through correlations with burnup which was considered as the only parameters which is effectively available for commercial fuels to be disposed of.

- Gap, fracture and grain boundaries inventories were jointly assessed through empirical correlations with the FG release which in turn is correlated to the burnup;
- Rim zone inventory was assessed by considering the mean rim burnup and the evolution of rim width with the mean pellet burnup;

A robust model of RN distribution within the rod after irradiation based on all the available data, both literature and unpublished CEA data, was hence acquired (D1, Johnson et al., 2004) (Table 1).

Table 1: Gap and GB inventory estimates (% of total inventory) for various radionuclides for PWR UO_2 fuel, based on BE values for burnups of 48 $GWdt_{iHM}^{-1}$ or less and PE values for higher burnups. (D1, Johnson et al., 2004).

BURNUP	37		41		48		60		75	
RN	Gap	GB	Gap	GB	Gap	GB	Gap	GB	Gap	GB
fission gas	1	1	1	1	1	3	4	8	8	14
$^{14}C^{*}$	10		10		10		10		10	
^{36}Cl	5		5		10		12		25	
^{79}Se	0.1	1	0.1	1	0.1	2	0.4	8	0.8	14
^{90}Sr	1	-	1	-	1	-	1	8	1	14
^{99}Tc	0	1	0	1	0	2	0	8	0	14
^{107}Pd	0	1	0	1	0	2	0	8	0	14
^{126}Sn	<0.01	1	<0.01	1	<0.01	2	<0.01	8	<0.01	14
^{129}I	1	2	1	2	1	3	4	8	8	14
^{135}Cs	1	1	1	1	1.5	1	4	8	8	14
^{137}Cs	1	1	1	1	1.5	1	4	8	8	14

Furthermore, a theoretical approach on the diffusion process within the rod, in particular the diffusion enhanced by the alpha self-irradiation, was performed (D2, Lovera et al., 2003). A Booth's type diffusion model was implemented using the upper estimate of for the alpha self irradiation enhanced diffusion coefficient in order to assess the evolution of the RN distribution with time (Table 2).

Table 2: % of RN inventory released by alpha self irradiation enhanced diffusion towards grain boundaries as a function of time (UO_2 at 55 GWd/t)

Time	1 000 y.	10 000 y.	100 000 y.
% of inventory released through ASIED within the grain boundaries	3	5	7

This new IRF model is able to account for the potential fuel evolution before water ingresses the canister is one of the major outcomes of the SFS project and is easily usable by any end-user due to its intrinsic flexibility in the uncertainty management, *i.e.* in the definition of the zone to allocate to IRF (D3, Johnson et al., 2005).

- **WP2: Reaction mechanistic aspects of radiolytic dissolution of spent fuel (Coordinator FZK, M. Kelm).**

This WP aimed to determine the nature and amount of the radiolytic products generated at the UO_2/water interface and model the radiolytic reactions at work during fuel alteration. In order to quantify the production and consumption of radiolytic oxidants, several experiments were conducted: (i) a UO_2/H_2O interface has been irradiated in a representative geometry by a 5MeV alpha particle flux supplied by a cyclotron (D6, Corbel et al., 2005), (ii) external irradiation by gamma source (^{60}Co) or alpha solution (^{238}Pu). The aim was to depict the mechanisms of oxidation at the fuel surface, to assess the influence of other chemical species on the radiolytic reactions and to update the available radiolytic kinetic model. Focus was put on brines (one of the German reference condition) and carbonate-rich water (relevant for argillaceous media like the argillites). The results show that dissolution is clearly enhanced by external alpha irradiation at high dose rate. The experiments performed out of irradiation but with similar bulk H_2O_2 concentration have lower dissolution rate demonstrating the likely influence of radiolytic radicals on the fuel corrosion. At the highest concentration, an hydrated uranium peroxide, called studtite, precipitates at the fuel/water interface, regardless of O_2 presence.

New experimental results obtained on the long lived products formed under γ- and α- irradiation in brines allowed to update the Christensen's kinetic model which has been implemented in the CHEMSIMUL or MAKSIMA code. Comparison with new experimental data leads to introduce new reactions to account for some additional reactions with brines contaminants like Fe^{2+}, Br^- and Ni^{2+} and some of the kinetics constants were updated (D7, Christensen, 2004a,b; D4, Kelm and Bohnert, 2004).

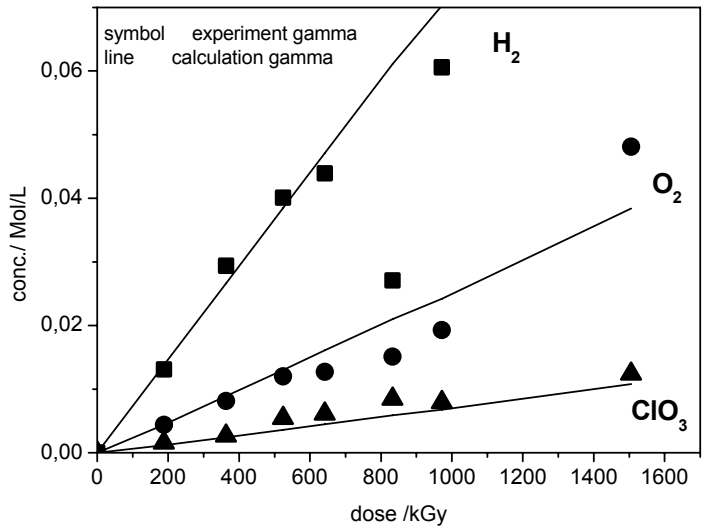

Figure 1: Formation of alpha radiolysis products in 5 M NaCl solution: Comparison of experimental and modelling results

Concerning the influence of secondary phases on radiolysis, very little data are available under reducing conditions, in contrast with the abundant literature under oxidising conditions. Many experts agree that no or very little secondary phase is to be expected under repository conditions (i.e. reducing). However the issue of formation of thick layers of secondary phases containing UO_2 is not ruled out (D8, Christensen, 2003).

Finally, several modelling approaches have been conducted in order to better depict the actual dose profile and radiolytic products distribution at the fuel/water interface. These models (like TRARAMO) account for (i) diffusion of molecular and radical radiolytic species from the fuel/water interface, (ii) reaction of the radiolytic species with the fuel surface and (iii) spatial and temporal variations of alpha and beta-gamma dose rates (D5).

- **WP3: Key experiments using α doped UO_2 and real spent fuel (Coordinator SKB, K. Spahiu).**

This WP tackled two major objectives which were to (i) relate the fuel alteration rate to the α radiation field and identify therefore whether there is a dose threshold beyond which no radiolytic dissolution occurs, and (ii) determine the potential influence of hydrogen on spent fuel alteration.

The relation between the fuel alteration rate and the alpha residual activity

Static or dynamic leaching experiments have been carried out with ^{238}Pu-doped and ^{233}U-doped UO_2 pellet or ^{225}Ac doped colloids with different doping level simulating fuel at various cooling time, from fresh fuel up to 10^6 y. old fuel.

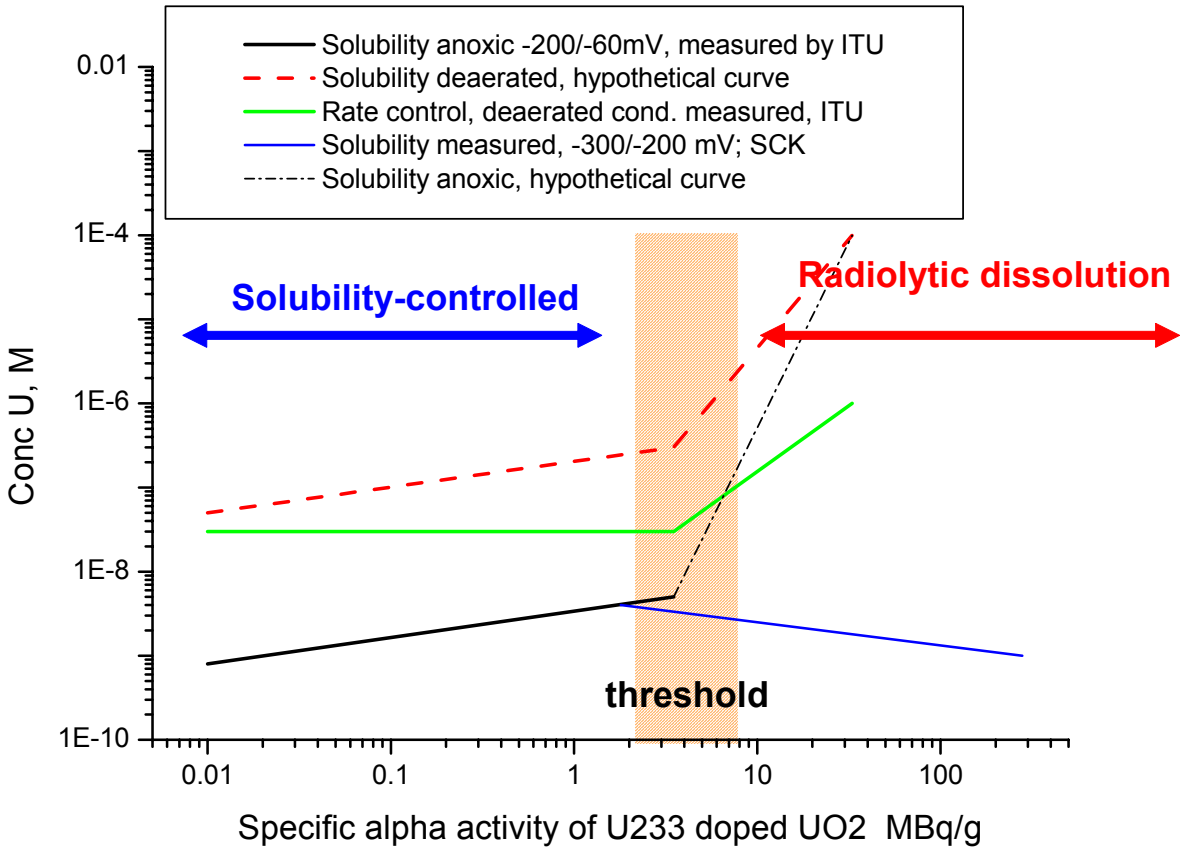

Figure 2: Effect of alpha activity on solubility and rate controlled release of U from alpha-doped UO_2 (D9, Cachoir et al., 2005)

From this large dataset, major conclusions are (Figure 2):

- Fuel alteration rate increases with alpha activity except for the lowest activities for which the rate seems to be independent on the alpha activity;
- A specific activity threshold occurs below which no effect of alpha activity is observed. This threshold ranges between 3.5 and 33 MBq/gUO_2 for deionised water but basically depends on the environment. Indeed, this threshold is now understood as a relative measure of the ratio of oxidants produced by radiolysis to the global reducing buffer capacity of the medium. For instance, it is observed that in strongly reducing medium like the Boom clay porewater, the threshold is much higher than 245 MBq/gUO_2 due to the strong reducing capacity of this medium.

These major results demonstrate that radiolytic dissolution can only occur if the non-radiolytic redox-acting couples in the near-field environment are not overwhelming the radiolytic oxidants: if non-radiolytic

reducers are majority, fuel alteration will be controlled by fuel solubility (alpha activity below the threshold) whereas if non-radiolytic oxidants are majority (oxidising conditions), fuel alteration will be oxidised by them independently of the water radiolysis.

The influence of the environmental aqueous species, in particular hydrogen

Corrosion of the iron-based container in reducing conditions will lead to the formation of large amount of hydrogen and Fe(II) within the near-field. Although H_2 is not supposed to be chemically active below ~100°C, hydrogen was envisaged as a potential fuel corrosion inhibitor prior to this project in preliminary experiments (Spahiu et al., 2000).

Numerous experiments have been conducted within SFS both on alpha doped UO_2 and on spent fuel to determine the H_2 influence, down to H_2 concentration. They all demonstrate a significant to complete inhibition of fuel corrosion with corrosion rates which are almost non measurable. These results are confirmed both under simultaneous α, β and γ radiations (fresh fuel) but also under pure α radiations (doped UO_2) (Figure 3).

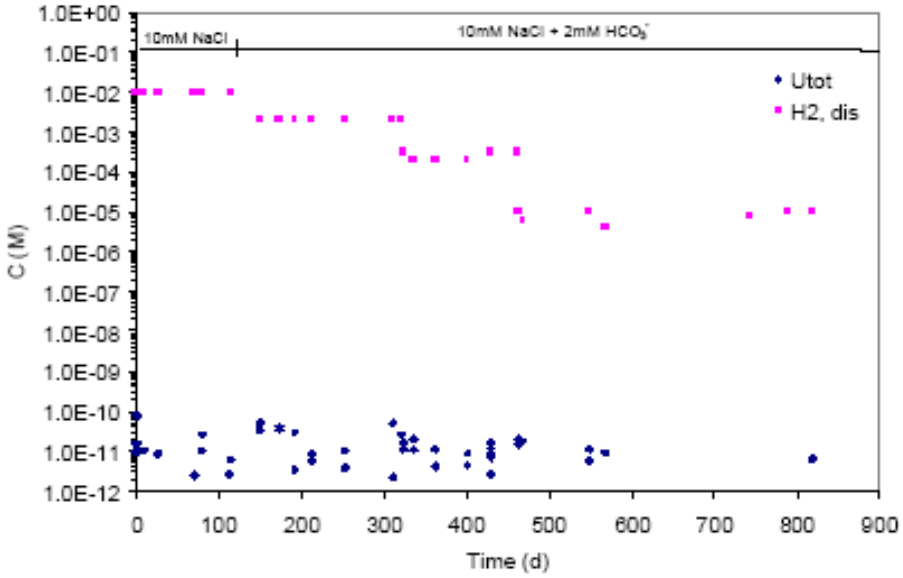

Figure 3: Measured H_2 and the total U concentration in the leachate as a function of time (D10, Carbol et al., 2005)

The mechanism of H_2 effect on fuel alteration is not yet completely understood and several interpretations have been proposed. New dedicated experiments are on-going within the 6th FWP NFPRO.

These findings on the fuel matrix alteration provide very important constraints on performance assessment modelling. Indeed, the first ten thousands years of a geological disposal should be dominated by strongly reducing species coming from the container corrosion like Fe(II) and H_2 and radiolytic dissolution is expected to be inhibited: radiolytic oxidants will be scavenged by the reducing species as evidenced by the high specific activity threshold observed in such conditions. For much longer term, fuel residual alpha activity will not be high enough to produce sufficient amount of radiolytic oxidants to oxidise spent fuel: the specific activity threshold in deionised water (with no real reducing buffer capacity by comparison to the geological medium) is in the range 3.5 – 33 MBq/gUO_2 which corresponds to fuel activity after 15 – 20 ky. Beyond this time, fuel dissolution will be governed by the fuel solubility kinetic rate law. Nevertheless, influence of local water radiolysis on fuel surface and solubility still needs to be assessed.

- **WP4: Matrix model construction (Coordinator ENRESA, A. Martinez).**

This WP developed the spent fuel alteration model by using results provided by WP2 and WP3 on water radiolysis, radiolytic dissolution and influence of hydrogen. Common views on the main mechanisms at work and their sequence arose from a dedicated workshop in Avila. Participants of different scientific

backgrounds shared viewpoints and ended up agreeing on the identification and ranking of the elementary processes to be integrated in a conceptual model (Figure 4).

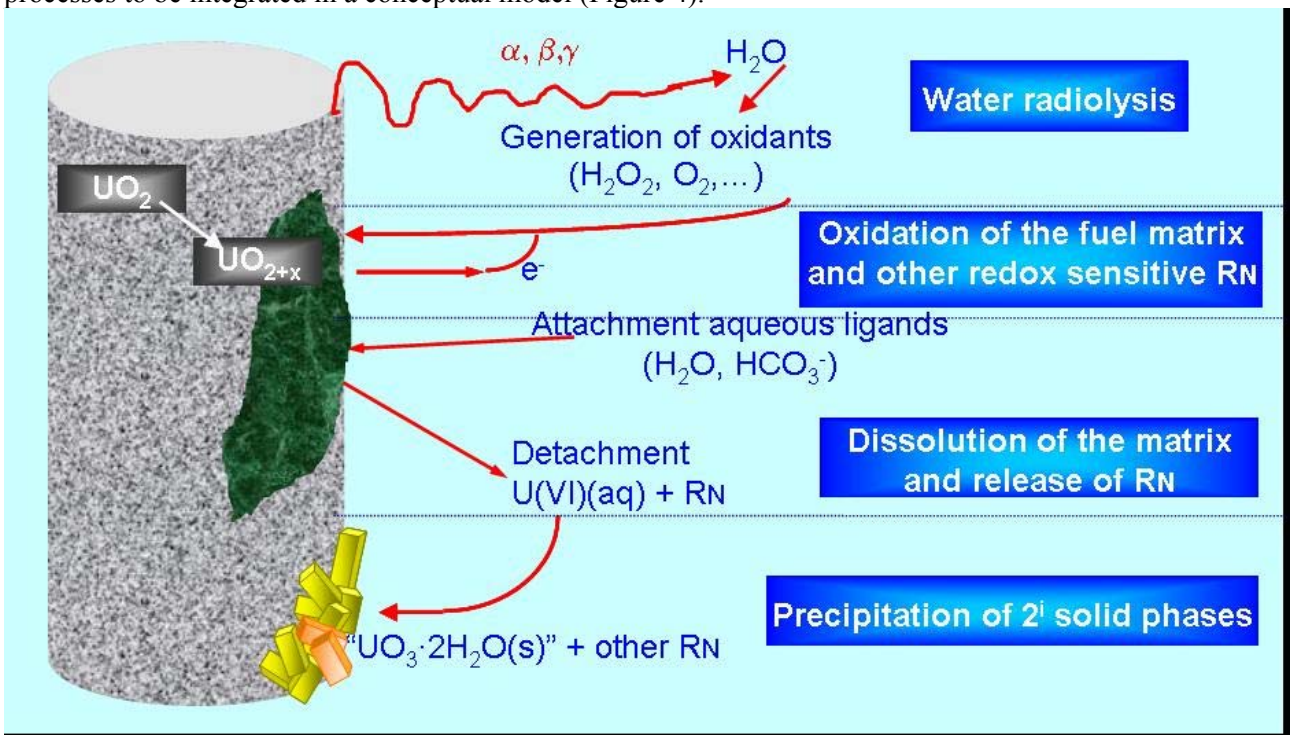

Figure 4: *Identification of the elementary processes governing the spent fuel alteration as discussed and agreed by all SFS partners (D12, Martinez-Esparza et al;2004a)*

When water reaches the fuel surface, water radiolysis will occur due to α irradiation. This radiolysis will generate reductants and oxidants. Local oxidative conditions are expected. As a consequence of these local conditions, the surface of the fuel will oxidise as well as any other redox sensitive radionuclides located close to the surface. The oxidation of the matrix and the attachment of aqueous ligands able to form strong complexes with uranium will favour the dissolution of the matrix. The release of the radionuclides embedded in the complexes will follow up. Finally, the precipitation of secondary pure or mixed solid phases (if solubility limits are reached) is expected to occur in the vicinity. Fuel oxidation is expected to be in many cases the limiting processes.

Based on these different mechanisms, a MAM was developed considering the following assumptions for each governing step (D13, Martinez Espara et al., 2004b):

- *step1, generation of oxidants by water radiolysis*: the amount of radiolytic oxidants was calculated using the updated Christensen's radiolytic kinetic scheme and was used as an input parameters in the MAM;
- *step 2, fuel oxidation by radiolytic oxidants*: this step was modelled by considering the surface complexation formalism. Both oxygen and hydrogen peroxide promoted oxidation was considered for the oxidation of the matrix
  - $>UO_2 + 1/2O_2 \Leftrightarrow >UO_3$
  - $>UO_2 + H_2O_2 \Rightarrow >UO_3 + H_2O$.
- *step 3: oxidised fuel dissolution under the influence of aqueous ligands*: this mechanism was modelled by a two-steps model :
  - Surface co-ordination of U (VI) by the aqueous ligands (H^+,H_2O or HCO_3)
  - Detachment (dissolution) of the product species.

  For H^+ and H_2O the rate-determining step will be the detachment of the product species [25]. For bicarbonate, the limiting process will be the surface co-ordination step [26]. Kinetic constants have been taken from the semi-empirical models developed by de Pablo
- *step 4, potential precipitation of secondary phases:* this process was not yet included in the current model (future update).

The model was calibrated against UO_2 experimental data and qualified on real spent fuel data, both from previous studies and SFS. It leads to a good agreement between MAM, previous semi-empirical models and experimental data as evidenced on Figure 5.

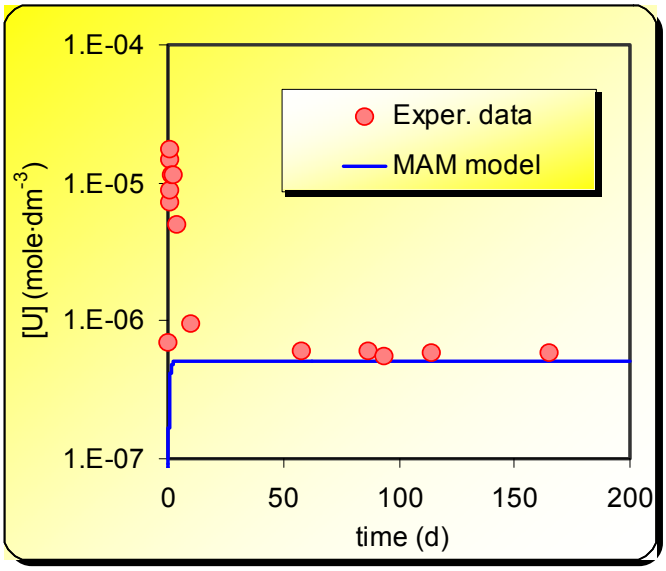

Figure 5: Comparison between the MAM and the SFS experimental results on doped UO_2 and spent fuel (Martinez Esparza et al., 2005)

Due to the recentness of the data on H_2 and activity threshold as well as the lack of understanding of the H_2 effect, they were not currently included in the current version of the MAM. Future development should integrate this point and also focus more on the solubility-controlled dissolution rate.

- **WP5: synthesis (Coordinator NAGRA, L. Johnson).**

Predictive calculations have been realised considering the IRF and the MAM models presented before respectively in argilites, granite and saline environment (D14, Martinez Esparza et al., 2004c). Environmental conditions were chosen to be generic but representative of the environment encountered in the different European sites with an initial hydrogen pressure of 3 bar when canister fails at 1000 y. Two reference engineered barrier system (EBS) have been chosen, respectively a container and a clay buffer for the granite and clay host rock, a container and a salt backfill for the saline host rock. Each canister is assumed to be composed of 4 fuel assemblies.
The fractional release rates of the 3 different environments are quite similar although the amplitude of the rock diffusion process is quite different (Figure 6).

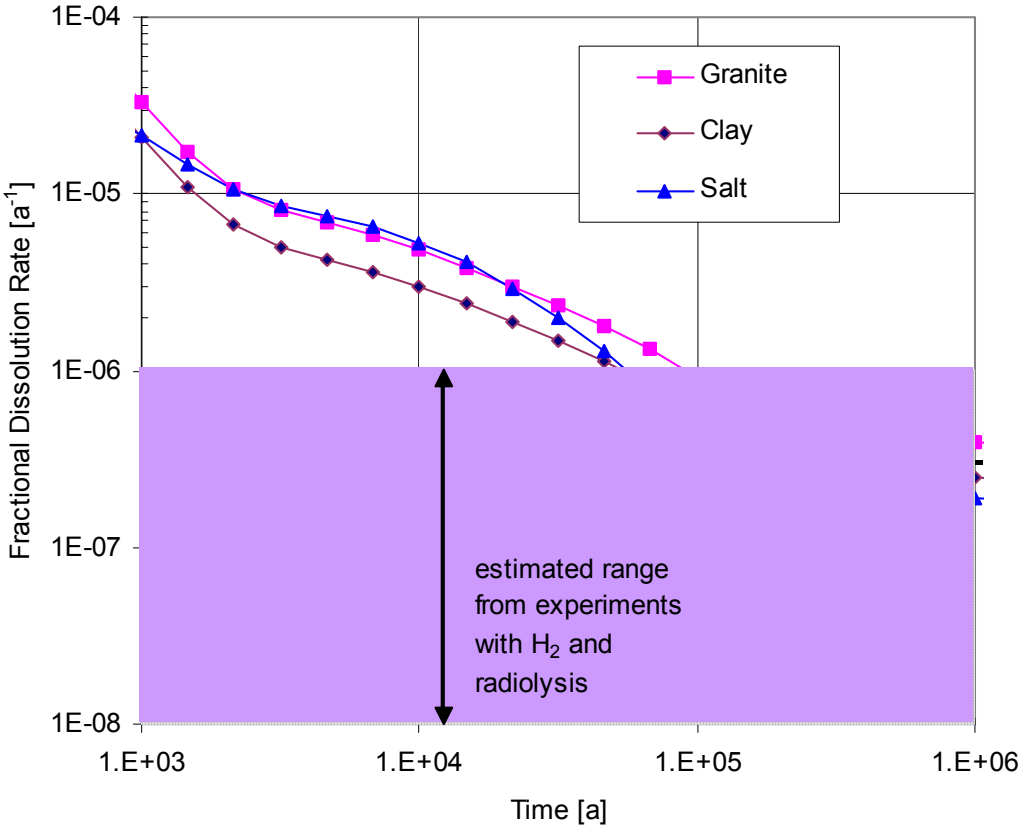

Figure 6: Comparison of fractional dissolution rates calculated using the MAM with the range of values estimated from experimental studies of dissolution of alpha-doped UO_2 and spent fuel in the presence of H_2 (D15, Johnson et al., 2005)

Although the inhibiting effect of hydrogen was not directly considered in these calculations, the fractional release of SNF was estimated to be in the range 10^{-5} to 10^{-7} y^{-1} and its lifetime beyond 10^6 y. Implementing the complete coupling between environmental reducing species (geochemical reducing buffer capacity, Fe(II) and H_2 produced by the container corrosion) will still significantly increase the performance of spent fuel by several orders of magnitude.

Finally, IRF contribution is quite significant for the most mobile elements during the earliest time but it progressively dominated by the matrix contribution as evidenced on Figure 7.

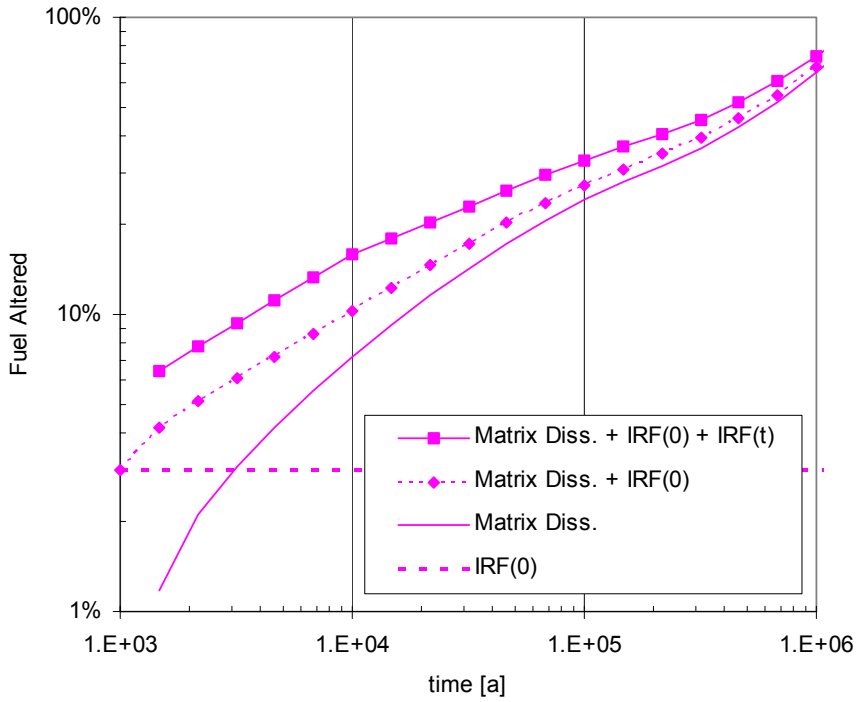

Figure 7: Integrated release of I-129 from spent fuel with a burnup of 41 GWd t_{iHM}^{-1} (granite case) considering matrix dissolution only (lower curve), matrix dissolution plus IRF (t=0) and matrix dissolution plus IRF(t=0) plus IRF(t). (D15, Johnson et al., 2005)

- **Future R&D developments**

As a conclusion, the studies performed within SFS allowed to strongly increase our understanding of spent fuel (UOX and MOX) behaviour and performances in geological disposal. The most significant findings and remaining uncertainties important for future R&D are:

1. IRF values for some radionuclides may be very high (15-25%) at burnups of 60-70 GWd t_{iHM}^{-1}. This is largely due to the rim restructuring, which leads to accumulation of volatile fission products in pores of the rim. There is very little information on the leaching behaviour of higher burnup fuels, on the leachability of the rim and on the stability of grain boundaries, leading to pessimistic assumptions in the IRF assessment. Considering the significance of IRF in PA, future studies should therefore focus in priority on (i) the long term stability of grain boundaries and (ii) the leachability of restructured zones which depends on the accessibility of the water inside them. In particular, it will be necessary to assess the He buildup in high burnup and MOX fuels may lead to high gas pressures in pores that might destabilise grain boundaries, possibly leading to cracking.
2. The uncertainties in alpha self irradiation enhanced diffusion cover several orders of magnitude. Although the final contribution of ASIED to the IRF and the overall RN release is limited, it will be necessary to refine and experimentally quantify this process to reduce the uncertainty.
3. Experimental results evidenced that radiolytic dissolution can not be studied solely but has to be coupled with the other redox couples which will be active in the near-field environment, in particular Fe(II), geochemical species and H_2. Our results demonstrated that radiolytic dissolution is the governing mechanism down to a dose threshold below which a solubility-controlled process becomes predominant. Furthermore, the threshold was demonstrated to be environment-dependent and to be at relatively high specific activity (3.5 – 33 MBq/gUO_2 for deionised water) , which means that SNF dissolution will be controlled by solubility after a relatively short period of time (~15 ky. in deionised water for instance, much less in reducing conditions). This finding implies that more effort has probably to be now focused on (i) characterization of environmental parameters controlling the specific activity threshold in order to specify its range value according to different environmental conditions (salt, high redox buffer as boom clay, metallic corrosion products), (ii) the quantification of the kinetic rate law associated with the solubility controlled dissolution. Finally, hydrogen activation at low temperature in spent fuel system still requires to be studied and understood before being implemented in an updated version of the MAM.

4. Fuel fractional alteration rate directly depends on the surface area accessible to water, which is not a easily accessible parameter. Indeed, measurements on fresh fuels are scarce and dispersed and probably not representative of what could be the surface area after some thousands years due to the potential evolution of grain boundaries. It is therefore of prime importance to better ascertain the evolution of grain boundaries to allow a realistic assessment of fuel fractional alteration rate.
5. A best estimate matrix alteration model (MAM) that has a strong mechanistic basis has been developed and successfully qualified. Fractional matrix dissolution rates calculated with the MAM are in the range of 3×10^{-5} yr^{-1} after 1000 y., gradually decreasing to 1×10^{-6} yr^{-1} after 10^{5} y. Experimental data from various studies using spent fuel and α-doped UO_2 with H_2 overpressures suggest that the dissolution rates may be in the range of 10^{-6} yr^{-1} to 10^{-8} yr^{-1}.
6. According the non congruent release observed for few radionuclides (Cs, …), some studies must focus on the behaviour of this type of RN.

A very significant increase of knowledge was therefore realised with the SFS EC-funded project which allowed all the European scientific community of spent fuel to gather data and develop common understandings and models. Although some very important questions are still addressed, the basis for the development of future models integrating the coupling with the near-field environment has been promoted and established by SFS and will make the development of future models easier.

1. Objectives and structure of the project, presentation of input data

1.1 GENERAL OBJECTIVES OF THE PROJECT

The EC 5th Framework Programme 'Spent Fuel Stability under repository conditions' (Contract FIKW-CT-2001-00192 SFS, referred to as SFS later on) was a collaborative experimental and modelling programme aimed at defining the radionuclide source terms for the disposal of spent nuclear fuel in a geological repository.

1.1.1 SOCIETAL OBJECTIVES

The **public acceptance** of nuclear fission as a reliable and sustainable source of energy strongly depends on whether European societies will successfully manage the nuclear waste issue. Among the various solutions and scenarios studied, *geological disposal* seems to be from the technical viewpoint the most reasonable. Implementing a geological repository requires the "demonstration" of **long-term safety** of such a facility in every envisaged scenario by ensuring that the radio-toxic impact will be below the levels established by safety regulations. In this demanding approach, particular effort has to be put on the **radionuclide release rate from the waste package to the environment**. This is in particularly true for spent nuclear fuel which has not been designed for long term radionuclide containment after removal from the reactor: At what rate will the radionuclides be released into the environment in relation to time and expected boundary conditions ? The answer to this question will directly determine (i) the potential radiation and radio-toxic impact on workers and public, and (ii) the way the repository has to be designed in order to guarantee long term safety. This is also the demanding task this project will face.

Public acceptance of nuclear waste disposal will never rely solely on individual or isolated scientific and technical studies, whatever their intrinsic merit. **Gaining public acceptance also requires the development of a common scientific and technical opinion throughout the European community and the building of a consensus** on the way the disposal system will evolve, and on what the most relevant mechanisms and processes are for modelling long term evolution. Therefore, coordinating the **work of high quality scientific institutions** working on spent nuclear fuel long term evolution is of prime importance for ensuring timely development of a European view on this issue, which is strategic for the energy independence of Europe.

In this context, the SFS project was designed to organize and optimise a critical evaluation of the various experimental and modelling approaches to obtain a first consensual European view on the sounded processes involved in the fuel alteration in repository and the subsequent radionuclides release while enhancing the soundness, quality and reliability of the model.

1.1.2 TECHNICAL OBJECTIVES

Among the various types of radioactive material that the European societies have to manage properly, safely and in economically viable conditions, much concern is focused on *spent nuclear fuel*. Indeed, in it is concentrated most of the residual activity generated during the fuel cycle if no reprocessing is performed, which is the current situation for some of the European countries. In addition, by comparison to other nuclear waste forms such as nuclear waste glass, spent fuel is quite a complex and heterogeneous system which has obviously not been designed as a waste form for disposal. A spent nuclear fuel assembly is composed of 264 fuel rods (a PWR assembly is considered as an example) held together by grids and thimble tubes, as illustrated in Figure 8. Each fuel rod is composed of 8mm diameter UO_2 pellets containing most of the radionuclide inventory after irradiation, and enclosed within a 0.5 mm thick Zircaloy-4 cladding.

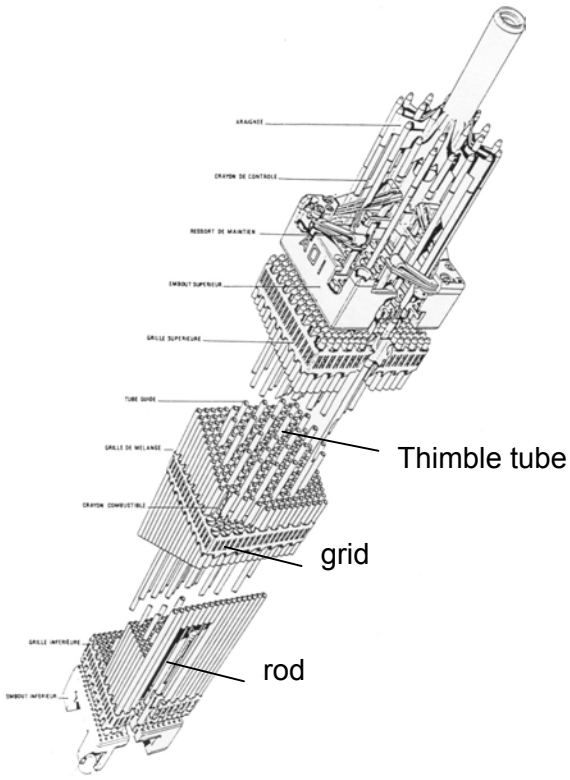

Figure 8: schematic of a typical PWR fuel assembly showing the complexity of the system

Assessing the performance of spent nuclear fuel in a potential future geological disposal system requires an understanding of the important time-dependent phenomena influencing its behaviour on a time-scale up to millions of years. Such a goal requires the development and qualification of models predicting the long-term evolution of the fuel assembly as well as models describing the release rate of radionuclides. These last models are usually referred to as "*radionuclide source term models*".

The fundamental aim of this project was to develop a **reliable and robust model for the spent fuel source term** which could then be used with *confidence* in the *various national performance assessment* exercises by the national agencies in charge of assessing the feasibility and safety operations of a potential geological disposal system, whatever the countries and disposal system designs are. The development of source term models is indeed intrinsically a scientific and technical challenge which requires an obvious **scientific consensus of what major mechanisms have to be accounted for**.

1.2 CONCEPTUAL MODEL OF RADIONUCLIDES RELEASE DISCRIMINATING THE RESPECTIVE ROLE OF IRF AND MAM

The classical RN source terms for spent nuclear fuel are schematically composed of two contributions :

(i) the so-called *Instant Release Fraction (IRF)* which is expected to be instantaneously released when water arrives in the waste package and which corresponds to the radionuclides located in microstructures which do not display any confinement properties;

(ii) The radionuclides located within the grains which are released with the alteration of the grains. This contribution is often referred to as the *matrix contribution.* Two processes were classically invoked as the potential long term matrix alteration governing mechanisms and the results were still lacking at the onset of the project to discriminate between them:

- A dissolution controlled by the *solubility of the grains* (roughly the UO_2 solubility) which will probably undergo a kinetic control;

- An *oxidative dissolution* related to the existence of a significant but decreasing α activity at the fuel/water interface (Figure 9) which yields oxidative species by *water radiolysis,* which then react with the fuel surface (radiolytic mechanism).

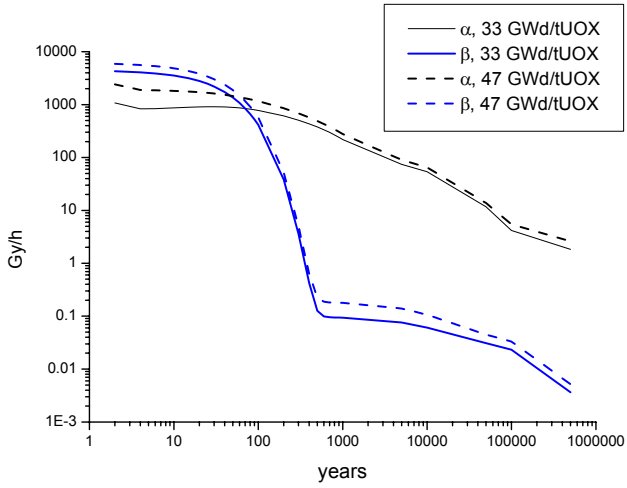

Figure 9: Evolution of α-, and β- dose rates at the fuel surface with time for two burnups: Average α dose rates at a distance of 30 μm from the fuel surface, β- dose rates calculated for a hypothetical water filled fuel/cladding void of 80 μm

The project therefore aimed to develop a consensual **model predicting the radionuclide release rate as a function of time** for the spent fuel in geological disposal conditions. Such a model subsequently provides reliable input for assessing the performance of spent nuclear fuel in geological disposal.

Key experiments and calculations were performed in the SFS project in order to determine:

(i) What is the *evolution with time of the IRF* which represents the major contribution to the radio-toxic impact on the biosphere (through the release of long-lived, mobile radionuclides such as, for example, ^{129}I, ^{36}Cl and ^{14}C) ?

(ii) How should *the radiolytic alteration process be modelled over time* in order to predict the spent fuel alteration rate? That is, how will the model

- relate the known residual α activity to the spent fuel alteration rate, and
- allow discrimination between the solubility-controlled and radiolytic mechanisms. In particular, due to the decrease with time of the residual alpha activity, it will determine if there is any *time threshold* beyond which spent fuel would alter under the control of the solubility and when it would occur.

1.3 STRUCTURE OF THE PROJECT

The participants were the Commissariat à l'Energie Atomique (CEA-France), the Association pour la Recherche et le Développement des Méthodes et Processus Industriels (ARMINES-France), the Agence Nationale de Gestion des Déchets Radioactifs (ANDRA-France), Empresa Nacional de Residuos Radioactivos SA (ENRESA- Spain), Forschungs Zentrum Karlsruhe (FZK-Germany), Joint Research Centre - Institute for Transuranium Elements (JRC-ITU), Svensk Kärnbränslehantering AB (SKB-Sweden), Nationale Genossenschaft für die Lagerung radioaktiver Abfälle (NAGRA-Switzerland), Belgian Nuclear Research Center, (SCK.CEN-Belgium), Centro de Investigaciones Energéticas, Medioambientales y Tecnológicas (CIEMAT-Spain), Universita Politecnica de Catalunya (UPC-Spain), Enviros (ENVIROS-Spain), Studsvik Nuclear AB (STUDSVIK-Sweden), Ecole Nationale Supérieure des Mines de Nantes (ENSTIMN-France). This program lasted from November 2001 to October 2004.

In order to propose a model able to predict the release rates of radionuclides as a function of time, the project has developed, on the one hand, a model to predict the evolution of the IRF with time, and on the other hand, a model to predict the release rates of radionuclides from grain dissolution (matrix contribution) as a function of time.

1.3.1 ASSESSING THE INSTANT RELEASE FRACTION IRF (WP1)

From the most recent results obtained in national programs, it appears that spent nuclear fuel may evolve with time before water access to the waste form in a repository (after resaturation of the site, and corrosion and failure of the canister …) and that this evolution may influence the subsequent radionuclide release in the repository. In particular, (i) radionuclide diffusion processes within the rod may be active and modify the known radionuclide location, and (ii) the fuel microstructure may alter under the influence of the He buildup within the pellet, and because of the accumulation of irradiation damage in a temperature domain where little or no recovery is expected.

The radionuclides associated with the IRF term are expected to be located within the gap zone, the grain boundaries and also in the high burnup restructured zones as the rim in UO_2 fuel. The significance of the IRF for the long term safety is therefore directly related to the inventory of RN which are located within these microstructures. In order to evaluate the IRF inventory, the project therefore modelled the evolution versus time of the radionuclide inventories which are located in the gap, grain boundary and rim zones by:

1- Synthesising the current knowledge on the radionuclides location within a spent fuel rod at the end of the irradiation, in particular by accounting for the existing leaching data;

2- Computing the potential migration of these radionuclides through time under the influence of thermal and α self-irradiation-enhanced diffusion.

All this work was performed in the Work-Package WP1 coordinated by C. Poinssot (CEA).

1.3.2 DEVELOPING A TIME-DEPENDENT RADIOLYTIC MODEL (WP2-WP3-WP4)

Research conducted on water radiolysis under α irradiation shows that water radiolysis leads to an increase in the oxidative properties of the aqueous solution due to the production of oxidative species such as H_2O_2. Since UO_2 is not stable in presence of oxidants and tends to oxidize to U_3O_7/U_4O_9 phases, any increase in the solution redox potential at the fuel surface would enhance the reactivity of spent fuel and increase the driving force for its alteration. In this framework, radiolysis was early evoked as a potential governing mechanism for the spent fuel alteration rate on time scales which were unknown.

Despite the general agreement on the significance of α radiolysis, no data were available at the beginning of the project to relate the α spent fuel residual activity to the concentration of oxidants produced and thus to the spent fuel alteration rate (although an electrochemical model based on corrosion potentials on UO_2 arising from α radiolysis was developed for the Canadian performance assessment (Johnson et al. 1996). In this context, the SFS project aimed to provide new experimental high quality reliable data on these two aspects:

1- Develop and upgrade the radiolytic kinetic scheme by conducting experiments on simplified systems in representative conditions in order to discriminate the relevant reactions and aqueous species. This work was performed within the Work-Package 2 (WP2) coordinated by M. Kelm (INE).

2- Conduct key experiments on more realistic systems (α-doped UO_2 and spent fuel) in order to (i) derive an empirical relation between the residual α activity and the alteration rate, (ii) determine the existence of any thresholds beyond which alteration is governed by the matrix solubility, (iii) evidence any potential influence of near-field H_2 which will be produced by container corrosion. This work was conducted within the Work-Package 3 (WP3) coordinated by K. Spahiu (SKB).

From the results of WP2 on the radiolytic scheme and processes at a microscopic level, and of WP3 on the more general alteration process at a macroscopic level, a Matrix Alteration Model (referred to as MAM) has been developed in order to reproduce the anticipated long term performance of the fuel matrix. This work was performed within the Work-Package 4 (WP4) coordinated by A. Martinez (ENRESA).

1.3.3 ASSESSING THE GLOBAL FUEL PERFORMANCE IN REPOSITORY (WP5)

Based on the boundary conditions defined by the agencies involved in the project and representing the various potential environments for a deep repository (clay rocks, granitic rock, salt), a global source term model was proposed by combining the IRF assessment from the WP1 with the MAM from WP4. This model was used to illustrate representative release rates of RN in different repository environments. It was performed within Work-Package 5 (WP5) coordinated by L. Johnson (NAGRA).

The global structure of the project can therefore be represented as follow:

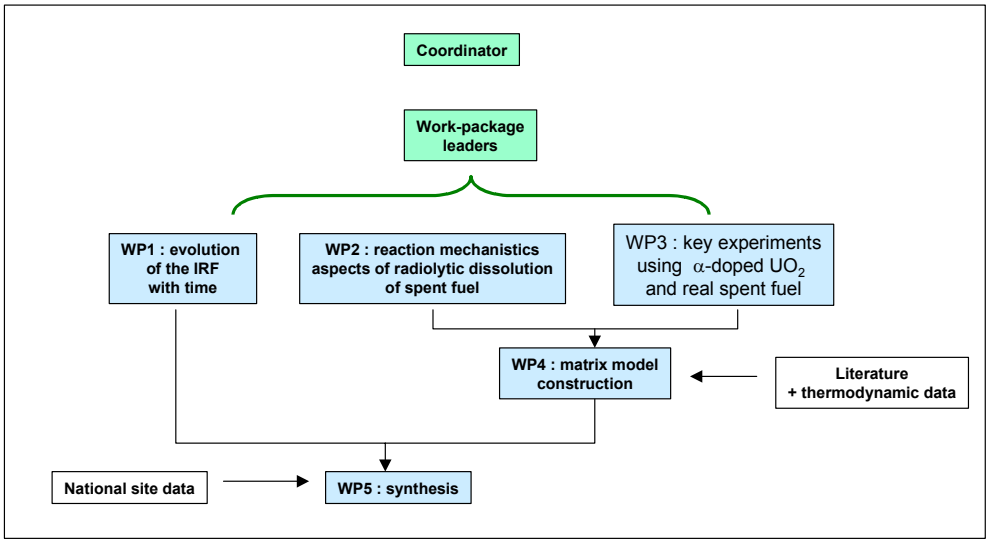

Following tables summarises the respective objectives, resources and partners of each work-package.

Name	Coordinator	Total manpower	partners	Objectives
WP1: Evolution of the IRF with time	C. Poinssot (CEA)	11	CEA, NAGRA	model the evolution with time of the IRF which correspond to the major contribution to the long term dose. Focus was put on estimating IRF values for various burn up and evaluating potential diffusion process
WP2: reaction mechanistic aspects of fuel radiolytic dissolution	M. Kelm (INE)	33	CEA, INE, ARMINES, ENSTIMN, STUDSVIK	determine the nature and the amount of the radiolytic products generated at the UO_2 / water interface and develop a model to predict these radiolytic reactions, which could be used thereafter within a wider matrix alteration model.

WP3: Key experiments using a-doped UO2 and spent fuel	K. Spahiu (SKB)	91	ITU, FZK, INE, CIEMAT,ENRESA, SKB, SCK-CEN, ARMINES, ENSTIMN	relate the spent fuel alteration rate to the α and gamma radiation field, assess the potential existence of an activity threshold and determine the potential influence of hydrogen on spent fuel alteration.
WP4: Development of a Matrix Alteration Model	A. Martinez (ENRESA)	56	UPC, ENVIROS, ENRESA, CIEMAT, INE, ARMINES-ENSTIMN, CEA, ANDRA	develop the spent fuel alteration model by using results produced within WP2 and WP3.
WP5: synthesis	L. Johnson (NAGRA)	18	All partners	produce the global spent fuel alteration model and RN release including both IRF and matrix contribution. First assessment of the spent fuel stability under repository conditions were subsequently performed using this model.

The CD-ROM attached to this report contains the compositions of UOX and MOX spent nuclear fuels used as reference and all deliverables produced by the project.

1.4 CHARACTERISTICS OF THE SPENT FUEL CONSIDERED WITHIN THE PROJECT

The SFS project focused on relevant spent nuclear fuels used in existing industrial reactors in Europe. Because of their relative importance, the work was focused on fuels used in current Pressurized Water Reactor (PWR) having burnups of 33, 41, 47.5 and 60 $GWd.t^{-1}$, although IRF studies also considered BWR fuels. One MOX spent fuel burnup value of 41.5 $GWd.t^{-1}$ was also considered. This choice was done at the initial step of the project in order to cover the current burnup range and the anticipated trends in burnup as well as considering limitations in the available data.
Quantitative assessment of the inventory after irradiation was provided by CEA as well as the assessment of their evolution with time under the influence of radioactive decay. The calculations were issued from the CESAR 4.0 code, a simplified evolution code for industrial use consistent with the DARWIN reference formulary (Marimbeau et al., 1998; Roque et al., 2002).

Reference composition of UOX and MOX spent nuclear fuels can be found in the CD-ROM attached to this report.

1.5 ENVIRONMENTAL CONDITIONS STUDIED AND ASSOCIATED BOUNDARY CONDITIONS

In order to cover the situation of the different European countries, three types of environmental conditions have been considered: salt formations based on the data provided by the German teams, argillaceous rocks based on the data provided by the French, Belgium and Swiss teams, and the crystalline rocks based on the data provided by the Spanish and Swedish teams involved within the project. Table 1 gives the different components of the repository system for spent fuel disposal in different European countries.

Table 1: Different components of the repository system for spent fuel in different European countries (Andriambololona and Johnson, 2005)

Site	Engineered barriers	Container	Backfilling materials inside the container
Clay	Clay	Carbon steel	Silica sand In most cases, no backfill. materials are present inside the container
		Stainless steel	
Granite	Clay	Carbon steel	
		Stainless steel	
		Copper with cast iron insert	
Salt	No engineered barrier	Carbon steel	
		Stainless steel	

Representative water chemistries and hydraulic conditions, to which the SF will be exposed after container breaching, are briefly summarised in Table 2 and Table 3.

Table 2: Chemical and transport conditions for a breached spent fuel container in a granite or clay repository from D15 (Johnson et al, 2005)

Parameter	Name	Variation range
Temperature		
	T	25°C -60°C
Hydraulic parameters in bentonite		
Diffusion coefficient (species dependent)	D_e	3 x 10^{-12} m^2/s (anions) 2 x 10^{-10} m^2/s (cations)
Porosity	ε	0.36
Hydraulic conductivity	k	$<10^{-12}$ m s^{-1}
Composition of the ground water		
	pH	7-10
	Eh (mV)	-130 (pH 7) to –300 (pH 8)
Carbonate system (mol/l)	HCO_3^-	10^{-4} – 6 x 10^{-2}
Major cations (mol/l)	Na^+	2 x 10^{-3} – 0.4
	K^+	10^{-4} - 10^{-3}
	Ca^{++}	10^{-4} - 10^{-2}
	Mg^{++}	10^{-5} –2 x 10^{-3}
Species influencing redox conditions	PH_2	1 to 10 MPa
	Fe(II)	1 x 10^{-7} - 3 x10^{-4}
	Fe(II)/Fe(III) phases	magnetite, siderite, green rust
Major Anions (mol/l)	Cl^-	1 x 10^{-3} - 0.4 (min. - Boom Clay, max. - saline water in granite)
	SO_4^{--}	10^{-5} – 0.14

Table 3: Chemical and transport conditions for a breached spent fuel container in salt repository from D15 (Johnson et al., 2005)

Parameter	Name	Variation range
Temperature	T (°C)	25 - 100
Hydraulic parameters		
Diffusion coefficient		
Porosity		
Composition of the ground water		
	pH	7 - 9
	Eh	
Total Carbonate (mol/l)	HCO^{3-}	
Major cations (mol/l)	Na^{+}	~ 6
	K^{+}	> 1
	Ca^{++}	> 0.2
	Mg^{++}	> 5
Anions (mol/l)	SO_4^{--}	> 2
	Cl^{-}	~6
Species controlling redox conditions	Fe(II)/Fe(III)	magnetite, green rust
	pH_2	10 - 20 MPa

2. EVOLUTION OF THE INSTANT RELEASE FRACTION AS A FUNCTION OF TIME (WP1)

It is now recognized that spent fuel may evolve during the first confinement phase before container corrosion and water ingress (Poinssot *et al.*, 2001, Poinssot *et al.*, 2002). The aims of this WP were to assess the impact of this first stage of evolution on the subsequent radionuclide (RN) release and to subsequently develop a model to predict the IRF as a function of time. The work was divided in three major tasks:

- to define as precisely as possible the initial location of RN after removal from the reactor based on post-irradiation examinations and leaching experiments on fresh fuels (deliverable D1);
- to assess the relevant diffusion processes to consider and thereafter to develop a diffusion model (α self-irradiation enhanced diffusion, αSIED) which will allow modelling of the evolution of RN location within the pellet as a function of time (deliverable D2);
- to finally model the IRF as a function of time considering the potential evolution of fuel microstructure (deliverable D3).

Based on the available knowledge arising from Post Irradiation Examination and leaching data, WP1 focused on potential long term confinement properties of the various fuel microstructures to allocate them either to the IRF or to the matrix. Due to the lack of common consensus throughout all the partners on the respective confinement properties of these microstructures on the long term, the project proposed several options to the end-users as shown in Table 4.

Table 4: Expected distributions of radionuclides in fuel assemblies and possible modelling approaches (Johnson et al., 2004)

Components	Key radionuclides	Characteristics and possible modelling approach
Fuel assembly structural materials		
Zirconia	^{14}C (organic?)	Oxide film typically about 40 to 80 μm thick is formed in reactor (about 10 % of cladding thickness).The oxide has a low solubility; the outer part is porous and ; may incorporate nuclides present in Zircaloy as the film grows. ***Limited data on Zircaloy indicating preferential release; consider ^{14}C as part of IRF. No data on steels.***
Zircaloy, Inconel and steel	^{14}C (organic?), ^{36}Cl, ^{59}Ni, ^{63}Ni	Very low general corrosion rate. ***Release of all nuclides plus remaining ^{14}C congruent with the slow corrosion rate***
Uranium oxide		
Gap	Fission gases, volatiles (^{129}I, ^{137}Cs, ^{135}Cs, ^{36}Cl, ^{79}Se, ^{126}Sn(?)). Also ^{14}C (non-volatile but partially segregated)	Good data for some nuclides. Assessment through fission gas release measurements and correlation with leaching experiments. ***Part of IRF***
Rim porosity	Fission gases, volatiles (^{129}I, ^{137}Cs, ^{135}Cs, ^{36}Cl, ^{79}Se, ^{126}Sn(?))	Rim width a function of burnup; good data available. Large proportion of nuclides in rim region segregated into pores and secondary phases during restructuring. No experimental data indicating release. ***Pessimistically could be part of the IRF;***
Rim grains	Actinides, FP	Release through dissolution when water arrives. FP may also diffuse to rim pores by αSIED. ***FP inventory may thus be part of IRF or MAM***.
Grain boundaries	Fission gases, volatiles (^{129}I, ^{137}Cs, ^{135}Cs, ^{36}Cl, ^{79}Se, ^{126}Sn(?)) Segregated metals (^{99}Tc, ^{107}Pd)	Limited data. ***As for rim pores, pessimistically considered part of IRF,***
Grains	Actinides, remaining FP and activation products	Belongs to **MAM**, WP4

As a conclusion, we can consider the following options with an increasing conservatism:

- **gap zone**: consensus to allocate it to IRF. It corresponds roughly to the initial labile fraction measured in laboratory experiments.
- **Rim porosity and grain boundaries**: their long term stability is currently difficult to demonstrate due to the potential impact of He production which could lead to the nucleation of nanobubbles within the grains (grain swelling ?) or the ingrowth of He bubbles within the grain boundaries. No significant conclusion can be drawn from the current knowledge and the choice of the IRF model is left open to the end-user.
- **Rim grains**: if rim grain boundaries progressively open with time, rim grains may present a very high specific surface area accessible and therefore alter relatively fast (by comparison to the hundred thousands years of prediction which is researched) due to their very small size (grain diameters ~0.1 μm).

Consequently, it was agreed by all the partner that WP1 will produce synthetic tables summarizing the best estimate evolution of the RN location as a function of time and end-user will have to decide whether they consider each zone as part of the IRF or not.

2.1.1 ASSESSMENT OF THE RN LOCATION AFTER IRRADIATION (NAGRA, CEA)

A general synthesis of the available data on the initial IRF has been realised by NAGRA with the support of CEA. This synthesis includes the data coming both from the Post Irradiation Examination (PIE) and from

short term leaching experiment. This synthesis benefits not only of the available data in the open literature but also of some unpublished data from CEA, in particular on fission gas release versus burnup. This work has been performed with the aim of identifying which radionuclides are located in the gap, the rim pores, the rim grains and the grain boundaries after irradiation. It was demonstrated from the available data that fission gas release provides a good bounding estimate of the RN inventories within the gap and the grain boundaries.

Table 5 summarises pessimistic estimates of the initial IRF for PWR UOX fuels.

Table 5: IRF estimates (% of total inventory) for various radionuclides for PWR UO_2 fuel, assuming IRF comprises gap, grain boundaries and all fission products in rim region (grains plus pores). BE (Best Estimate) values, with PE (Pessimistic Estimates) values in brackets (Johnson et al., 2004)

BURNUP	37	41	48	60	75
RN	IRF	IRF	IRF	IRF	IRF
fission gas	2 (2)	2 (3)	4 (6)	10 (16)	18 (26)
$^{14}C^{*}$	10	10	10	10	10
^{36}Cl	5	5	10	16	26
^{79}Se	1 (1)	1 (2)	3 (4)	7 (11)	11 (17)
^{90}Sr	1 (1)	1 (2)	3 (4)	7 (11)	11 (17)
^{99}Tc	1 (1)	1 (2)	3 (4)	7 (11)	11 (17)
^{107}Pd	1 (1)	1 (2)	3 (4)	7 (11)	11 (17)
^{126}Sn	1 (1)	1 (2)	3 (4)	7 (11)	11 (17)
^{129}I	3 (3)	3 (3)	4 (6)	10 (16)	18 (26)
^{135}Cs	2 (2)	2 (2)	4 (6)	10 (16)	18 (26)
^{137}Cs	2 (2)	2 (2)	4 (6)	10 (16)	18 (26)

The quantities of fission gas in the gap and pores of large Pu rich agglomerates of MOX fuels are summarised in Table 6. The IRF values proposed here assume that water penetrates all pores rapidly.

Table 6: Distribution of the fission gas in MOX fuel for various burnups (BU); best estimate and pessimistic values; IRF values taken into account inventories in the gap and pores of Pu rich agglomerates (Johnson et al., 2004)

BU (GWd t_{iHM}^{-1})		40	45	55	60
Gap (%)	average	2	3.2	5.6	6.8
	pessimistic	3.8	7.0	13.4	16.6
Restructured Pu rich agglo-merates (%)	average	25	30	30	35
	pessimistic	50	50	50	50
IRF estimates	average	27	33	36	42
	pessimistic	54	57	63	67

2.1.2 ASSESSMENT OF THE RN DIFFUSION WITHIN THE PELLET (CEA, NAGRA)

On the one hand, thermal diffusion is considered as non-significant in the temperature range considered (diffusion coefficient < 10^{-30} $m^2.s^{-1}$). On the other hand, α self-irradiation enhanced-diffusion (αSIED) has been proposed to be a relevant process based on a comparison with the effect of fission fragments on diffusion within reactors. A complete review of the data existing in the literature and some theoretical attempts to assess this process have been performed by CEA:

- Scaling approach based on the Matzke's reactor data (1983). The fission rate is corrected to the volumic alpha activity and the number of defects by fission to the total number of defects created by alpha decay. Values around 10^{-25} $m^2.s^{-1}$ are found for activity corresponding to fresh fuels.
- Development of atomistic and kinetics calculations. They lead to values ranging roughly three orders of magnitude lower than the previous reactor scaling approach.
- Natural analogues. Assessment of lead loss in Oklo uraninites is modeled in terms of diffusion and rough diffusion coefficient are therefore derived leading to value close to 10^{-24} $m^2.s^{-1}$.

Based on this assessment, a conservative value for ASIED coefficient was proposed versus the volume alpha activity as:

$$\textit{Eq. 1:} \qquad D^{\text{extrapolation}}_{\alpha-\text{sied},\,(m^2.s^{-1})} \approx (2.0 \pm 0.6)\ 10^{-41}{}_{(m^5)} \times A_{v\,(Bq.m^{-3})}$$

which can be modelled by considering the alpha decay for reference PWR fuel:

$$\textit{Eq. 2:} \qquad D(t)_{m^2.s^{-1}} \approx (1.0 \pm 0.3) \times 10^{-25} \quad \textit{for } t < 100 \textit{ years}$$

$$\textit{Eq. 3:} \qquad D(t)_{m^2.s^{-1}} \approx (3.7 \pm 1.2) \times 10^{-24}\ t^{-0.77}\ (\text{years}) \quad \textit{for } t > 100 \textit{ years.}$$

A report has been written by CEA and NAGRA detailing the literature review and the calculations performed on the various approaches (D2 deliverable) (Lovera et al., 2003, Ferry et al, *in press*).

2.1.3 DEVELOPMENT OF THE GENERAL IRF MODEL

Using the previous estimation for the αSIED diffusion coefficient, a Booth's type model has been developed to predict the evolution with time of the IRF. This model assumes:

- Grains as spheres of 8 μm;
- That the diffusion within the grain boundaries is much higher than in the grains, which leads to an assumption of zero concentration within the grain boundaries.
- That RN diffuse only under the influence of the αSIED with the previous conservative value for the diffusion coefficient (Eq. 1).

These hypotheses are therefore quite pessimistic and are not shared by all partners. They correspond to the definition of an upper bounding estimate of the contribution of diffusion to IRF. Although an upper estimate of the αSIED diffusion was taken into account, the contribution of diffusion enhanced by alpha self-irradiation is not so significant for the relevant time of water ingress considered in the European countries. It is about 5% after 10,000 years of cooling (Figure 10).

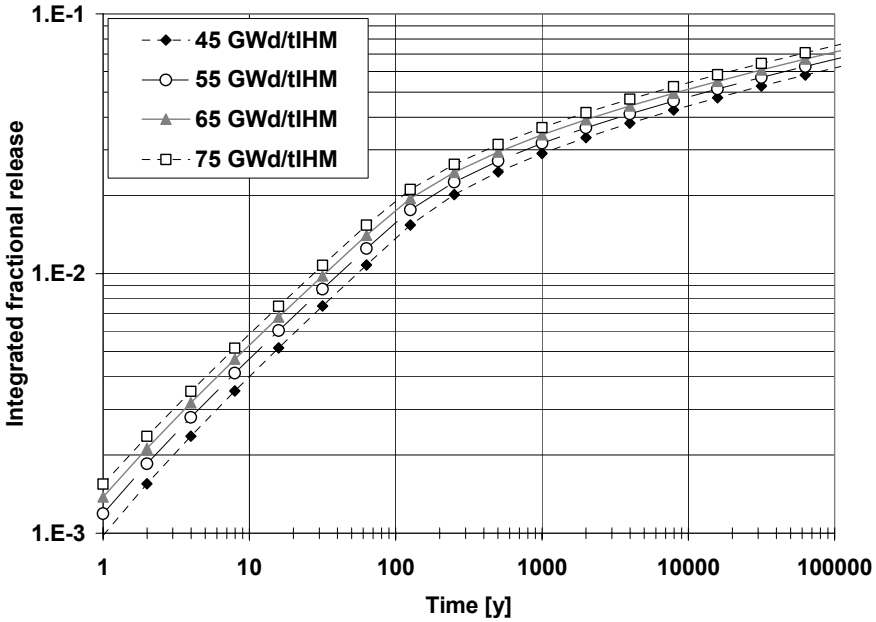

Figure 10: Calculated released fraction from grains due to α self irradiation enhanced diffusion for UO_2 fuels with burnups of 45, 55, 65 and 75 GWd t_{iHM}^{-1} (Ferry et al., 2004)

Using this model, Table 7 gives the bounding estimates of IRF versus time for the most mobile elements. The values proposed in Table 7 assume that water rapidly penetrates grain boundaries and pores and are based on pessimistic estimates of the inventories located in gap, grain boundaries and pores of restructured zones.

Table 7: Bounding estimates of the IRF at t = 0 y, 1,000 y, 10,000 y and 100,000 y of key RN for a PWR UO_2 fuel with a burnup of 55 GWd/t_{IHM} (Ferry et al., 2004)

	Bounding IRF values (%)			
Nuclide	**After irradiation**	**Container failure time**		
		1,000 y	**10,000 y**	**100,000 y**
^{14}C	10	13	14	16
^{36}Cl	11	14	15	17
^{79}Se	11	14	15	17
^{129}I	11	14	15	17
^{135}Cs	11	14	15	17

2.1.4 CONCLUSIONS AND PERSPECTIVES

The WP1 proposed the development of a model to predict the evolution of IRF with time which is based on the known distribution of radionuclides in the various microstructures of the spent fuel rod. The proposed model takes into account the potential evolution of the spent fuel pellet after removal from the reactor before contact with water. This work benefited from the complementary competencies of both partners but major uncertainties exist concerning the physical evolution of the fuel pellet on the long term in a closed system. As there is no consensus on how to treat these uncertainties in the IRF values, the WP1 produced a synthesized table giving the evolution of the RN inventories in the various microstructure (gap, rim grains, rim pores, grain boundaries) as a function of time so that every end-users can therefore decide which is to be associated to the IRF. Some work is necessary today in order to reduce the uncertainties on the IRF values.

Particularly, due to the lack of leaching data on high burnup fuel and MOX fuel, the distribution of radionuclides in the spent fuel microstructures is based on fission gas distribution which should lead to overestimates of the IRF. Major improvement will depend also on the demonstration of the grain boundaries and pores stability on the long term.

3. REACTION MECHANISTIC ASPECTS OF RADIOLYTIC DISSOLUTION AT THE FUEL/WATER INTERFACE (WP2)

This work-package aimed to depict the elementary mechanisms which occur during the radiolytic step of fuel oxidation. In order to quantify the production and consumption of radiolytic oxidants, several experiments were conducted: (i) a UO_2/H_2O interface has been irradiated in a representative geometry by a 5 MeV alpha particle flux supplied by a cyclotron, (ii) external irradiation by gamma source (^{60}Co) or alpha solution (^{238}Pu). The aim was to depict the mechanisms of oxidation at the fuel surface, to assess the influence of other chemical species on the radiolytic reactions and to update the available radiolytic kinetic model. Focus was put on brines (one of the German reference condition) and carbonate-rich water (relevant for argillaceous media like the argillites).

3.1 BASIC REACTIONS AT THE UO_2 / H_2O INTERFACE IN WATER

3.1.1 DESCRIPTION OF EXPERIMENTS

In order to investigate the effects of alpha irradiation on the release of uranium and the alteration of UO_2 in aqueous solution, pure water was irradiated through a thin UO_2 window with a high flux of alpha particles from a cyclotron. In parallel, UO_2 corrosion experiments without radiation were carried out with the same cell and UO_2 disk. As corroding medium a H_2O_2 solution was used with a concentration equal to the mean H_2O_2 concentration achieved by radiolytic water decomposition. The conditions in the irradiation experiments were adjusted so that the energy of the particles emerging from the UO_2 disk was 6.5 ±1.5 MeV. This energy is comparable to the typical energy of alpha particles emitted from spent fuel. Prior to the experiments the UO_2 disk was annealed in Ar/H_2 and afterwards pre-leached. In both cases the concentrations of uranium and H_2O_2 were measured after 4 to 7 consecutive leaching procedures of 1 hour duration each were carried out, starting always with a fresh solution. The UO_2 surface was analyzed after the leach experiments by means of Raman backscattering spectroscopy.

3.1.2 RESULTS

Prior to irradiation or H_2O_2 addition the UO_2 disk was leached in aerated and deaerated water, respectively (experimental blank). As expected, more U was released in the experimental setup used under irradiation (aerated water) compared to that for H_2O_2 addition (Figure 11). Afterwards the solutions were deaerated in both experiments. It was found that the amount of dissolved uranium is about 100 times higher under irradiation compared to the addition of H_2O_2. The H_2O_2 concentrations (mean value in the bulk) achieved by radiation or by addition were about 10^{-3} Mol/L. After 4 one-hour experiments the sequential irradiation yielded roughly 1800 times higher U concentrations compared to the blank. The U concentration measured in the experiments with added H_2O_2 decreased from sample to sample and was about 17 times higher than the blank after 7 one-hour experiments (Figure 11).

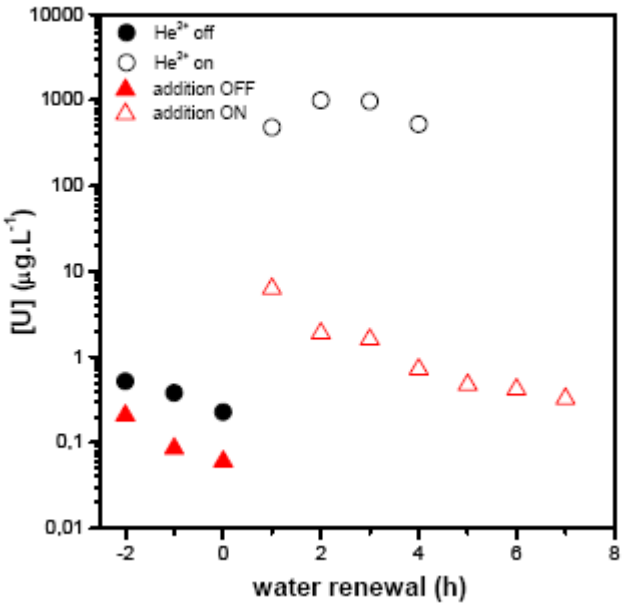

Figure 11: Comparison of UO_2 dissolution under irradiation and by adding H_2O_2. Experiments under irradiation (black symbols) have been acquired in aerated medium whereas experiments with H_2O_2 have been obtained in deaerated conditions. The increase of uranium release is much higher under irradiation than by adding H_2O_2.

The observed 100 fold higher UO_2 corrosion rate under irradiation (compared to experiments with added H_2O_2) can be explained by the fact that radiation creates radical species at the UO_2 surface that are more reactive than H_2O_2. The low radical yield under alpha radiation does not contradict this, as the fraction of oxidized uranium is small compared to the total amount of oxidants formed. On the other hand, the local H_2O_2 concentration in the water layer adjacent to the solid during the irradiation is much higher than the mean bulk concentration. This could explain the higher corrosion rate too, but is jeopardized by the result of Raman backscattering experiments. They showed that a layer of studtite is formed on the UO_2 surface under irradiation as well as in experiments with added H_2O_2. In the latter case the layer is more pronounced and leads obviously to a reduction of the corrosion rate in the course of the sequential experiments (Corbel *et al.*, 2005).

3.2 KINETIC RADIOLYSIS MODEL

The first step of radionuclide mobilization from spent fuel which is buried in the deep underground and exposed to ground waters is -besides the dissolution of the instant release fraction- the oxidative matrix dissolution through radiolysis. To predict the long term performance of spent fuel in a final disposal the mechanism of the radiolytical processes involved must be understood. This includes not only the processes in pure aqueous systems but also the influence of possible contaminants and of long-lived radiolysis products on the radiolysis. Furthermore one has to distinguish between the effect of low and high linear energy transfer radiation (LET): β, γ and α, respectively. A kinetic reaction model, compiled from published data of elementary reactions is assumed to be adequate to describe the radiolytic processes in the course of time in homogeneous solution (Kelm & Bohnert, 2004a). For the integration of the heterogeneous dissolution of solid UO_2 additional assumptions have to be made and kinetic parameters have to be calibrated by using dedicated experimental data. In this way the alteration of the spent fuel with time (decay and diffusion processes, formation of surface layers etc.) can also be described. In the following the reaction model is described including its basics, adaptation into program codes, application to solid UO_2 corrosion and experimental verification of modelling results.

3.2.1 PRIMARY RADIOLYTIC YIELD

The radiolytic effect in solution is the generation of reactive species in the early stages after the absorption of radiation energy. The yield of primary species (expressed as G-value, i.e. number of species formed per 100 eV absorbed energy) is that of species available for reactants in homogeneous solution after energy absorption and homogenization of species concentration by diffusion out of the spurs and tracks and is sometimes called 'escape yield'. This definition indicates that the term 'primary yield' is not very precise, but for dilute near neutral solutions at room temperature the primary G-values for β/γ and for α radiation are well established. The yield is proportional to the dose and depends strongly on the linear energy transfer (LET) of the radiation.

The early radiolysis processes in concentrated NaCl brine are different from those in diluted aqueous solutions. Whereas Na^+ is under radiation chemically inert, the Cl^- reacts very efficiently with oxidizing radicals. Because of the high Cl^- concentration such reactions take place already in the tracks and spurs. In this way -with less radical recombination in the tracks and spurs- the total yield of species diffusing out of the tracks and spurs increases. Furthermore, there is a change in the species spectrum reaching a homogeneous distribution and becoming available for other reactants (Fig. 2 and 3 in Kelm & Bonhert, 2004). In contrast to dilute solutions, there is a direct radiation effect on the solute in concentrated chloride brine. From the number of electrons attached to the Cl^- ions compared to all electrons present in the solvent and the solute a portion of 15 % for the direct effect on Cl^- can be estimated for 5 M NaCl solution.

For gamma radiolysis experimental values for the primary yields in brine are published or can be derived from other experimental data. As no experimental data are available for alpha radiolysis one has to rely on the very general deduction for the interaction of scavengers with short lived species in the tracks and spurs and its effect on the primary yield. The G-values for alpha and gamma radiolysis in water and 5 Mol/L NaCl solution are listed in Kelm & Bonhnert (2004a).

3.2.2 EQUATIONS

Even though the number of species created radiolytically in pure water is limited, the number of equations describing the interaction of the species is large and increases further with each dissolved species added. Within the SFS project only reaction schemes for water, Cl^-, Ni^{2+}, Fe^{2+}, CO_3^- and Br^- were considered. They are compiled in the annex of Kelm & Bohnert (2004a). The rate constants are usually given for room temperature and zero ionic strength. Therefore the model works only near room temperature. In the calculations the rate constants for reactions between charged species need to be corrected for the kinetic salt effect. As the radiolytically formed gases can interact with radical species one has to specify if or to what extend the gases are desorbed from the solution, thus not taking further part in the radiation chemical reactions.

To make the model applicable for the corrosion of UO_2 one has to differentiate between reactions, which mobilize U from the surface of UO_2 and others, which describe the fate of dissolved U species in the bulk of the solution. For the UO_2 dissolution calculations a combined transport and radiolysis model code was developed (TraRaMo) (Lundstrom, 2003). In the model the aqueous solution surrounding the UO_2 is divided into an arbitrary number of small compartments and the time is divided in an arbitrary number of time steps. A radiolysis calculation is carried out in each compartment for each time step, allowing for diffusion between the compartments after each time step. A combination of 3 types of radiation with different LET is accepted. Calculated 'mixed' G-values are used in the compartments according to the actual combination of radiation type. A shortcoming of TraRaMo is the use of a single diffusion coefficient for all species and the long calculation time.

Two much simpler two-compartment approaches were used in WP4 to describe the UO_2 dissolution under pure alpha irradiation. Both approaches consider that in the compartment adjacent to the UO_2 surface with the thickness equal to the maximum range of the alpha particles emitted from the solid into the solution, UO_2 is oxidized to the hexavalent state from radiolytically produced oxidants. The U(VI) drained from that 'active' layer into the (radiation free) bulk of the solution by diffusion is addressed as mobilized uranium. The first step of the UO_2 dissolution is formulated as a pseudo first order oxidation reaction with radical and/or molecular oxidants. Actually the models contain second order reactions. The 'Christensen' approach

assumes a constant 'concentration' of 10^{-4} mol.L^{-1} solid UO_2 in the 'active layer' which results in second order rate constants comparable to rate constants found in homogeneous solution for U(IV) species. For the 'new alteration scheme' the 'concentration' of solid UO_2 in the active layer is derived from a measured 'active site density'. As in the 'Christensen' approach the 'concentration' is taken fixed. In the simplified model the (elevated) real surface of UO_2 (compared to the geometric surface) is simulated by an elevated 'concentration' of solid UO_2 in the active layer.

3.2.3 DOSE RATE

While the gamma dose rate in solutions close to spent fuel mainly depends on the geometry of the assembly (and can be treated as constant in a first approximation), the dose rate caused by beta and alpha radiation has its maximum at the solid surface and becomes zero beyond the range of the particles. For alpha radiation the dose rate near the solid surface and the energy fraction transferred into the solution can be approximately estimated from geometric considerations (flat large solid surface, straight alpha path, constant energy loss along the path):

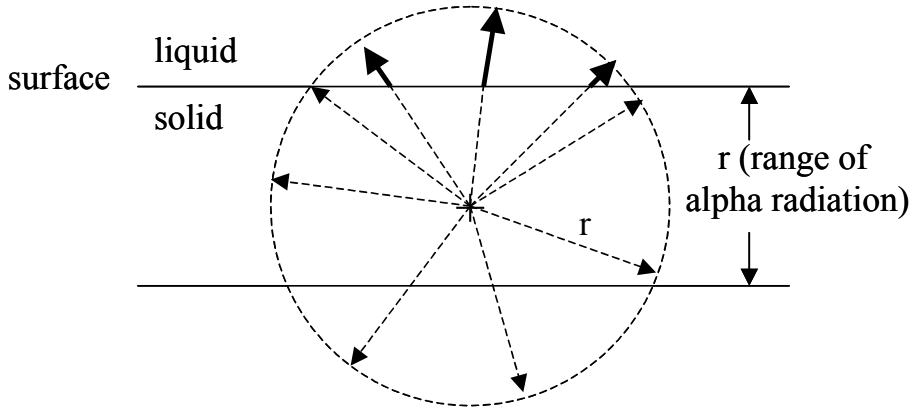

Figure 12: Alpha radiation emerging from a solid: The mean volume of sphere segments represents the fraction of energy released into the liquid.

As an example one can calculate for a UO_2 solid containing 6.10^{-3} Bq.µm^{-3} of a 5.8 MeV alpha emitter:

- Energy absorption per volume in the bulk of the solid:

$$\text{Eq. 4:} \qquad \frac{6.10^{-3} \times 10^{18} \times 5.8 \times 1.6 \times 10^{-13} \times 3600}{1000} = 20044 \ \ (J.h^{-1}L^{-1})$$

  At the solid surface the energy absorption is only half, i.e. 10022 J.h^{-1}L^{-1}.
  (Because the surface is only irradiated from one side)

  The energy absorption per volume in the solution at the interface can be estimated from the different alpha particle path lengths in both media:

$$\text{Eq. 5:} \qquad \frac{10022 \times 14}{45} = 3120 \ \ (J.h^{-1}.L^{-1})$$

  this equals 3120 Gy/h in water.

- The fraction of energy f(E) emitted in the surface layer of the solid with the thickness of the alpha particle range r (=14 µm) that reaches the adjacent liquid can be estimated from the mean volume of sphere segments (representing the escaping energy, solid arrows in Figure 12) compared to the total sphere volume (representing the total emitted energy, all arrows in Figure 12). The two-dimensional sketch Figure 12 illustrates this consideration: Depending on the depth in which the decay occurs the sphere segment volume ranges from 0 (depth = r) to 50 % (depth = 0). The mean fraction of the sphere volume is:

Eq. 6:
$$f(E) = \frac{\int_0^r \frac{\pi}{3}.(r-x)^2 \times (2r+x).\frac{dx}{r}}{\frac{4\pi r^3}{3}} = 0.188$$

The total energy E emitted in the 14 µm thick solid layer per mm^2 and second is hence:

Eq. 7:
$$E = 6.10^{-3} \times 10^9 \times 0.014 \times 5.8 \times 1.6 \times 10^{-13} = 7.8\ 10^{-8}\ J$$

18.8 % of this energy is absorbed in a 45 µm layer of the adjacent solution. Practically all that energy is already absorbed in the first 30 µm as will be shown later (Figure 13). On that condition the mean dose rate $\frac{dE}{dt}$ is:

Eq. 8:
$$\frac{dE}{dt} = \frac{1.47 \times 10^{-8} \times 10^6 \times 3600}{0.03} = 1760\ Gy.h^{-1}$$

Considering the Bethe-Bloch equation for the energy transfer in UO_2 and water, using an iteration scheme with 50 to 100 cells per trajectory and summarizing over all trajectories one can calculate the correct dose rate profile as shown in Figure 13 (Cachoir et al., 2005).

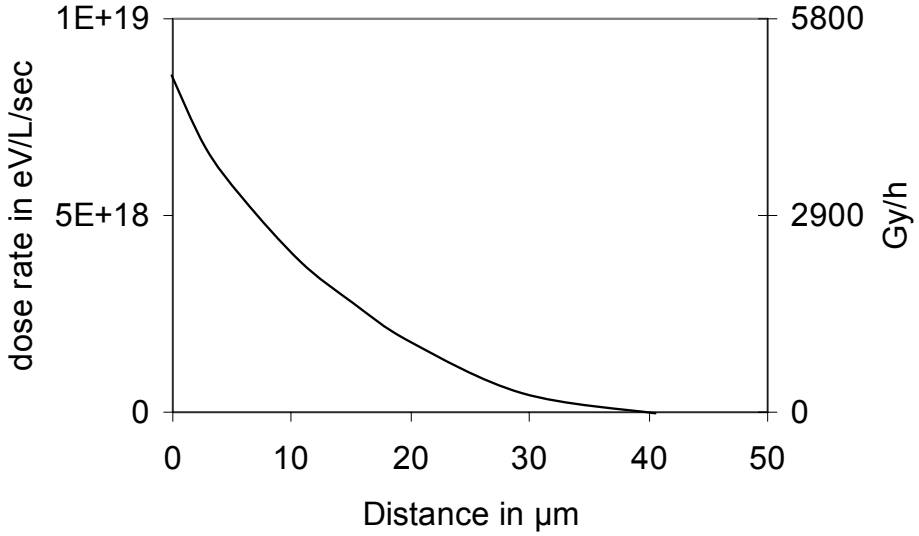

Figure 13: Calculated dose rate profile in solution adjacent to a cylindrical pellet (Activity concentration: $6*10^{-3}$ Bq/ $(\mu m)^3$, Alpha energy: 5.8 MeV)

The shape of the curve in figure 3 shows that in 30 µm distance from the surface practically all energy emitted from the solid is absorbed. For the activity concentration given above, the maximum and mean dose rates based on geometric considerations and the calculation are compared in Table 8. There is practically no difference in the mean dose rates. The estimated maximum dose rate is about twice the mean value, the calculated maximum dose rate is about three times the mean value.

Table 8: Comparison of maximum and mean alpha dose rates in a 30 µm suface layer of solution from geometric estimation and calculation

Dose rate (Gy/h)	Estimation	Calculation-Bethe-Bloch equation
Maximum at surface	3120	4880 (from Figure 13)
Mean in 30 µm layer	1760	1680

The radiolysis calculations in WP4 were carried out with the simple 2-compartment model using a mean dose rate for the surface layer. There is only a small difference between the approximation and the calculation. The dose rate profile however has to be considered in multi-compartment calculations with TraRaMo.
The dose rate profile in front of a solid caused by beta radiation cannot be easily estimated as beta radiation is not mono-energetic and many fission products with quite different decay energies contribute. But a similar derivation from the Bethe-Bloch equations as carried out for alpha particles is possible, if mean beta energies are used. This might be sufficient for a first approximation (Cachoir et al., 2005).

3.2.4 CALCULATION CODE

Two different kinetic codes with slightly different capabilities were used in the SFS project: MAKSIMA CHEMIST and Chemsimul. In the D12 report (Martinez et al., 2004a) of this project it is worked out that concentrations calculated with both codes deviate from each other by less than 1 %.

3.2.5 SENSITIVITY AGAINST PARAMETER VARIATIONS

The results of modelling with respect to long-lived radiolysis products are mainly influenced by the kinetic rate constants and the G-values and less by the dose rate. To determine which rate constant or G-value has a strong impact on the calculated concentrations the numerical values of both were varied and the output with respect to the concentration of the molecular products H_2O_2, H_2D, H_2, O_2 or O_2D in water and H_2D, H_2, O_2D, O_2 or ClO_3^- in chloride brine was compared to calculations with nominal values. For the sensitivity analysis the dose rate for gamma irradiation was chosen to be 8000 Gy/h that for alpha irradiation 1400Gy/h. The concentrations after 1000 y. of irradiation were compared. The general behaviour of the radiolysis systems under investigation and their general performance in the sensitivity analysis are shown in Table 9. Details are given in Kelm & Bohnert (2004a).

Table 9: Calculated behaviour of different radiolysis systems (open= constant gas release; closed= no gas release): x= formation proportional to dose; o = establishment of steady state conditions; bold and underlined symbols mark species concentrations which are influenced only by a few parameters in the sensitivity analysis.

	H_2O			5 M NaCl solution		
System	H_2	O_2	H_2O_2	H_2	O_2	ClO_3^-
gamma-open	x	x	o	x	x	x
Gamma-closed	o	o	o	o	o	o
Alpha-open	**x**	**x**	**o**	**x**	**x**	**x**
alpha-closed	**x**	**x**	**o**	x	x	o

3.3 VALIDATION, CALIBRATION AND APPLICATION OF THE MODEL

The model described in section 3.2 was validated with respect to pure radiolysis by comparing calculated concentrations of long-lived radiolysis products with the respective results from gamma- and alpha

experiments. The rate constants for the UO_2 oxidation reactions were fitted according to experiments with real spent fuel. Furthermore the model was applied to experiments with alpha-doped UO_2.

3.3.1 MODEL VALIDATION WITH 5 M NACL BRINE

The calculated production of radiolysis species in brine were compared to a variety of experiments conducted under gamma and alpha irradiation. The standard deviation of gamma experimental results in an open system with respect to the formation rate of the molecular products H_2, O_2 and ClO_3^- is under most conditions (pH, concentration of Cl^- and contaminants) in the range of some 10 %. The deviation between experimental and calculated concentrations is approximately of the same order (Figure 14).

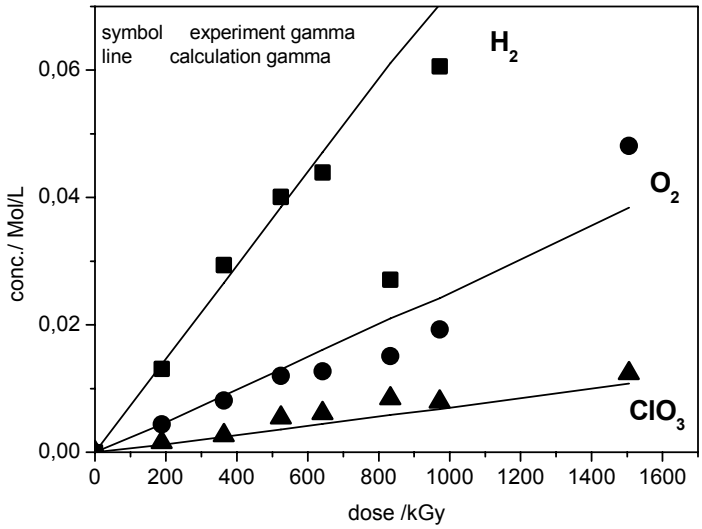

Figure 14: Formation of gamma radiolysis products in 5 M NaCl solution: Comparison between experiments and model results

Only for Fe^{2+} containing solutions the degree of compliance is poorer. The compliance between experimental and calculation results for the alpha radiolysis of brine with respect to H_2 and O_2 is similar to that for gamma radiolysis. But all chlorine species are underestimated in the calculation (Figure 15). The formation of ClO_3^- proportional to the dose (at higher dose) and the steady state formation for HClO however is simulated correctly.

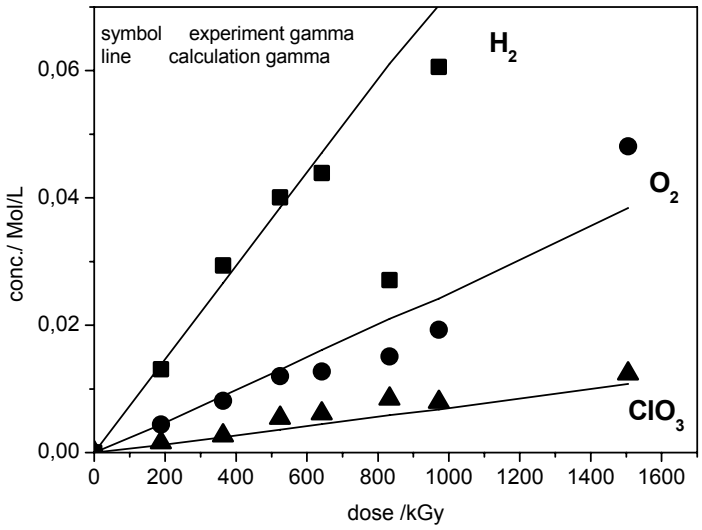

Figure 15: Formation of alpha radiolysis products in 5 M NaCl solution: Comparison of experimental and modelling results

The gamma radiolysis mechanism in a closed system without any gas release with the formation of steady state concentrations for H_2, O_2 and ClO_3^- as observed in experiments is correctly modeled if a reaction between H_2 and Cl_2^- is considered in the scheme and if the strong pH dependence is correctly described by the model. The experimentally observed "protecting" effect of dissolved H_2 and the effect of added Br^- acting in the opposite direction is reasonably modeled. The deviation between experiments and calculation is for H_2 and in most cases for O_2 in the range of some 10%. The already low ClO_3^- concentrations found in experiments however are orders of magnitude lower in the calculation (Kelm & Bohnert, 2004a).

3.3.2 MODEL CALIBRATION WITH RESPECT TO UO_2 DISSOLUTION REACTIONS.

The equations and rate constants describing the dissolution of UO_2 according to section 3.2 are arbitrary. Therefore the rate constants need to be calibrated to achieve agreement between experiments and simulation. For the 'Christensen' approach the rate constants of the reactions between UO_2 and oxidants from the water radiolysis (OH, HO_2, O_2^-, H_2O_2 and O_2) and HClO were determined earlier (Poinssot et al., 2004). In this project the rate constants for reactions of U species with the Cl_2^- radical were fitted using measured corrosion data from real spent fuel (Christensen & Lundstrom, 2004). The fitting result and a comparison with experiments are given in Table 10.

Table 10: Effect of considering oxidation reactions with Cl_2^- radicals. Fitting result.

calc. / exp.	Reaction rate constant ($M^{-1}s^{-1}$) for		Corrosion rate
	$UO_2 + Cl_2^-$	$UO_3H + Cl_2^-$	µg $*cm^{-2}*d^{-1}$
calc.	4 E08	8 E08	2.6
Calc	1.7 E05	3.4 E05	0.84
Exp.			0.84

A sensitivity analysis similar to that mentioned in section 3.2.5 shows for pure alpha irradiation that the reaction scheme yields remarkably higher corrosion rates if the molecular oxidant HClO is partially replaced by radicals (Cl_2^-, $ClOH^-$ and OH).

3.3.3 EFFECT OF SECONDARY PHASES ON THE UO_2 DISSOLUTION

A literature search shows that layers of secondary phases are formed in drip tests and in studies of natural analogues, minerals and in leaching experiments under oxidizing conditions. But very little secondary phase is formed under the reducing conditions of deep ground water. A number of minerals such as schoepite, dehydrated schoepite, studtite, becquerelite, rutherfordine and uranophane are identified as secondary phases. In some cases layer thickness and in a few cases the porosity of the layer are measured. A reliable prediction of the properties of a secondary phase formed in a repository in deep ground waters has not been found. However, methods have been developed to make calculations of corrosion rates possible, when such information becomes available (Christensen, 2003).

The UO_2 corrosion rate predicted by the radiolysis model is a product of a calculated concentration increase over time of oxidized, released uranium species and a 'reactive' solution volume. Accordingly, if the porosity is 20 %, the 'reactive ' water volume and therefore the corrosion rate will be reduced by a factor 5. As the alpha particle path length is shorter in a layer of a dense secondary phase (compared to the solution), one can expect a further reduction in 'reactive' water volume and thus in the corrosion rate. Radionuclides precipitated in the secondary phase on the other hand will increase the dose rate in the pore water. It can be shown however that the tortuosity factor of such a layer, which might reduce the diffusivity by a factor of 2 or more, has a negligible effect. Such consideration assumes that the radiolysis effect occurs in the pore water only but that the radiation chemical processes are the same as in the bulk water.

3.3.4 MODEL APPLICATION ON UO_2 CORROSION UNDER ALPHA IRRADIATION

The model was applied to various experiments (Christensen, 2004). A comparison between calculation and experiments carried out with ^{238}Pu-doped UO_2 pellets and different solutions are compiled in Table 11. The agreement in all cases is reasonable, even though the assumptions for calculating the effective dose rate that is used for modelling in Christensen (2004 a,b) differs slightly from that made in section 3.2.3.

Table 11: Comparison of experimentally measured UO_2 corrosion rates with model calculations (a): Stroess-Gascoyne et al., 2002; (b) Kelm & Bohnert, 2004a; (c) Cobos et al., 2002.

Ref. No	Method	Activity concentration Bq/g	Mean surface dose rate Gy/h	Solution	Corrosion Rate µg/(cm^2.d)	
					Exp.	Calc.
a	Corr. Potential	$3.7*10^8$	1.13	0.1 N $NaClO_4$	0.07	0.21
		$3.7*10^9$	11.3	pH 9.5	1.3	0.85
b	Amount of dissolved U	$3.8*10^8$	1.02	5M NaCl	0.48	0.20
		$3.8*10^{10}$	102	pH 8	3.9	0.76
		$3.8*10^{10}$	102	5 M NaCl, pH 11	0.89	0.57
c	Amount of dissolved U	$3.8*10^8$	1.16	H_2O	0.65	0.21
		$3.8*10^{10}$	116	pH 6-7	3.4	1.87

The calculated corrosion rates deviate by less than one order of magnitude from each other, regardless of the experimental conditions and for a maximum factor of 100 between the different dose rates. The range of experimental results is larger but in most cases the deviation between experiment and calculation for certain conditions is less than a factor 3.

Under certain experimental conditions the agreement between experiments and calculation is poorer:

- In experiments at Whiteshell laboratories (Sunder & Shoesmith, 1997), UO_2 was alpha irradiated with an external source in a narrow distance from the UO_2 surface. The calculated corrosion rate was more than 10 times higher than observed;
- Kelm and Bohnert (2004b) corroded UO_2 pellets in a ^{238}Pu containing brine. The calculated corrosion rate was more than 10 times lower compared to the experiments probably because the UO_2 oxidation from the added Pu(VI) was not considered;
- The model was unable to simulate experiments using extremely high dose rates as provided from a cyclotron (Sattonay et al., 2001).

4. ASSESSMENT OF THE DISSOLUTION RATE EVOLUTION WITH TIME IN GEOLOGICAL REPOSITORY (WP3)

4.1 ASSESSMENT OF THE RADIATION FIELD INFLUENCE

4.1.1 INTRODUCTION

European repositories become soon reducing, after a short oxic post-closure phase. Under such conditions unirradiated UO_2 becomes thermodynamically stable. Reducing environments favour also the stability of natural uraninite minerals for billions of years. However, the radiation field created by the α-, β- and γ-

decay of the radionuclide inventory of this material may establish locally oxidising conditions. The effect of radiation initiated spent fuel instability is of temporary nature since the radiation field decreases with time. With respect to the radiation field, the spent nuclear fuel samples available today for experimental work are not representative of aged fuel after hundreds or thousands years of storage. As a consequence of radioactive decay the short-lived radionuclides dominating the radiation field of present day spent fuel will disappear soon and already after a few hundred years of storage, α-decay will dominate the radiation field in and around the spent nuclear fuel. A key factor in determining the dissolution behaviour of spent fuel exposed to groundwater might be then the radiolysis of the water in a film approximately 50 µm thick surrounding the surface of the fuel caused by the α-decays. Radicals and molecular species radiolytically produced near the fuel surface could oxidise the fuel matrix, thus enhancing its dissolution, in spite of the nominally reducing conditions, which characterise the repository near field environment.
UO_2 containing short-lived alpha-emitters, the so-called alpha-doped UO_2, simulating the level of activity of spent fuel after different storage times, was used to study the effects of radiolysis on the corrosion behaviour of aged spent fuel exposed to groundwater. Figure 16 shows the alpha-activity as a function of storage time for different types of spent fuel. Also indicated in the figure as horizontal dashed lines are the activity levels of various alpha-doped UO_2 materials used in the SFS project.

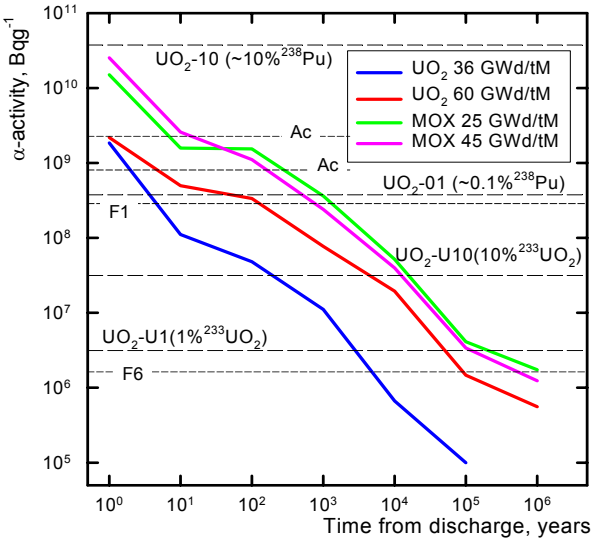

Figure 16: Alpha-activity of spent LWR fuels as a function of time (Rondinella et al., 2000). The horizontal lines indicate the activity of the various alpha-doped UO_2 prepared for the present studies (this activity can be assumed to be constant during the timeframe of this project, sample description and preparation methods are given below).

Due to the decrease in the radiation field one can expect that spent fuel stability will increase with the time after disposal. Static and dynamic leaching experiments and electrochemical experiments were performed by SCK.CEN, ITU, ENRESA and ARMINES under reducing conditions both with fresh spent fuel and with UO_2 doped with well selected quantities of α-emitters, simulating either artificially enhanced high alpha dose rates or the much lower alpha dose rates expected after disposal times of up to 10^6 years. These experiments are combined with pre- and post leaching characterisation of the specimen. In some cases the production of radiolytic species has been analysed as well. In the following, first a brief description of the experimental programme, materials and procedures is given, followed by a description of the results and their discussion in the context of literature data. More detailed descriptions are given in the deliverable D9 (Cachoir et al., 2005).

4.1.2 EXPERIMENTAL METHODS

^{233}U-doped UO_2 and other alpha-doped samples were produced at ITU by the sol-gel method with an α-activity simulating a large range of fuel ages after discharge. ^{225}Ac doped samples were fabricated by ARMINES by an electrochemical coprecipitation method. Sample names, doping levels, target fuel ages and

organisations using the samples are summarised in Table 12. To provide a comprehensive picture of the effects of different alpha activities on the leaching behaviour of UO_2, previously obtained data from experiments performed at ITU using higher activity alpha-doped UO_2 containing ^{238}Pu are also shown (Rondinella et al., 1999).

Table 12: Summary of some properties of the α-doped materials used for the leaching tests

Material	additive weight fraction %	α-activity of mixture $Bq \cdot g^{-1}$	Target fuel age f(burnup) yr	Dose rate Gy/h (30μm zone)	Organisation
UO_2-10	^{238}Pu: ~10.0	$3.8 \cdot 10^{10}$	high activity enhanced dose	114000	ITU/ ENRESA
UO_2-01	^{238}Pu: ~0.1	$3.8 \cdot 10^{8}$	5-1000	1140	ITU/ ENRESA
UO_2U10	^{233}U: 10.0	$3.3 \cdot 10^{7}$	200-20000	99	ITU/ ENRESA
UO_2-U1	^{233}U: 1.0	$3.5 \cdot 10^{6}$	3000-200000	10.5	ITU/ ENRESA
UO_2-0	0	$1.1 \cdot 10^{4}$	$>10^{6}$	0.033	ITU/ ENRESA
F1	^{233}U: 0.42 ^{238}Pu: 0.0385 Sr : 0.09	$2.45 \cdot 10^{8}$	5-1000	735	SCK·CEN
F6	^{233}U: 0.43 Sr: 0.09	$1.62 \cdot 10^{6}$	10^{4}-10^{6}	4.4	SCK·CEN
Ac	^{225}Ac: 10^{-5}	$5\text{-}50 \cdot 10^{8}$	high activity	0.6-3	ARMINES

The pellet sized samples (2-3 g each) fabricated by ITU were characterised using density measurements (~95 %TD for (UO_2-U1, UO_2-U10), ~93 %TD for F1 and F6), SEM, XRD, α-autoradiography, α-track analysis of the surface. Colloids of uranium dioxide doped with a short-lived α emitter, ^{225}Ac, were prepared by coprecipitation in a 1 $mol.L^{-1}$ NaCl solution at fixed pH = 6 and Eh= -500 mV / SHE.

Average dose rates in a 30 μm water film were calculated using the Bethe-Bloch equation, considering energy loss in the spent fuel (maximal escape depth about 11 μm). The model does not apply to Ac-doped colloids since the particle diameter is much smaller than the escape depth of alpha particles. In this case a model for homogeneous activity distribution in aqueous solution was used.

Before the leaching tests, all the ITU produced samples (alpha-doped and undoped UO_2) were annealed for several hours at 1000°C in Ar/(6%)H_2 to reduce the specimens to stoichiometry and to recover alpha-decay damage and mechanical stresses accumulated during the sample preparation. A continuous pH constant reduction procedure (-800 mV, -300 μA) was used in the case of UO_2 colloid dissolution tests of SUBATECH/ARMINES.

The leachant used by ITU-CIEMAT-ENRESA consisted of deionised water (MQ) and commercial carbonate water (CW). SUBATECH utilised pure oxygen and carbonate free 1 M NaCl solution denoted solution S1 at a pH of 6.0. The test medium used by SCK•CEN is Real Boom Clay water (RCW), sampled in the underground laboratory of SCK•CEN. The RCW is characterised by its high carbonate concentration, its high content of organic material- mainly humic acids - and its reducing capacity. The water composition of CW and RCW water is given in the deliverable D9 (Cachoir et al., 2005). The values of the ratio of the sample surface to the solution volume (S/V ratio) were calculated using the geometric surface, in case of powders a sphere model was used together with the average particle size. S/V values employed by ITU/ENRESA were between 0.2 and 4 m^{-1}, 300-1000 m^{-1} for SCK and 20000m^{-1} for SUBATECH/ARMINES.

ITU/ENRESA experiments were performed either under sequential deaerated (purging with inert gas) or under static anoxic conditions. All tests were performed at room temperature, using borosilicate or Pyrex glass vessels, in glove boxes with N_2 atmosphere under static conditions (no water flow). All the leachates were filtered through 450 nm membrane filters. The sequential leaching experiments (same sample through

increasing leaching times) were performed either with total renewal of the leachant and replacement of the vessel after each contact period (CW and MQ) or by taking aliquots of leachate (typically 2 ml) from the reaction vessel (CW). The duration of single contact periods ranged from 0 to ~600 days. The total timeframe of the experiments was of the order of 3 years.

SCK experiments (samples F1 and F6) were performed under dynamic conditions in a Teflon made flow through reaction cell of 7.6 mL volume using powdered samples (particle diameter of 200-300 μm). Five experiments were performed with fuel F6, with flow rates of 10.4, 10.9, 25.1, 40.2 and 80.5 $\mu l.min^{-1}$, corresponding to residence times of 12.2, 11.6, 5.0, 3.2 et 1.6 h of the leachant in the flow cell. Two experiments were also carried out with fuel F1, with flow rates of 10.5 and 40.2 $\mu l.min^{-1}$, corresponding to residence times of 12.2 and 3.2 h of the leachant in the flow cell). ^{238}U, ^{233}U and ^{238}Pu were analysed by ICP-MS, the radiolytic products such as H_2, O_2 by gas chromatography, H_2O_2 by chemiluminescence and ClO_3^- by IC.

Static colloid dissolution tests of SUBATECH were realised with a suspended quantity of 90 mg $UO_2.L^{-1}$ and a specific Ac activity of 520 $MBq.g^{-1}$ UO_2. After colloid fabrication, the supernatant solution was removed and replaced by the same volume of fresh oxygen-free solution (NaCl 1 $mol.L^{-1}$, pH 6). The start of the dissolution experiment was the moment when fresh solution was introduced in the reaction cell.
Electrochemical testing (free corrosion potential measurements and impedance spectroscopy (EIS)) of α-doped UO_2 was done at ITU with electrodes made from undoped and α–doped UO_{56} and with spent fuel in deaerated 0.1 mol/l NaCl solution under inert gas purging (O_2< 1 ppb) in an inert gas glove box. Prior to testing, the electrodes were cathodically polarised to reduce oxidized surface layers.

Three dynamic dissolution tests of spent fuel were performed at ITU under oxidizing conditions at 25°C in 0.001 M $NaHCO_3$ /0.019 M NaCl to study the dissolution rates in the absence of secondary phase precipitation. A continuous flow-through reactor (70 mL) was installed in a hot cell. Two combined pH and Eh electrodes (ThermoOrion Low maintenance triode and Platinum Redox electrodes, respectively) monitor the conditions in the reactor during the experiment. Two irradiated UO_2 fuel samples from pins with average burn-ups of 53 and 29 MWd/kg U were used in pellet form; the high burn-up material was also leached in powdered form. Mean particle size of the powdered fuel was 9 ± 4 μm. Oxidising conditions were maintained by equilibrating the leachant solution with air. The flow rate of the leaching solution was kept within the range of 0.06-0.5 mL/min. The whole length of the experiment was more than 5 months. Details for dissolution rate calculations from the flow-through test results can be found in the deliverable D9.

4.1.3 RESULTS

4.1.3.1 STATIC DISSOLUTION TESTS WITH α-DOPED UO_2, ITU/ENRESA/CIEMAT

Figure 17 summarises the results of leaching of alpha doped UO_2 containing ^{233}U in CW and MQ water under deaerated conditions, in terms of U concentration as a function of leaching time. Four independent experiments were performed, labelled **B**, **C** and **D**, **BC,** in CW, **D** in MQ water. **B** were performed with aliquot sampling; **C** and **D** with total renewal of the leachant after each contact period. The pH was 7. A clear enhanced release is observed for UO_2 with 10% ^{233}U compared to the other two types of samples. The values for UO_2 with 1% ^{233}U are indistinguishable from those for undoped UO_2 within the timeframe considered so far. There is good agreement among all sets of data, and, in particular, between the results in CW for the tests with and without replenishment. The enhanced dissolution measured only in the case of UO_2 with 10% ^{233}U indicates that, *under these experimental conditions and for the experimental timeframes considered*, the lowest threshold to observe an alpha-radiolysis enhancement of UO_2 dissolution lies between $\sim 3 \cdot 10^6$ and $\sim 3 \cdot 10^7$ Bq/g. Figure 18 shows data from leaching in MQ of the alpha-doped UO_2 containing ^{238}Pu (UO_2-10, UO_2-01 and UO_2-0) (Cobos et al., 1999; Rondinella et al., 2001). A comparison between Figure 19 and Figure 20 illustrates that the release values for UO_2 containing 10% ^{233}U converge after 1000 h of leaching to those obtained for the Pu-doped samples.

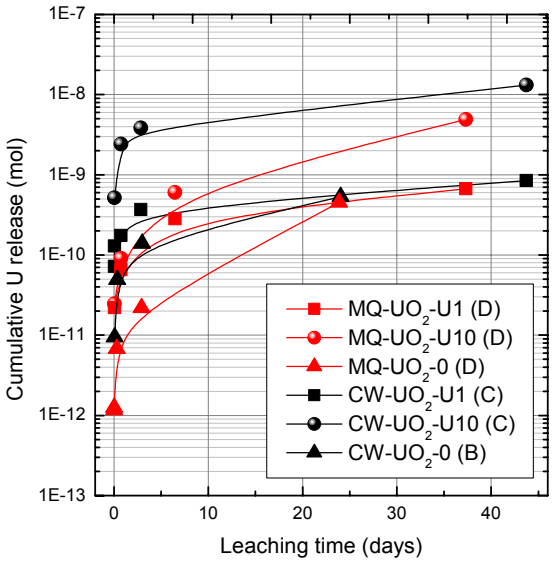

*Figure 17: α-radiolysis effect on corrosion behaviour of UO_2 pellets doped with ^{233}U under unaerated conditions. Comparison between CW water (experiment **C**) and MQ water (experiment **D**). Sequential leaching with total renewal. Cumulative U release vs. time.*

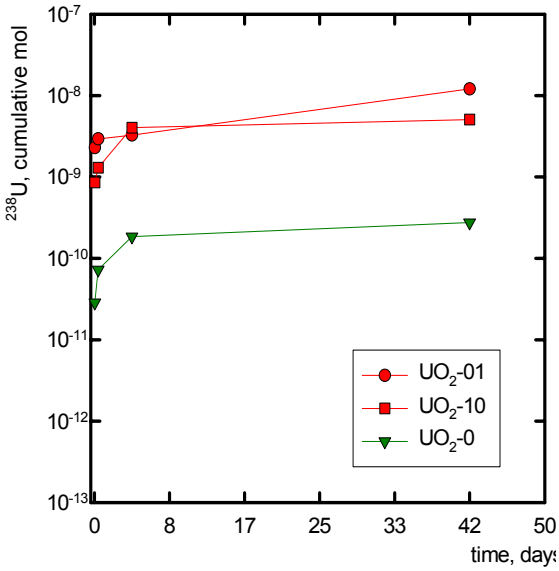

Figure 18: α-radiolysis effect on corrosion behaviour of UO_2 pellets doped with ^{238}Pu under unaerated conditions in MQ water. Cumulative U release vs. time. Sequential leaching with total renewal (pH 5.85 – 6.15) (Cobos et al., 1999; Rondinella et al., 2000)

For anoxic conditions and CW water (0.02% CO_2) Figure 19 shows for undoped UO_2 that no significant uranium dissolution could be observed under these conditions, similar to what was seen in the leaching experiments performed under reducing conditions. However, in the case of UO_2–U10 the concentration of ^{238}U in solution was more than 10 times higher than that for undoped UO_2-0. The concentration of ^{238}U versus time increases only in the test performed with UO_2-U10. Concerning UO_2-U1, the results indicate that no release occurred after the initial contact times. Figure 20 shows the results obtained under similar "low" S/V conditions (but in MQ water) for the ^{238}Pu-doped samples UO_2-10, UO_2-01 and undoped UO_2-0 (Rondinella et al., 2001, 2003).

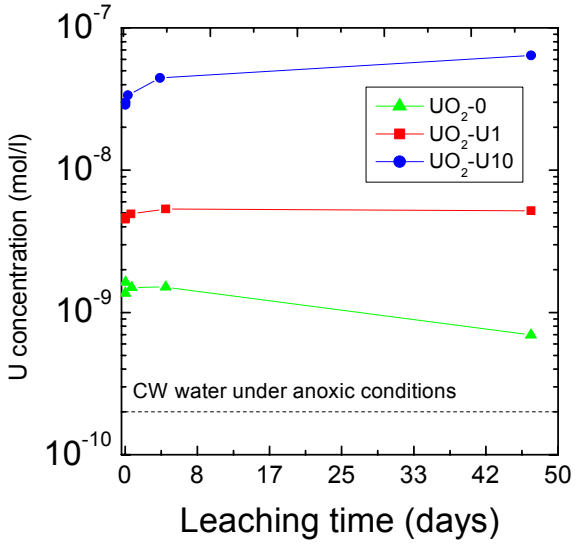

Figure 19: Concentration of U under anoxic conditions (flushing Ar, 0.02%CO_2) with carbonated groundwater (pH=7.5). The dashed horizontal line represents the nominal (blank) concentration of U in the CW under these experimental conditions

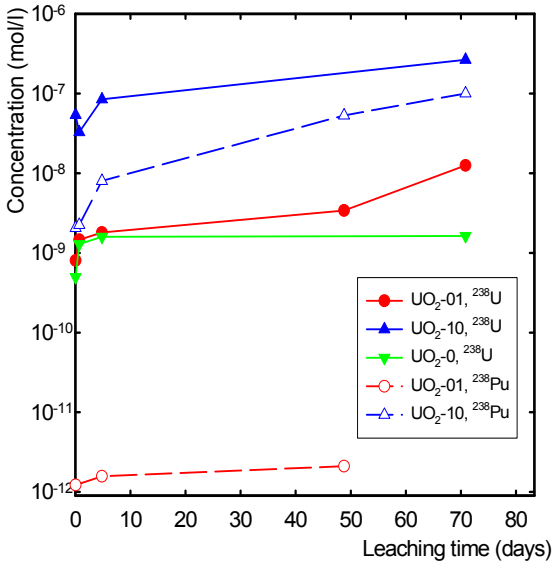

Figure 20: Concentration of U, ^{238}Pu versus leaching time in experiments performed under anoxic conditions (flushing N_2 permanently) with deionised water (pH 5.6 – 6.5) (Rondinella et al., 2001, 2003)

4.1.3.2 DYNAMIC TESTS IN REDUCING CONDITIONS (SCK.CEN)

The ^{238}U results are presented for sample F1 and F6 in Figure 21. The uranium concentrations are presented after subtraction of the background U concentration of the RCW water (U_0 = 0.25µg.L^{-1}). The uranium concentration is lower when the alpha activity is higher. The maximum dissolution rate of the UO_2 in Boom Clay water is determined by means of a plot of the uranium concentration [U-U_0] in function of the inverse flow rate (Table 13 and Table 14). When the alpha activity of fuel increases, the dissolution rate decreases from 2 to 0.77 µg.m^{-2}.d^{-1}, respectively for fuels F6 and F1. When the uranium found in an acid strip of the reactor at the end of the test was included in the calculation, dissolution rates were up to an order of magnitude higher. The lower dissolution rate of F1 may be due to the presence of Pu in F1 (F6 is a ^{233}U doped fuel, containing only traces of Pu). Similar behaviour has been observed in Figure 20. It is, however, not clear why the presence of Pu would decrease the dissolution rate, in spite of the higher alpha activity. Alternatively scavenging of radiolysis products by humic acids (reducing species) from Boom Clay water, passivating surface films or modified corrosion potentials may explain the different behaviour. The inverse relation between alpha activity and UO_2 dissolution rate, observed when we use ^{238}U as dissolution indicator, is not confirmed with ^{233}U or ^{238}Pu as dissolution indicators.

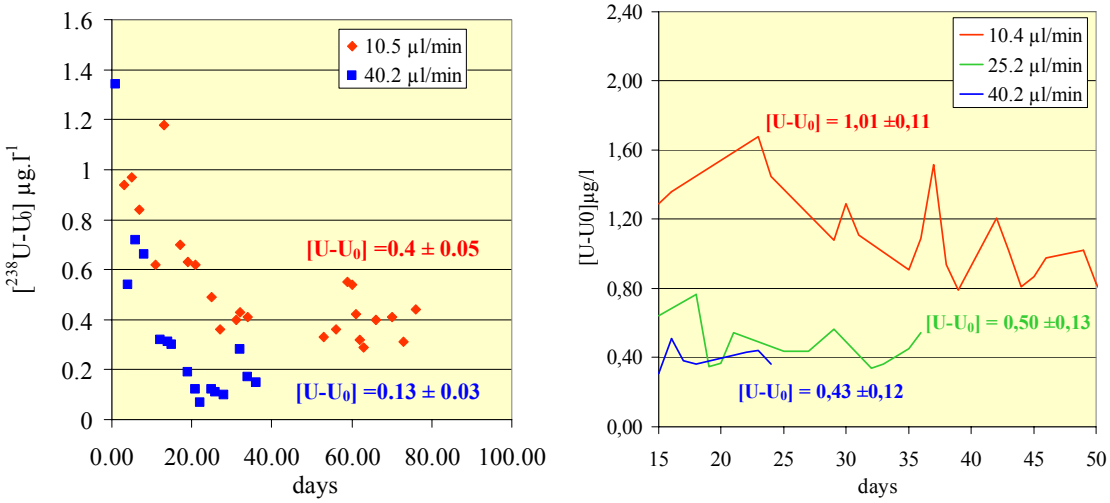

Figure 21: [^{238}U-U_0] at equilibrium for the experiments with fuel F1 (left) and F6 (right)

Considering the ^{233}U and ^{238}Pu concentrations, the maximal UO_2 dissolution rate would actually increase with the alpha-activity of the fuel (for details see deliverable D9), so the results for the different isotopes are internally inconsistent. We have no explanation for these discrepancies.

The ^{238}U-based dissolution rate is lower than the values found in the literature. It is about two orders of magnitude lower than for ^{233}U and ^{238}Pu doped UO_2 in deaerated or anoxic carbonated or MQ water (see Figures 12 to 15). The lower dissolution rate in these experiments is probably due to the reducing conditions, the presence of organic matter and to the absence of clay. Concerning the radiolytical species, the H_2O_2 concentrations are equivalent for all experiments, and around 10^{-7}-10^{-6} mol.l^{-1}.

Table 13: Dissolution rate calculation for Fuel F6

Flow rate (ml.min^{-1})	**Q (cm³.d^{-1})**	**1/Q (d.cm^{-3})**	**[U-U_0] (µg.l^{-1})**
0.0402	57.888	0.017	0.43 ± 0.11
0.0251	36.144	0.028	0.49 ± 0.12
0.0104	14.976	0.067	1.01 ± 0.11
0.0805	115.92	0.009	< 0.32

R (µg.m^{-2}.d^{-1})= 2.04

Table 14: Dissolution rate calculation for Fuel F1

Flow rate (ml.min^{-1})	**Q (cm³.d^{-1})**	**1/Q (d.cm^{-3})**	**[U-U_0] (µg.l^{-1})**
0.0402	57.888	0.017	0.13 ± 0.03
0.0251	36.144	0.028	
0.0104	14.976	0.067	0.4 ± 0.05

R (µg.m^{-2}.d^{-1})= 0.77

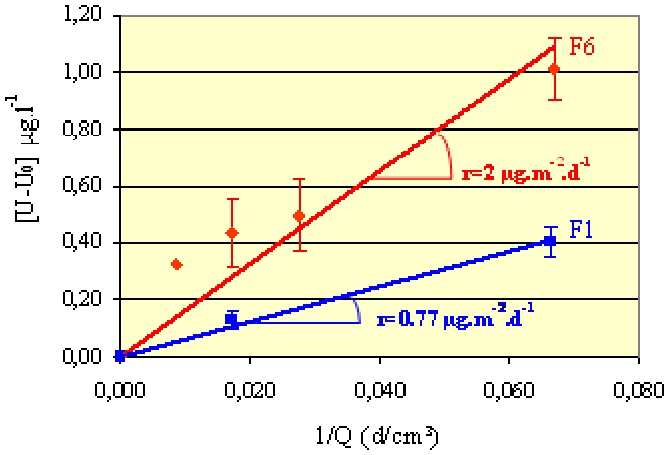

Figure 22: Dissolution rate of α-doped UO_2 in Boom Clay water in function of flow rate; because most U concentrations for 1/Q = 0.009 (F6) were below detection limit, the actual value of $[U-U_0]$ is lower than indicated.

Although the alpha activity of the low- and high-activity fuel were different by a factor 150 (Table 12), the maximal fuel dissolution rates differed only little. This means that the alpha effect on the fuel dissolution rate is relatively small in these test conditions. The main cause of the absence of pronounced alpha-dose effects is probably the high concentration of organic matter, reacting with radicals or the oxidising radiolytic species like H_2O_2.

4.1.3.3 DISSOLUTION BEHAVIOUR OF COLLOIDS OF UO_2 DOPED WITH ^{225}AC (SUBATECH)

The dissolution of UO_2 nanoparticles was very fast. Initial concentrations were $[U]_i = 5 \times 10^{-7}$ mol.L^{-1} while at the end of the experiment the concentration increased to a value of $[U]_f = 1 \times 10^{-5}$ mol.L^{-1}. Under reducing conditions (Eh ≈ -800 mV/SHE), a certain fraction of U(VI), formed by radiolysis could become reduced again to U(IV) and reprecipitate as UO_{2+x}. Congruent behaviour shows that La and U are homogeneously distributed in the colloids as is suggested by the crystal lattice variation measured by XRD (Rousseau, 2002). The dissolution rate increased as a function of the average alpha dose (Figure 23). Dissolution rates were of the order of a few mg.m^{-2}.d^{-1}. The α-radiation apparently has induced oxidising conditions near the surface of the solid despite strongly reducing conditions in the bulk. Even in the case of the experiment with the smallest dose rate, the effects of radiation remained dominant. The lowest dissolution rate was of the order of 1.4 mg.m^{-2}.d^{-1} for a dose rate of 0.26 Gy.h^{-1}.

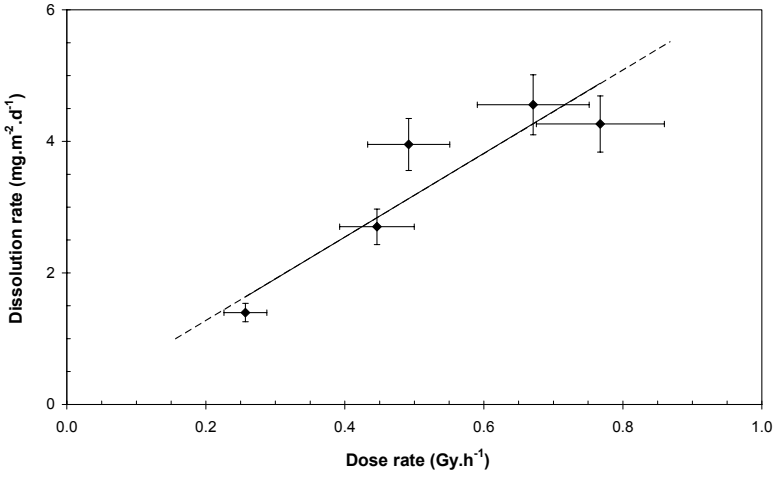

Figure 23: Dissolution rate of Ac doped UO_2 colloids as a function of the dose rate.

The question is, why are the dissolution rates as high as for irradiated fuel pellets even though the average alpha dose is 10000 times lower (Table 12). If one would use the published relation between alpha dose rate and UO_2 dissolution rate (Sunder et al., 1997), we should have dissolution rates lower than 10^{-7} g.m^{-2}.d^{-1}. Calculations of the radiolytic reactions using the MAKSIMA code with the reaction scheme published by

Christensen et al. (1994) gives for H_2O_2 2 x 10^{-8} mol.L^{-1}, and U concentrations in the range of 10^{-10} mol.L^{-1}. Observed U concentrations are much higher. One explanation would be that the effect of radicals is more important for our small particles than for large pellets. In the case of pellets, radical species (with generally a short lifetime) created at few μm of distance from the surface will hardly react with the material, because they recombine before being able to diffuse to the surface and react with it. In the case of colloids, many particles were located within the range of radical species. Another explanation could be that the colloids are more reactive than standard fuel pellets, or have a higher oxygen content x in UO_{2+x} than pure UO_2. Some additional data (Mennecart et al., 2004; Grambow et al., 2004) show that even under external irradiation by the alpha beam of a cyclotron the colloids behave like pellet sized UO_2 since it was found that the measured corrosion rates were similar to those measured in the absence of irradiation for fuel pellets exposed to similar H_2O_2 concentrations. Our results indicate that the relation between local surface dose and UO_2 dissolution rate may be more complicated than initially considered.

4.1.3.4 RESULTS OF ELECTROCHEMICAL EXPERIMENTS

UO_2 corrosion is an electrochemical process consisting of anodic dissolution (UO_2 to UO_2^{2+} + $2e^-$) accompanied by a cathodic reduction of an oxidant such as oxygen: e.g. $O_2 + 2H_2O + 4e^- \rightarrow 4OH^-$ for neutral and basic solutions. Various electrochemical methods have been applied to the aqueous corrosion of UO_2 under anoxic conditions typical for a final repository. These have given reasonably consistent results down to 10^{-10}A/cm^2. Detailed applications to measurement results (corrosion potential, Eh measurements, U concentrations) for 0, 1 and 10% ^{233}U are given in deliverable D9 (Cachoir et al., 2005).

AC impedance spectroscopy offers another possibility to determine corrosion rates. Details are given in deliverable D9. Due to the resistivity of UO_2 the errors of this method are large. Derived corrosion rates of 10% ^{233}U and 1% ^{233}U doped UO_2 in 10mM NaCl solution were respectively about 30 and 8 mg/m^2 d under N_2. Despite the fact that the corrosion rates are overestimated the data show (see deliverable D9) that the corrosion rate in case of the 10% doped UO_2 is higher by an order of magnitude than in the case of the 1% doped UO_2.

4.1.3.5 DYNAMIC LEACHING OF SPENT FUEL (ITU/ENRESA/UPC)

The long term steady state redox potential for the three flow through performed experiments were 510 mV/SHE, 470 mV/SHE and 400 mV/SHE for pellets of 53 and 29 MWd/kgU and powdered 53 MWd/kgU samples respectively. U dissolution rates were 1.4±0.6 and 6±3 mg/m^2d for pellets of 29 and 53 MWd/kgU respectively. The obtained results for pellets indicate that uranium dissolution rate depends on burn-up. Due to the low surface area of the used pellets (ca 1.3 cm^2) only uranium could be analysed by ICP-MS. Spent fuel dissolution rates agree with results obtained by Gray and Wilson (Gray, 1998; Gray and Wilson, 1995) using a similar experimental device under the same experimental conditions.

The release of radionuclides other than uranium could only be measured with powdered spent fuel. Congruency/selective release relationships between uranium dissolution and the other radionuclides were studied determining dissolution rates for each radionuclide taking into account their abundance related to uranium in the spent fuel from data obtained using the ORIGEN code. Results are shown in Figure 24. There is congruency of Np with U. Lower dissolution rate is obtained for Pu (14 times smaller than U) while higher rates are found for Sr and Cs (2 and 5 times higher than U, respectively). These results are comparable with those obtained from bibliography (Röllin et al., 2001).

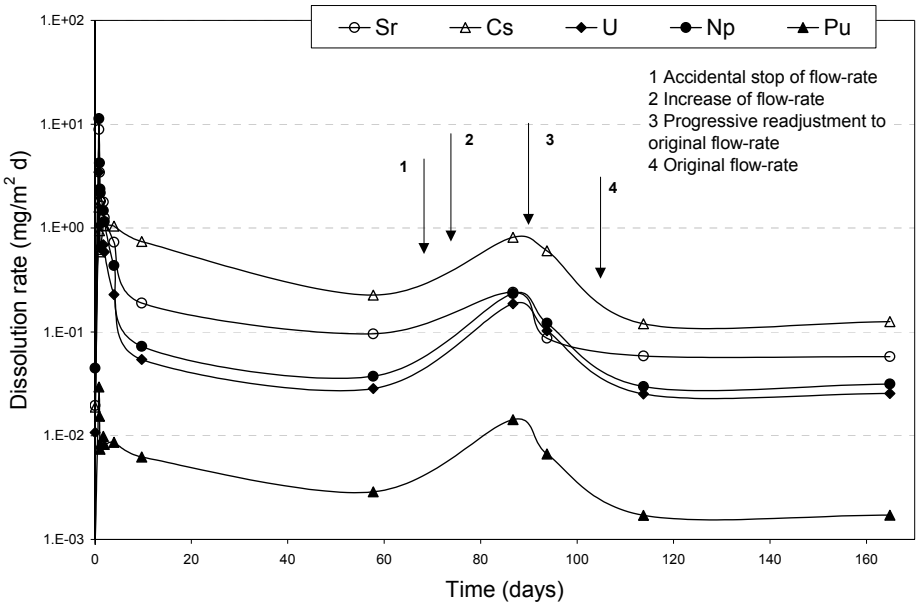

Figure 24: Normalised dissolution rates in equivalent mg_{UO2}/m^2 d obtained from the elemental concentrations in dynamic leaching of powdered spent fuel (burn-up ca. 53 MWd/Kg U) in oxidising conditions . The short rate increase after 80 d is due to an interruption of oxidizing conditions

After five months leaching of the milled sample, steady state conditions were reached for all studied elements: Sr, Cs, U, Np and Pu, with an estimation of uranium dissolution rate of 0.03 mg m^{-2} d^{-1}. There is congruency of Np with U. 14 times lower dissolution rate than U is obtained for Pu, while higher rates are found for Sr and Cs (2 and 5 times higher than U, respectively). These results, including the difference between pellets and powder, are comparable with those obtained from bibliography (Loida et al., 1996; Röllin et Spahiu, 2001).

4.1.4 COMPARISON OF RESULTS TO IDENTIFY ALPHA ACTIVITY EFFECTS

The experimental results of the present study are compared with literature data in Figure 25 using the specific alpha activity as criterion governing dissolution rates. Details for the data in this figure are given in table 43 of deliverable D9 (Cachoir et al., 2005).

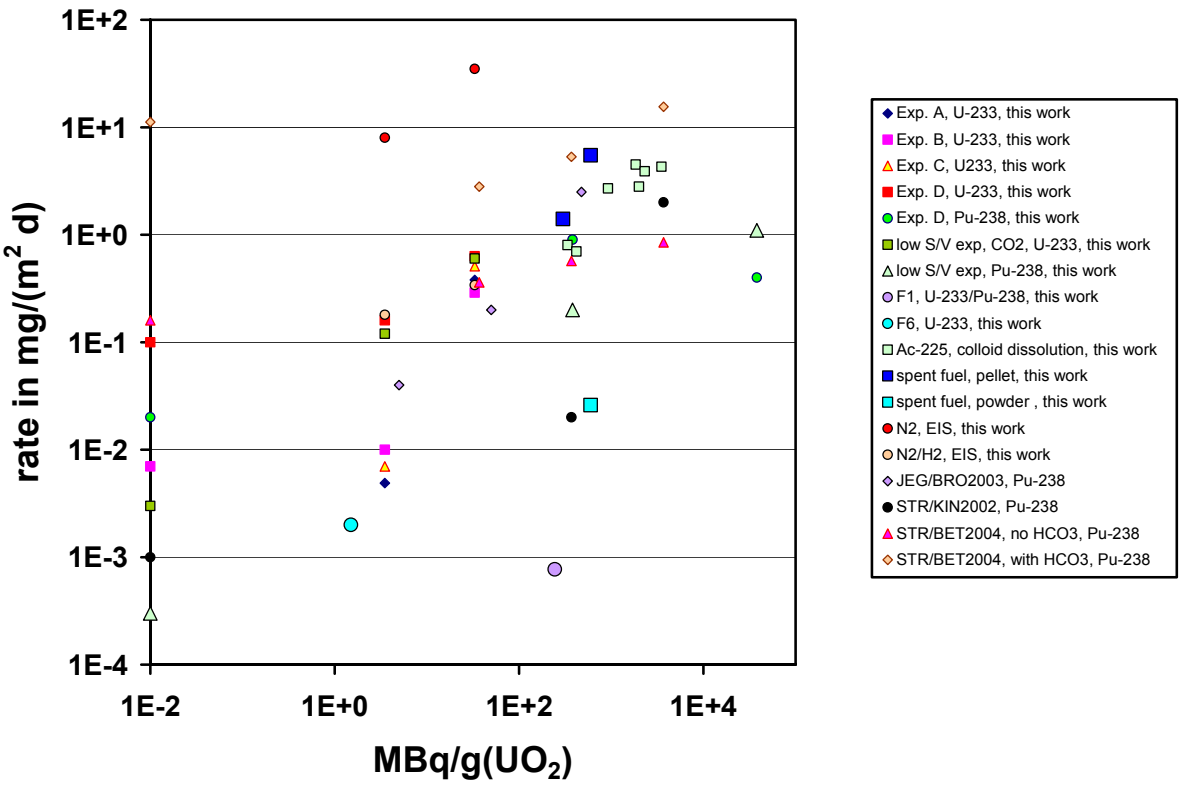

Figure 25: Corrosion rates of alpha doped UO_2, non doped UO_2 (0.01 MBq/g) and spent fuel and comparison with literature data (all references are given in deliverable D9)

The results show for most data a clear trend of increasing corrosion rates with increasing specific alpha activity. It looks like there is a specific activity threshold below which no effect of specific alpha activity is observed and above which an increase of corrosion rates with alpha activity is observed. The threshold activity itself cannot yet be located exactly. It depends probably on environmental parameters. Values below the threshold were observed under strongly reducing conditions, as in Boom Clay water, even up to 245 MBq/gUO_2. It was observed between 3.5 and 33 MBq/g_{UO2} in the case of deaerated water but it may be even below 3.5 MBq/g_{UO2}under better controlled anoxic conditions. It may be as high as 300 MBq/gUO_2 in carbonate rich water with oxidant contamination. In oxidising waters with corrosion rates in the range of 1-6 mg/m^2d the threshold is beyond 300 MBq/g_{UO2}, a value, which is indicative of fresh spent fuel. This threshold shows that alpha radiolysis is insignificant for spent fuel exposure to strong oxidising conditions. Below the threshold activity, the corrosion behaviour of unirradiated UO_2 should well describe long term spent fuel matrix dissolution behaviour (of course this does not account for the instant release fraction). Above the specific activity threshold, in general a less than proportional relationship is obtained.

Pu-doped samples seem to have somehow lower uranium corrosion rates than other alpha doped materials at the same specific alpha activity. Hence, the alpha-radiolysis enhancement of uranium dissolution rate is not observed when rates for Pu-doped high activity samples are compared with rates for ^{233}U-doped lower activity UO_2.

In order to clarify the environmental constraints on an activity threshold for alpha irradiation field effects on spent fuel long term corrosion rates, it may be useful to distinguish between two different types of irradiation effects: irradiation effects on dissolution rates and irradiation effects on UO_2 solubility. The observed threshold may hence be interpreted in this context. Solubility control is expected at rather reducing conditions, rate control at mildly to strongly oxidising conditions. One may use in the absence of large concentrations of dissolved hydrogen the measured Eh as indicator for the redox potential in solution. Concerning the surface oxidation state, some preoxidation cannot always be avoided and might have influenced experimental results. The theoretical solubility of crystalline UO_2 based on the thermodynamic data bank of OECD/NEA would be about $4 \cdot 10^{-10}$ M (Grenthe et al., 1992). However, a theoretical solubility value is hardly directly applicable. Independent of the uncertainties due to impurities and particle size, the

trend in solubility as a function of solution constraints (pCO2, pH, Eh…) shall be independent on the stability of the solid phase. Under reducing conditions no pH dependency of solubility is expected in the pH range of the present study and pCO_2 is of little influence. The threshold in Eh at which an increase in solubility occurs due to stabilising of U(VI) in solution depends both on pH and on pCO_2. For illustration, Table 15 gives the Eh at which the solubility increases by a factor of two, due to hydrolysis and carbonate complexation of U(VI). At lower Eh, the pH and CO_2 independent solubility of UO_2 under reducing conditions is rapidly obtained, at higher Eh the solubility increases rapidly with further increasing Eh.

Table 15: Eh values (mV) at which the solubility of UO_2 under reducing conditions is increased by a factor of 2 due to U(VI) formation in solution.

	pH 6	pH 7	pH 7.5	pH 8
0 atm CO2	105	70	30	-10
0.01 atm CO2	80	-10	-80	-165

If the Eh is much higher than the values in Table 15, solubility constraints are rather unlikely and rate constraints are invoked. If the Eh is lower than the values given in Table 15, and if U solution concentrations are lower than 10^{-9} M (a somewhat arbitrary criterion) we consider that solubility constraints are highly likely. If, furthermore, solution concentrations stay constant or decrease rather then increase with time, we consider this tentatively as a confirmation of solubility constraints even though other explanations like decrease in solubility due to dissolution of an oxidised surface phase cannot be ruled out. Rate constraints are also invoked if a clear increase of solution concentrations with time is observed, except in cases where solution Eh is close to the values in Table 15 and where an increase in solubility might be expected due to an increase of Eh with time. Finally for datasets without reported Eh values or for datasets with Eh values which may be erroneous, due to high hydrogen concentrations one only has the evolution of solution concentration with time and the magnitude of the solution concentration as a criteria to distinguish between solubility and rate control. Figure 26 gives a sketch indicating how one might be able to separate the effect of alpha radiolysis on either solubility of UO_2 or on reaction rates.

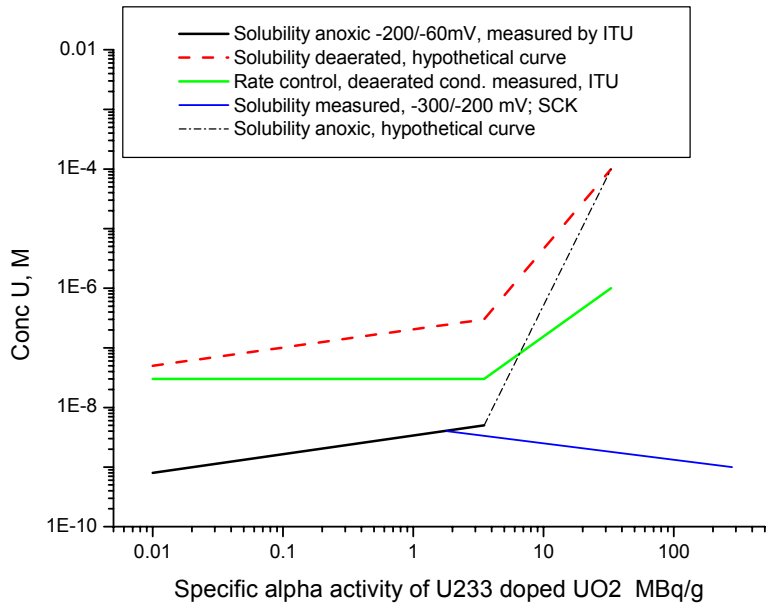

Figure 26: Effect of alpha activity on solubility and rate controlled release of U from alpha-doped UO_2.

Lowest Eh conditions are observed at SCK (experiments with samples F1 and F6) under very reducing conditions in Boom Clay water . Radiolysis changes the Eh (from –200 in case of UO_2-0 to –60 for UO_2-U1 to +200 mV for UO_2-U10 in the case of ITU experiments with low redox buffer capacity, but it changes only very little from –260±10 for F6 to –220±60mV for F1 in case of the Boom Clay water of SCK). Considering

that U solubility is independent of redox conditions for Eh values lower than about –160 mV (calculated for RCW water at pH 8.2 and log pCO_2= -2.5), one would expect no effects of radiolysis on the solubility-controlled release in the case of reducing Boom Clay water. Steady state solution concentrations of U in the range of 10^{-9} M in the flow reactor decreased with time, consistent with solubility constraints, not with surface reaction rate control. The empirical solubility/activity curve is included in Figure 26. However, in case of solubility-controlled release, constant steady-state concentrations are expected and it is not consistent with solubility-controlled release that the steady state U concentrations decrease with increasing flow rate.
Low Eh values were also observed by ITU under anoxic conditions (Experiment D) for a specific activity < 33 MBq/gUO_2 .The concentration of U in the experiment D of ITU under anoxic conditions is slightly increased between 3.5 and 33 MBq/gUO_2 (samples UO_2-0 and UO_2-U1) due to an increase in Eh from –200 to –60 mV, considering that at pH 7.5 the thermodynamic solubility in carbonate rich waters (pCO_2=0.01 atm) increases between these two Eh values by a factor of 6. The evidence for solubility rather than rate control in case of the ITU experiment D is the constant or decreasing U concentration in case of anoxic conditions for the experiments with undoped UO_2 and with 1% ^{233}U doped UO_2. In contrast, for UO_2-U10 the Eh is positive, indicating high solubility. The solubility is sufficiently high, for not being anymore rate controlling. Indeed, an increase of U concentrations with time is observed. The empirical solubility/activity curve is included in Figure 26. The high solubility value at 33 MBq/gUO_2 is only a hypothetical value calculated for U(VI) solid phases at + 200 mV. The present interpretation indicates that it is possible but not necessary to invoke activity dependent preoxidation of the fuel surface as a cause for increased solution concentrations of uranium with increased alpha activity. Why is there for experiment D (ITU) an effect of alpha irradiation field on the solution concentrations of U leading to rate control at 33 MBq/gUO_2 while this is not observed in Boom Clay water at even higher activity? The difference between these two datasets is the much lower Eh in Boom Clay water and the higher redox buffer capacity. This hinders the radiation field to drive the solution Eh in positive direction.

A hypothetical solubility curve for deaerated conditions is indicated in Figure 26. This curve is constrained by the fact that U solubility must be higher than the measured solution concentrations of U of $3 \cdot 10^{-8}$ M since U concentrations increased with time. At low activities the solubility is not known since redox conditions were not reported. Hence, since solubility is higher that rate controlled U concentrations, the release is controlled by reaction kinetics. Rate controlled release is first independent on specific alpha activity and increases then with alpha activities between 1 and 10% ^{233}U doped UO_2. The rate of dissolution of 10% ^{233}U doped UO_2 is similar for anoxic conditions (experiment D) than observed under deaerated conditions for the same specific alpha activity (0.3-0.6 mg/m^2d). A curve for rate controlled U concentrations is included in Figure 26.

4.1.5 GENERAL CONCLUSIONS

On the basis of the above arguments, we can conclude that an effect of alpha radiolysis on the dissolution kinetics of UO_2 can only be obtained under not so oxidising and not so reducing conditions. In the present work it was mainly observed under deaerated conditions and here an activity threshold was observed between 3.5 and 33 MBq/g. Below this activity threshold no effect of alpha activity on reaction rates is observed. On the other hand, rate control of U concentrations is only possible if U concentrations are lower than the solubility limit. In the presence of significant redox buffers like H_2, Fe(II) or Boom Clay organics, no effect of alpha radiolysis either on reaction rates or on solubility is expected to be observed, even for very high alpha activity of 280 MBq/g.

These findings provide very important constraints on performance assessment modelling. Initially, depending on repository concept, for a period of 1000 yrs up to 100000 yrs the container corrosion will assure high buffer capacity for reducing environment due to high Fe(II) and H_2 concentrations. Hence no effect of the alpha irradiation field on the long-term corrosion is expected for this period. Once this period is passed, anoxic conditions will prevail and it is expected that the solution redox potential will be lower as those operative in the experiments performed at ITU under deaerated conditions. Hence, even if we assume kinetic rather than solubility control we have to consider that the radiation field is also much lower. It will take few 1000 yrs or less for UOX fuel and as much as 20000 yr for high burnup MOX fuel until the alpha activity is lower than the threshold of 33 MBq/gUO_2 for an effect of alpha activity on the dissolution rates.

Hence we may conclude that even after the stop of hydrogen production by container corrosion, no effect of alpha activity on dissolution rates of spent fuel is expected.

However, the distinction between alpha radiolysis effect on either U solubility or U dissolution rates applies possibly only to Uranium. Vessel rinse analysis shows that total release might be higher than U release. In case of solubility controlled U concentrations and a stop of increase of U release to solution one cannot exclude that the release rate of fission products is higher than zero. A limiting rate value cannot yet be given. Experiments with alpha-doped UO_2 containing a soluble matrix dissolution tracer would be necessary. The present results of SCK.CEN with Sr and alpha doped UO_2 are non-conclusive in this regard probably due to the heterogeneous incorporation of Sr in the matrix.

4.2 ASSESSMENT OF THE EFFECT OF DISSOLVED HYDROGEN ON THE RADIOLYTIC DISSOLUTION

In the framework of the SFS project, experimental studies on the effect of the dissolved hydrogen on the dissolution of spent fuel were performed by ITU, FZK-INE, CIEMAT/ENRESA and SKB, both with high burn-up spent fuel and MOX fuel, as well as with UO_2(s) doped with different quantities of α-emitters to simulate the much lower dose rates expected in spent fuel after long disposal times. Detailed experimental studies of the effect of α-radiolysis on UO_2(s) matrix oxidation/dissolution were carried out by different methods and under different conditions. The methods include static leaching and electrochemical tests using different gas compositions to vary redox conditions and autoclave leaching under higher than atmospheric pressure. New analytical methods were developed for measurements of very low radionuclide concentrations and besides intensive parameters as pH and Eh, radiolytic product concentrations and other parameters were measured as well. The experiments were combined with a detailed pre- and post-leaching characterization of the solid specimens. In all the experimental studies presented here, a considerable effect of hydrogen in the dissolution rates of radioactive materials was observed. All the experimental information gathered within the SFS project has contributed to an improved experimental basis for a reliable evaluation of long term dissolution rates of spent fuel and an increased credibility in its stability as a waste form in presence of H_2 issued from the anoxic corrosion of the container.

4.2.1 LEACHING OF ^{233}U DOPED UO_2(S) AND ELECTROCHEMICAL TESTS

4.2.1.1 EXPERIMENTAL: MATERIALS AND METHODS

Alpha radiation is expected to persist for a long time in the spent fuel. A material that resembles old fuel is alpha-doped uranium dioxide, where different quantities of an alpha-emitting isotope are homogeneously distributed in the uranium dioxide matrix. ^{238}Pu or ^{233}U doped UO_2 samples were produced at ITU by the sol-gel method with an α-activity simulating large ranges of fuel ages after discharge. The $^{233}U_3O_8$ powder used to fabricate the pellets was analysed for impurities (Carbol et al., 2000). The ^{233}U-doped UO_2 pellets (1% and 10wt-% ^{233}U) were fabricated by the sol-gel method (Somers et al., 2001; Fernandez et al., 1999). At the end of the fabrication the pellets were sintered at 1700°C for 6 hours in an Ar/6vol-% H_2 atmosphere. Some of the pellets were used for characterisation and the results are reported elsewhere (Carbol et al., 2003).

4.2.1.1.1 Static leach tests (ITU-CIEMAT-ENRESA)

The specimens used in the static tests were discs approximately 1 mm thick cut from sintered pellets. Before the leaching tests, all the samples (alpha-doped and undoped UO_2) were annealed for several hours at 1200°C in Ar/(4%)H_2. The annealing was performed at the same time for all samples of a given batch of tests. Commercial carbonated water (CW) was used for the static leaching tests, while de-ionized water (MQ) was used in the leaching of ^{238}Pu doped pellets under anoxic conditions (Rondinella et al., 2001; Rondinella et al., 2003). Static batch (with same leachant and same vessel for each leaching time) leaching experiments were performed on discs in pyrex glass leaching reactors with a total volume of 500 mL and a volume of leachant (CW) of 400 mL. A pH and a redox glass electrode allowed logging of these parameters every 30

minutes. During the experiment the gas volume above the electrolyte was purged with N_2. During these initial stages the fuel sample remained suspended in a quartz sample holder above the water. The leaching experiments started when the sample holder was immersed to the center of the water volume, preventing the sample from contacting the water until low Eh values (-400 mV_{SHE}) were achieved. Sampling of ~8 mL of leachate using a tight four-valve system was performed. The system consisted of three needle valves and one on/off valve that minimized the ingress of air inside the reactor. At the end of the experiment, the vessels were rinsed with 50 ml 2M HNO_3 for 3 hours.

4.2.1.1.2 Autoclave test (ITU/SKB)

The pellet used in the *autoclave leaching* was cut in two parts and the part used in the experiments had a height of 3.75mm, a diameter of 6.58mm, a weight of 1.2643g and a geometric surface area of $1.5 \cdot 10^{-4} m^2$. The pellet was annealed one day before start of the leaching experiment. The annealing was performed at 1200°C in a gas mixture of 4 vol.-% H_2/Ar at a flow rate of 2 ml/min for 12 hours. Thermo-gravimetric analysis according to the method outlined in ASTM [AST 1980] was used to check the oxidation state of the U in the UO_2-pellets. The pellet was only slightly oxidised (O/U=2.002±0.010) before the annealing process and the annealing process yielded a ^{233}U-doped UO_2-pellets with a composition of $UO_{2.000\pm0.007}$. Directly after the annealing the pellet was washed with H_2-purged 10mM NaCl solution for 20 min and thereafter placed in the autoclave. The initial leaching solution in the *autoclave test* of ITU/SKB consisted of 10 mM NaCl and was also pre-purged with H_2. Its composition was changed after 113 days to 10 mM NaCl, 2 mM $NaHCO_3$ by addition of a $NaHCO_3$ solution.

4.2.1.1.3 Electrochemical tests (ITU)

For electrochemical tests electrodes from different materials have been prepared. Slices of ~1 mm thickness were cut from ^{233}U-doped UO_2 pellets. These were then cut into 2 halves. After annealing to maintain UO_2 at stoichiometry the halve slices were mounted upright with conductive resin on the gold coated electrode holder. Then they were impregnated under vacuum in epoxy resin (EPOTHIN). To reduce higher uranium oxides which may have formed at the sample surface during polishing, the electrode was cathodically polarised for 10 minutes at -2.5 V at the beginning of the experiment. A 10 mM NaCl solution was used in the electrochemical tests.

4.2.1.2 RESULTS AND DISCUSSION

4.2.1.2.1 Static leaching of alpha doped pellets under Ar + 6%H_2

Figure 27 shows the concentrations of ^{238}U and ^{233}U in solution as a function of time for the experiments performed while bubbling Ar/(6%)H_2. The pH did not show any significant variations during the leaching time. In all cases during the contact time the pH was between ~7.1 and ~7.5. The redox potential measured in the solutions shows a general increasing trend with time, but remains negative throughout the duration of the experiment. The dissolved U results show that both in the case of un-doped UO_2 and of UO_2 containing 10% ^{233}U no uranium dissolution could be observed during almost 1 year of leaching. In the UO_2 with 10% ^{233}U the initial concentration of the ^{238}U in solution was higher than that for un-doped UO_2. However, no additional dissolution occurred after the initial release. The measured concentrations in solution actually tended to *decrease* for longer leaching times. The initial release can be attributed to the surface pre-oxidation conditions occurring before sample immersion. The $^{233}U/^{238}U$ ratio in solution was essentially the same as that in the solid pellets. This means that congruent dissolution of the material occurred. Also shown in the figure are the results of the analysis of the rinse solutions of the leaching vessels. Relatively low concentrations are found also in the rinse, considering that the values plotted in Figure 27 for the rinse are concentrations in 50 ml HNO_3, that is a volume 8 time smaller than the nominal volume of the leachant. Furthermore, the presence of fines in addition to the sorbed material cannot be ruled out. Data for the leaching of UO_2 with 1% ^{233}U are not shown, due to problems with the leaching setup which caused the results of this experiment to be discarded.

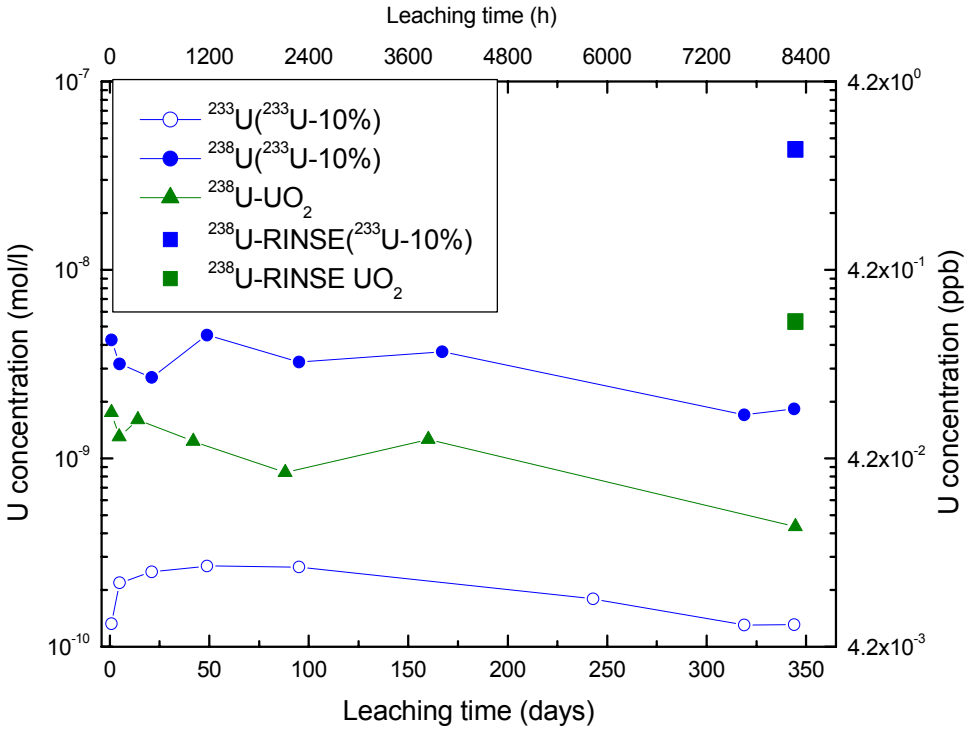

Figure 27: Concentration of U versus leaching time in experiments performed under 6% hydrogen in CW water (pH=7.5)

4.2.1.2.2 *Results from autoclave leaching of α-doped UO_2(s) under different H_2 pressures*

The study of the influence of dissolved molecular hydrogen on the leaching rate of UO_2 was performed using α-doped UO_2 doped with 10wt-% ^{233}U to simulate an old fuel. The leaching was started with a 10 mM NaCl solution under a hydrogen pressure of 16 bar. Samples of the solution were taken at different times and analyzed by α-spectrometry. After four months, the estimated uranium concentration in the solution was still less than $3 \cdot 10^{-10}$ M. To dissolve all oxidized uranium from the pellet, a bicarbonate solution was added to the autoclave, but no changes were noted in the uranium concentration. No measurable dissolution of uranium could be observed, not even when the hydrogen pressure was reduced to 1.6 bar during a 178-day period. The hydrogen pressure was further reduced by a factor of ten to 0.16 bar (1.6 bar of argon with a hydrogen concentration of 6.08 % by volume) during a 141-day period. Finally all hydrogen was substituted by pure Ar. The results from alpha radiometric analyses of uranium-233 are shown in Figure 28.

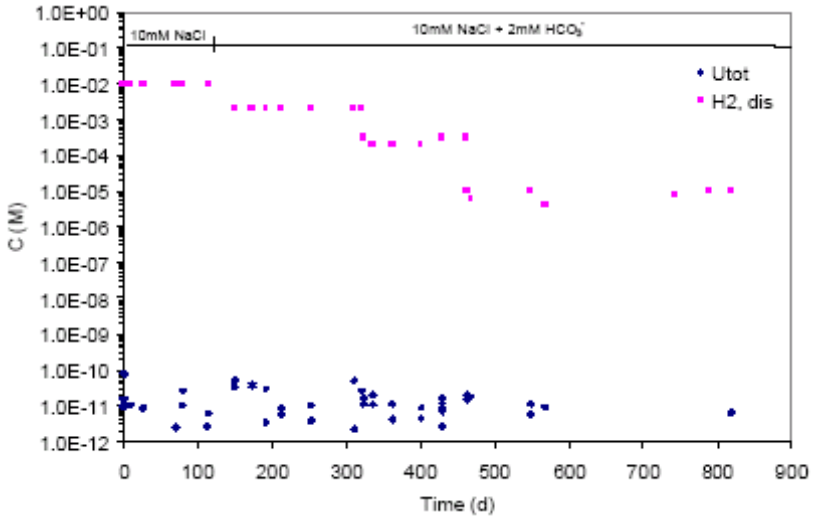

Figure 28: Measured H_2 and the total U concentration in the leachate as a function of time

The results show that no measurable increase in the very low uranium concentrations in the solution could be observed during the entire test period (more than 2 years). If, in this case, uranyl carbonate species were produced in a layer several tens of microns thick near the surface (range of alpha particles), some of them would diffuse away and contribute to an increase of the uranium concentration in the solution. These results are confirmed by the measured levels of radiolytic oxygen, which lie below the detection limit (10^{-8} M) for the oxygen sensor present in the autoclave solution during the entire test.

The same applies to any radiolytic oxygen or hydrogen peroxide: some of it would diffuse away from the surface and cause an increase in the oxygen levels, which would eventually be recorded by the oxygen electrode, given the long duration of the test. Literature data (Pastina & Laverne, 2001) with 5 MeV helium ions and preliminary measurements in the NF-PRO project (Jensen & Albinsson, 2004) indicate that there is no influence of hydrogen on oxidant consumption in the bulk solution. This indicates that the consumption of radiolytic oxidants by hydrogen is a surface process. At the end of the test, the examination of the uranium dioxide surface by spectroscopic methods (XPS) showed that the UO_2 pellet surface was stoichiometric $UO_{2.00}$, i.e. no oxidation of the surface had occurred even in the presence of Ar atmosphere. Published independent experiments with alpha radiolysis in hydrogen-saturated solutions and uranium dioxide surfaces show also that no oxidation occurs [SUN/BOY 1990]. The TiO_2 surfaces were also studied with respect to uranium using SIMS. The signal from mass 238 (^{238}U) was on the background level, clearly showing that no U was deposited on the TiO_2 particles.

4.2.1.2.3 Results from electrochemical tests

Corrosion rates can be determined by extrapolation of the current potential distribution from the anodic potential range in which the dissolution is the main process determining the free corrosion potential. This Tafel extrapolation gives the corrosion current from which the corrosion rate is calculated by Faradays law. Under oxic conditions the potential corrosion rate dependency was experimentally measured by Marx et al. (2000). He found a slope of 82 mV. Sunder and Shoesmith (1988) claim values of 40-60 mV for carbonate-free solutions and values of 90 mV for carbonate containing electrolytes. Current densities and charge during potentiostatic polarisation experiments performed on 1% ^{233}U doped UO_2. under $N_2/8\%H_2$ are given in the deliverable D9. The evaluation of the of the data in the strongly anodic range gives a straight line (the anodic Tafel line):

E_{pol} = ba * log(i) + n with b_a= (72 ± 12) mV and n = (1166 ± 12) mV (E_{pol} in mV, i in A/cm^2)

A comparison with the data measured by Marx et al. under oxic conditions shows about 1000 times lower corrosion rates under influence of hydrogen for the same potentials (Figure 29).

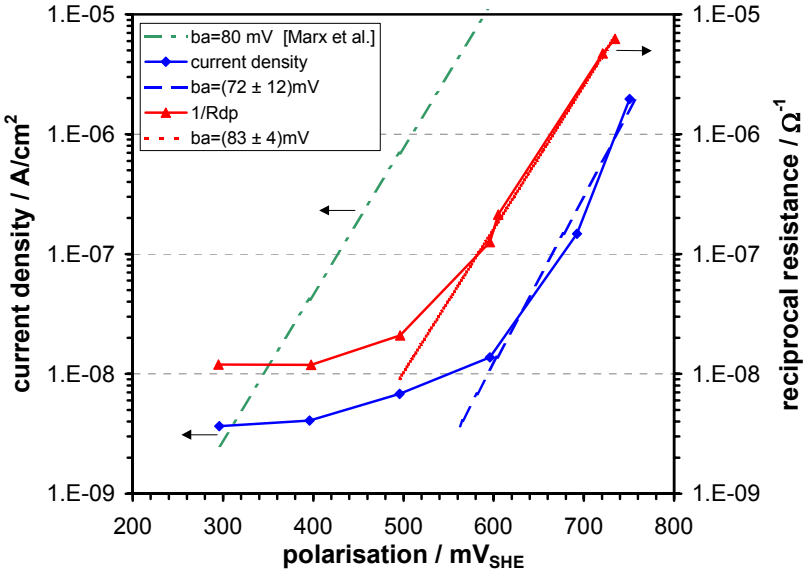

Figure 29: Comparison of anodic Tafel slopes derived from polarisation experiments under oxic conditions (Marx et al., 2000) and under N_2/H_2(8%) purging.

Figure 30 shows the measured U-concentrations with time for the experiment with 10% doped UO_2 under N_2+8% H_2 atmosphere. The U- concentration in solution is in the range of some ppb and is decreasing with time.

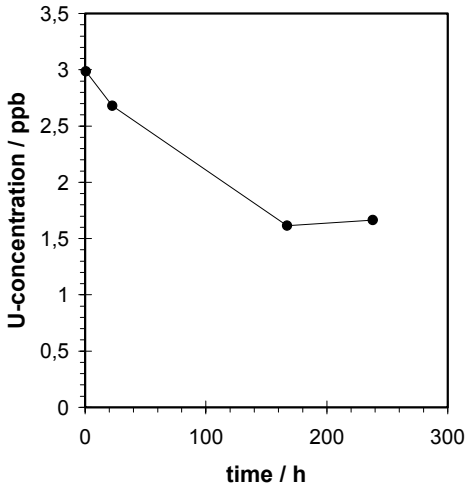

Figure 30: U concentration in solution during corrosion potential measurement of 10% ^{233}U doped UO_2 determined by α-spectrometry of ^{233}U

4.2.2 THE INFLUENCE OF DISSOLVED HYDROGEN IN THE PRESENCE OF THE MIXED ALPHA, BETA, GAMMA RADIATION FIELD OF THE SPENT FUEL

In the frame of this project, the leaching of a high burnup fuel in 5 M NaCl solutions saturated with 3.2 bar H_2 (FZK-INE) as well as the leaching of MOX fuel fragments in dilute bicarbonate containing solutions under 53 bar H_2 (ITU/SKB) were studied. The experimental details and the results obtained are presented below, together with a comparison with literature data and conclusions.

4.2.2.1 5.2.2.1 EXPERIMENTAL

4.2.2.1.1 Spent fuel corrosion experiment in 5 M NaCl brine under 3.2 bar H_2 (FZK-INE)

The study on spent fuel corrosion in brine is relevant to disposal in rock salt. The spent fuel pellet denoted as K8 (6.6 g fuel) had an average burn-up of ~50 MWd/kg U, while maximum burn-ups of 55 MWd/kgU during 4 cycles were reached. The average power ratings of the first two cycles were 30-32 kW/m. Pellet K8 was stored under Ar for 7 years, but inspection before leaching indicated oxidation by air and the presence of a white layer on its surface. Nuclide inventories of the fuel samples were calculated by means of the KORIGEN code (Fisher & Wiese, 1983). The experimental work was divided in two parts, i.e. the pretreatment of the fuel pellet by (1) several wash cycles under initially Ar atmosphere followed by (2) the static test under the external applied H_2 overpressure of 3.2 bar. The wash cycles were carried out in quartz glass vessels of approx. 280 ml volume. The leachate was replaced entirely by fresh Ar flushed 200 ml NaCl-solution (5 M) after 1, 3, 21, 42, 80 days; afterwards a static phase of 212 days followed. Sampling of gases and solution was performed 1, 3, 21, 42, 80, 157 and 292 days after start of the wash procedure. The effect of H_2 overpressure on the overall corrosion behavior of high burn-up spent fuel in 5 M NaCl brine was studied over a total duration of 3 years as a static test in a Ti/Pd-lined stainless steel autoclave of total volume 500 ml, equipped to take gas and solution samples under reverse Ar streaming. The starting salt solution volume was 200 ml and by inserting 40 bars of Ar / 8% H_2, a hydrogen partial pressure of approx. 3.2 bar was achieved. Sampling was carried out at 53, 117, 213, 461, 697, 915, 1095 days after start of the static test. After each sampling 40 bar Ar/ 8% H_2 was applied again and kept constant until the next sampling. This experiment was terminated unintentionally after a total duration of 1097 days due to a failure of the burst disk of the autoclave.

During the wash cycles and the static phase, samples from the gas atmosphere in the autoclave were taken each time before solution was sampled. The gas composition was analyzed quantitatively by a quadrupole mass spectrometer. Radiochemical and gas analyses procedures are described in detail in Grambow & Loida (1996). Measured pH – data were corrected for liquid junction potential as described in Grambow & Muller (1990). Reported $pH_{EQ3/6}$ values are consistent with Pitzer's pH convention (e.g. implemented in the EQ3/6 software package (Wolery, 1992)). A detailed discussion on the conversion of measured pH_{exp} values into $-\lg(m_{H^+})$ and $pH_{EQ3/6}$ values are given in Altmaier et al. (2003).

4.2.2.1.2 *Autoclave leaching of MOX fuel under 50 bar H_2 (ITU/SKB)*

The study of the influence of molecular hydrogen on the leaching rate of irradiated fuel was performed using MOX-fuel to investigate a fuel with higher α-activity as compared to irradiated UO_2 fuel. The MOX fuel used in this experiment had an average burn-up of 48MWd/kg U and was cut from a fresh fuel rod in a hot cell under nitrogen atmosphere (<2% O_2). The Zircaloy cladding was removed from a fuel slice ~1.1 mm thick and two fuel fragments with a surface area 50.8 mm^2 and total weight 0.399 g were selected, so that an initial fuel surface to leachant volume (S/V) ratio of 0.282 m^{-1} was obtained, similar to the ratio used in the ^{233}U-doped UO_2(s) experiment.

The leaching experiment was performed in an autoclave with a total volume of 200 ml. The initial solution consisted of 10mM NaCl and 2mM HCO_3^- and in the following will be referred to as leachate. The time that passed between the fuel cutting, de-cladding, sample transfer and the actual start of the leaching experiment was 2 weeks. The two MOX-fuel pieces were loaded into the fuel holder, which was dipped into 103.5 ml of a H_2 purged leachate for a period of 20min. After the wash, the fuel was directly lowered into the autoclave that was filled with 180.0 ml of H_2 pre-purged leachate. The leachate was purged with H_2 during the whole loading sequence. Direct after the mounting of the lid the autoclave was pressurized with pure H_2 to 53 bar.

The static corrosion experiment of the MOX fuel was run for a period of 494 days at a 53 bar H_2-pressure without opening the autoclave. The experiment was run at a room temperature of 22±4ºC. The sampling of leachate was made in two steps: first a rinse sample was collected (5ml) to remove the solution in the tubes and then the representative sample (approx. 3ml) was collected. Samples were taken after 3 hours, 26 days, 203 days and 494 days.

The MOX-leachate was sampled into PE-vials and analyzed for the leached fission products and actinides using high-resolution inductively coupled plasma mass spectrometry (HR-ICP-MS); radiometric methods

were also applied (UTEVA separation). Before the analysis all samples were acidified to give a 1M HNO_3 sample solution.

4.2.2.2 RESULTS AND DISCUSSION ON SPENT FUEL LEACHING IN THE PRESENCE OF H_2

4.2.2.2.1 Leaching of high burnup spent fuel in 5 M NaCl

The results of the gas analysis show that during the whole leaching test the radiolytic oxygen levels were below detection limit. The release of the fission gases ^{85}Kr and ^{144}Xe decreased by two orders of magnitude when H_2 pressure was applied, very close or below the detection limit and remained at these very low levels during the entire test. The evolution of solution concentrations of the different radionuclides is presented in Figure 31. The absence of oxygen together with the very low levels of uranium and other redox sensitive elements reached after a period of almost two years (697 days) indicate extremely low levels of radiolytic oxidants in the autoclave and a reducing atmosphere. The concentrations of U decrease from about 10^{-6} M to about 10^{-9} M, which together with the observed initial pH decrease indicate a potential reduction of U(VI), apparently precipitated during the wash cycles. This may be the one of the reasons for the initial decrease of Sr release rates and their consequent almost constant release rate of 10^{-7}/day. The prolonged washing cycles of the pellet K8 together with the washing of easily soluble fission products as Cs, were accompanied with the precipitation of relatively large amounts of U(VI) solids and it can not be excluded that some Sr was also incorporated into them. Against the hypothesis that this concentration of dissolved hydrogen (about 0.85 mM due to the low solubility of H_2 in brines) is not sufficient to completely hinder the dissolution of the spent fuel matrix or Sr originating from segregated phases in this "experimental" fuel are the data obtained with pellet K4 (Grambow & Loida, 2000) where in the presence of an even lower concentration of H_2 very low release rates of Sr ($<10^{-9}$/day) were measured. The presence of oxygen sensitive Fe corrosion products in these last test indicates that the radiolytic oxidants were consumed by the hydrogen produced by Fe corrosion and not by Fe(0) or Fe(II).

The decrease of the concentrations of uranium and other redox sensitive radionuclides is due to a reduction of their oxidized forms and is observed constantly in all other published studies (Grambow & Loida, 2000; Jensen & Albinsson, 2004; Spahiu et al., 2002; Ollila et al., 2003; Spahiu et al., 2004). Literature data (Jensen & Albinsson, 2004; Ollila et al., 2003) show that more than 99% of the uranium is precipitated on the surface of the fuel itself, since very low levels of U were found in the vessel rinse. The concentrations of U measured in the present experiment under 3.2 bar H_2 in 5.0 M NaCl solution based on the thermodynamic data-set for U(IV) and U(VI) aqueous species and solids of Neck & Kim (2001) and Neck et al. (2003), respectively, compare well with the calculated solubilities of UO_2(s).

During the next sampling after 915 days apparently an air contamination of the solution occurred, as indicated by the gas analysis, showing the presence of both oxygen and nitrogen.

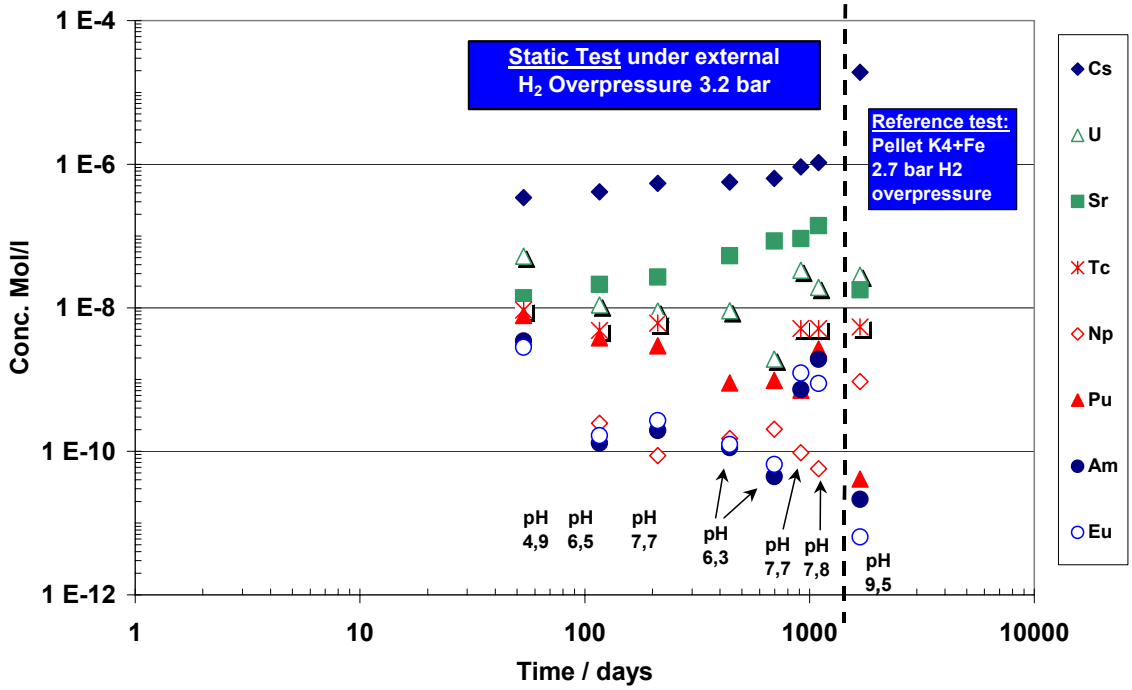

Figure 31: Radionuclide concentrations during 1095 days corrosion of spent fuel pellet K8 in 5 M NaCl solution under external H_2 overpressure.

The solution analysis data indicate that this apparently very small and short time air contamination was accompanied by a significant increase of the uranium concentrations and a simultaneous increase of the Am and Eu concentrations almost at their levels at the start of the leaching, whereas all other radionuclide concentrations remained unaffected (see also Figure 31). In the following period (697-1095 days) the concentrations of the U decrease again to reach the same final U concentration as observed in the reference test (K4+Fe) in the presence of corroding Fe (and 2.7 bar H_2).

4.2.2.2.2 Results from MOX fuel leaching

The results of the dissolution test of an irradiated MOX fuel studied under 53 bar H_2 pressure in a Ti-autoclave are presented in Figure 32. It can be concluded that 43mM $[H_2]_{dissolved}$ in 180ml of a 10mM NaCl + 2mM HCO_3^- solution inhibited the oxidative dissolution of 0.4 g irradiated MOX fuel, despite an α-dose rate of 13Gy/s and a β-dose rate of 2Gy/s. The concentration of U in the leachate decreased from an initial pre-oxidized [U] of $5 \cdot 10^{-7}$ M by three orders of magnitude ([U] after 494 day leaching was $3 \cdot 10^{-10}$ M, see Figure 32). This uranium concentration is below the ones calculated from the reported solubilities of pure UO_2(s) systems under similar pH and temperature ranges (Neck & Kim, 2001; Rai et al., 2003; Guillaumont et al., 2003) and corresponds to the same levels as the ones obtained with inactive crystalline UO_2 in the presence of chemically activated hydrogen at high temperatures (Parks & Pohl, 1988). No dissolution rate could be calculated since no U is oxidized after the initial dissolution that is presumed to come from the pre-oxidized UO_{2+x} layer.

The similar behaviour of the Tc, Mo, U, Np, and Pu in the leachate indicates that these elements were congruently dissolved during the initial fuel loading of the autoclave and thereafter precipitated or co-precipitated. The most probable explanation is that U, Pu, Tc and Mo were reduced to the tetravalent state and were precipitated as hydroxides.

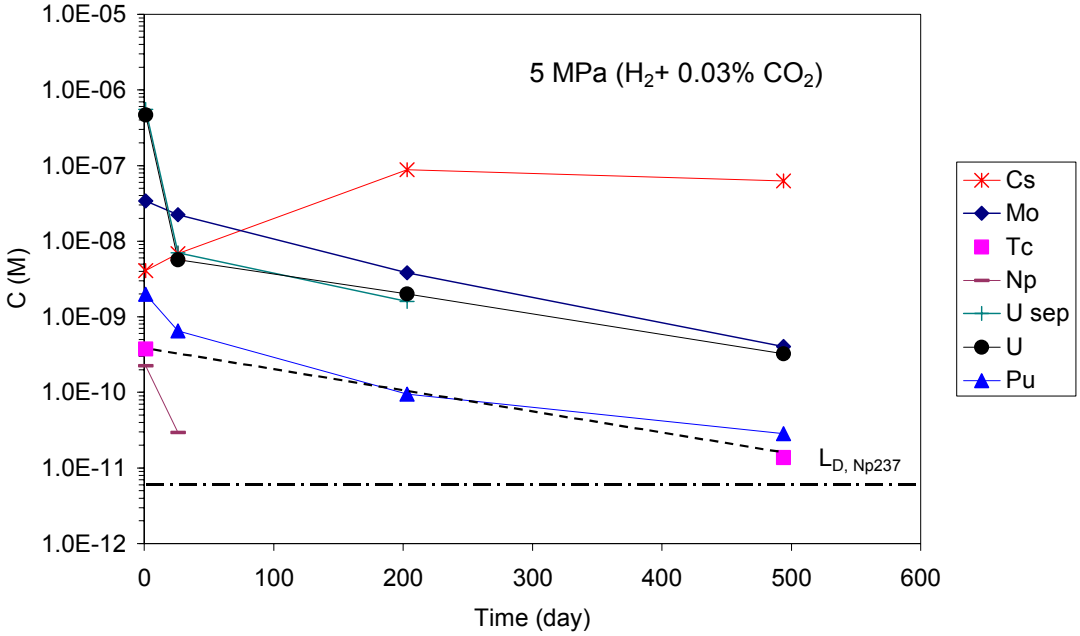

Figure 32: Concentration of fission products and actinides in the MOX leachate as a function of leaching time. The errors are in the range of 10-20% (1 s). The crosses represent an independent U determination using UTEVA separation

The concentration of ^{134}Cs and ^{137}Cs in the leachate was determined by γ-spectrometry and the results were confirmed by measurements using HR-ICP-MS. Additionally, the concentration of ^{135}Cs was determined by HR-ICP-MS. ^{133}Cs was detected in the leachate but was not used in the evaluation since the sample was contaminated with stable Cs. The ratios ^{134}Cs/^{137}Cs and ^{135}Cs/^{137}Cs were constant in the leachate. A strong indication of an inhibited oxidation of the UO_2 matrix is the fact that the Cs reached a steady state concentration of 10^{-7} M after 206 days of leaching. This was unexpected since Cs is non-redox sensitive element and the fraction of inventory in aqueous phase (FIAP) was only 10^{-3}. On the other hand, the ratio $(Cs_{tot}/U_{tot})_{leachate}/(Cs_{tot}/U_{tot})_{fuel}$ was found to be $2 \cdot 10^4$ after 494 days of leaching which shows that the Cs dissolves preferentially and probably originates from the grain boundaries.

Additionally, it must be pointed out that all elements present in a fuel were analyzed but only the most redox-sensitive and Cs could be detected. Even though radiometric methods were used to find short-lived radionuclides (^{125}Sb, ^{144}Ce, ^{154}Eu, ^{241}Am), no further elements than found by HR-ICPMS could be detected. Strangely, we could not find any lanthanide in the leachate. No chemical separations were made to determine ^{90}Sr. The higher Pu/U ratio in the fuel than in the leachate could be explained by most of the pre-oxidized UO_2 originating from the depleted UO_2 surrounding the Pu-enriched grains. The Pu-rich grains are the site of most of the fissions and contain most of the fission products, including the lanthanides that are known to stabilize the UO_2 matrix against oxidation. These facts explain the absence of lanthanides in the leachate.

4.2.3 CONCLUSIONS ON THE HYDROGEN EFFECT

In general, tests of a relatively high degree of complexity, mainly due to the extreme reducing conditions realized in some of the systems, were completed with good reproducibility and with a large number of test parameters varied and properties measured.

In connection with the studies on the dissolution of radioactive materials in the presence of hydrogen, the most important parameter affecting the dissolution process is the concentration of dissolved H_2 and should be preferably reported, instead of its partial pressure in the system. Due to the different hydrogen solubilities in various solutions, a H_2 partial pressure of e.g. 3 bar in salt brine corresponds to the same levels of dissolved H_2 in dilute solutions at 1 bar.

The effect of relatively low concentrations of dissolved hydrogen in successfully hindering the oxidative dissolution of α-doped UO_2(s), where the expectations based on the data from homogeneous radiolysis of hydrogen saturated solutions were relatively low, is one of the major outcomes of the SFS project.
The release rates of several spent fuel components in concentrated NaCl solutions decreases almost linearly with the partial pressure of hydrogen in the system, up to release rates of the order of 10^{-9}/day at relatively low partial pressures of hydrogen between 0.1 and 1 bar. Considering the low solubility of hydrogen in such concentrated solutions the impact of hydrogen concentrations in the range $2.7 \cdot 10^{-5}$-$2.7 \cdot 10^{-4}$ M is really large. These data indicate that molecular hydrogen is activated and participates in reactions with radiolytic oxidants.

In all existing radiolytic modelling studies, even when an extra reaction of the reduction/precipitation of a part of dissolved U(VI) (Jonsson et al., 2003; Liu & Neretnieks, 2002) the concentrations of uranium in solution are predicted to increase (even though with much lower rates) with time. Our experimental data as well as all published studies (Sunder et al., 1990; King et al., 1999; Grambow et al., 2000; Spahiu et al., 2000; Loida et al., 2001; Röllin et al., 2001; Spahiu et al., 2002; Ollila et al., 2003; Spahiu et al., 2004; King & Shoesmith, 2004) indicate that above a certain concentration of dissolved hydrogen, which depends on various factors, among others which the type and the intensity of the radiation field, the concentrations of molecular products of water radiolysis in the bulk solution reach extremely low values since the concentrations of U decrease to reach very low values.

Contrary to the expectations from the influence of dissolved hydrogen in the homogeneous radiolysis of water (Pastina & Laverne, 2001), it seems that this limit is much lower for pure α radiolysis than for the mixed α, β, γ radiation of the spent fuel.

From the long-term U concentrations measured in all studied systems, the presence of U(VI) solid phases can be excluded. Post-leaching characterization confirms their absence. The solid state chemistry of U(IV) is relatively simple:UO_2(s) in its microcrystalline (amorphous) form or UO_2(cr) are the only known solid phases (attempts to synthesize coffinite, $USiO_4$(s), have shown that it is a difficult task even under hydrothermal conditions favoring its formation).

During the leaching of spent fuel in hydrogen saturated solutions several factors contribute to the activation of hydrogen. A quantification of the various contributions is necessary and desirable but also related to difficulties. Besides the well known processes as homogeneous solution activation of hydrogen by radical rich radiations as β- and γ-radiation, the experimental data indicate also some effects of dissolved hydrogen that are difficult to explain with only a decrease of the levels of radiolytic oxidants in the bulk solution. Such are the very low levels of molecular radiolytic products after long leaching periods, the decrease of concentrations of uranium and other redox sensitive elements to very low levels corresponding to the solubilities of their reduced forms and indicating their reduction as well as the reported reduction of the UO_2(s) surfaces after tests with γ-radiation (King et al., 1999) or α-radiation (Sunder et al., 1990).

The experimental data obtained in this project together with literature data give a reliable background to use alteration/dissolution rates for spent fuel of the order of 10^{-6}/yr-10^{-8}/ yr, with a recommended value of 4 10^{-7}/y for dissolved hydrogen concentrations above 10^{-3} M and Fe(II) concentrations typical for European repository concepts.

The very low long term concentrations of uranium, measured in all systems studied make possible to exclude the presence of U(VI) solid phases, which in general have solubilities higher than 10^{-8} M. The evolution of U concentrations indicates in all cases no increase caused by the radiolytic oxidation of uranium from the UO_2(s) matrix. Since radiolysis continues to produce molecular oxidants in such systems, it follows that if they are not consumed to oxidize U(IV) to U(VI), the only remaining pathway for their consumption is their reaction with dissolved hydrogen to produce water.

The exact mechanism of this reaction in the case of inactive UO_2(s) surfaces would imply an activation of the reactants (H_2O_2, O_2 or H_2) on the surface of UO_2(s). Experimental evidence on the ability of UO_2(s) surfaces to activate hydrogen and cause the reduction of U(VI) carbonate species has been presented, while no such evidence for the combination of H_2 with O_2 could be obtained on depleted UO_2(s) (Devoy et al., 2003).

All experimental data indicate that this activation is more pronounced in the presence of different radiations. In the case of γ-radiation, a mechanism similar to photo-catalysis is proposed in (Petrick et al., 2001; King & Shoesmith, 2004), where the excitations produced by the absorption of radiation energy by oxides having

band gaps around 5 eV dissociate water molecules adsorbed on the surface to H and OH radicals (dissociation energy 5.1 eV). In H_2 saturated solutions the OH radicals are consumed through reaction with dissolved H_2:

Eq. 9: $H_2O + h\upsilon = H\cdot + OH\cdot$

Eq. 10: $OH\cdot + H_2 = H_2O + H\cdot$

In the case of α-radiation, the oxygen vacancies produced by the recoil atoms (Stultz et al., 2004) lead to the dissociative adsorption of water molecules and the production of atomic hydrogen.

The field of studies of α-doped UO_2(s) and spent fuel in hydrogen saturated solutions is relatively new and further studies are required to completely understand and quantify the various contributions to hydrogen activation as well as to confirm the obtained results. This should be considered especially in the different contexts of the discussion of the obtained data: their use in performance assessment and the scientific understanding of the phenomena.

5. MATRIX ALTERATION MODEL DEVELOPMENT (WP4)

5.1 REVIEW OF THE AVAILABLE MODELS AND DEVELOPMENT OF A CONCEPTUAL APPROACH BASED ON THE MAJOR PROCESSES

5.1.1 DESCRIPTION OF THE DISSOLUTION PROCESSES IN PRESENCE OF WATER RADIOLYSIS

Significant previous work was carried out on the development and testing of source-term models developed in the former EU framework program (1994 - 1998) and on the development of a simplified kinetic model based on mass balance equations for the radiolytic dissolution of spent fuel (Bruno et al, 1996-1998, Cera et al., 2000). The work package activities started with a workshop held in Avila, for presentation and discussion of the different model approaches and on the understanding of the alteration/dissolution processes to allow the system to be correctly formulated in terms of oxidants consumption and radionuclide release, assuming that the radionuclides embedded in the matrix will dissolve with the same rate as the UO_2 matrix.

The review of these different models, radiolytic, thermodynamic and electro-geochemical models were published as proceedings (Martínez Esparza et al., 2002).
These documents and discussions with WP2, WP3 and WP5 participants have constituted the basis to build the conceptual model. This basis and the conceptual model are described in detail in the D12 of the project *"Conceptual Model of the Matrix Alteration Model (MAM)* (Martinez Esparza et al, 2004a)". The final objective was to give a tool, for WP5, able of predicting the spent fuel matrix alteration in various environmental conditions.

The stability of the spent fuel will depend on a few variables of the system. Groundwater composition with carbonate and chloride contents as the main aqueous ligands, pe and pH constitute the master variables of this chemical system. Among these, the pe is the most critical one.
The main processes affecting the oxidation and dissolution of the spent fuel matrix and consequently affecting radionuclide release are depicted schematically in Figure 33.

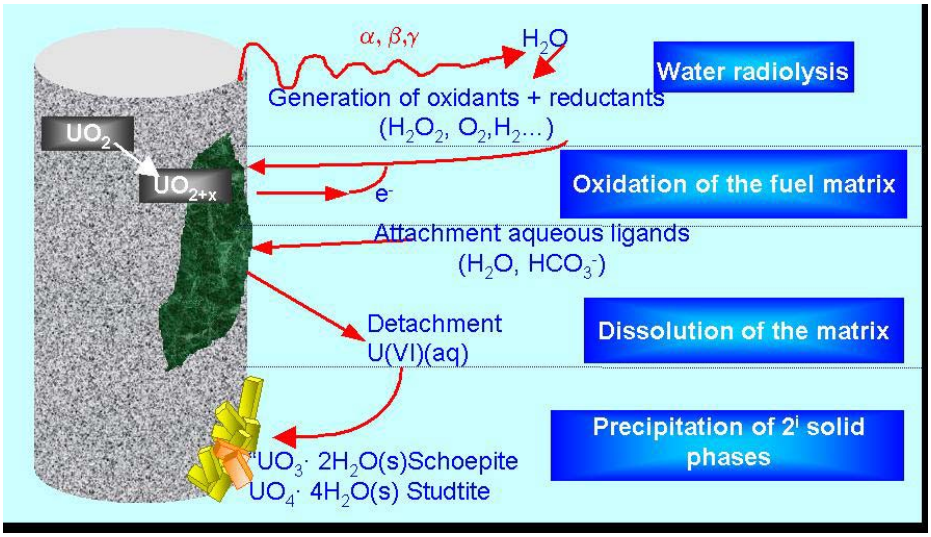

Figure 33: Main processes of oxidation-dissolution of the UO_2 matrix under radiolysis of water

When water contacts the surface of the fuel, the first process we may expect is the radiolysis of water. This radiolysis generates oxidants and reductants and, in spite of nominally anoxic or reducing conditions we can expect local oxidizing conditions.

Due to these local oxidant conditions, the surface of the fuel will oxidize as well as other redox sensitive radionuclides with the destabilization of the matrix. The attachment of aqueous ligands available to form strong complexes with its major component will favour the dissolution of the matrix and the consequent release of radionuclides (RN) embedded in it.

Finally, the precipitation of pure or mixed secondary solid phases is expected if solubility limits are reached. The main processes that are taken into consideration as well as the used approaches are described hereafter:

Process 1. Generation of oxidants and reductants by water radiolysis.

Eq. 11: H_2O + radiolysis $\Rightarrow$ oxidants + reductants.

The main oxidants generated by radiolysis or recombination reactions are O_2, H_2O_2 and radicals like OH, CO_3 etc. The main reductant generated radiolytically is H_2.

Process 2. Oxidation of the spent fuel matrix and other redox sensitive radionuclides

Eq. 12: U (IV) - 2e-$\Rightarrow$ U (VI)

Process 3. Reduction of the oxidants present in the system.

Reduction processes will occur according to the following reactions

Eq. 13: $O_2 + 2H_2O + 4e^- \Leftrightarrow 4OH^-$

Eq. 14: $H_2O_2 + 2e^- \Leftrightarrow 2OH^-$

In groundwater systems with chloride concentrations above 2 moles/dm^3, other oxidants such as Cl^-, ClO_3^- radicals and HClO are relevant.

Process 4. Dissolution of the spent fuel matrix and radionuclides release

Eq. 15: $(U,RN)O_{2(s)} \Rightarrow RN^{n+} + U(VI)_{(aq)}$

U(VI) speciation in the aqueous phase will depend on the groundwater composition contacting the fuel. The radionuclides embedded in the matrix are assumed to be congruently dissolved with the matrix.

Process 5. Precipitation of secondary solid phases

There is a limited knowledge about the precipitation kinetics and solid phases in repository conditions. The lack of information on precipitation kinetics has made to simplify the system and consider a thermodynamic approach.

This is the main difference with the three first processes that are kinetically controlled.

Like the dissolution process, precipitation of secondary phases will depend on water chemistry inside the canister: pH, pe and concentration of complexing anions. Radiation source strength has showed the formation of different phases. Formation of schoepite $UO_3.XH_2O$ and studtite $UO_4{\cdot}4H_2O$ or uranium peroxides respectively at lower and higher alpha radiation fields (McNamara, 2002; Clarens et al, 2003; Colbert et al, 2003).

5.1.2 CODE INTER-COMPARISON

Radiolytic models do not have a wide acceptance for heterogeneous systems due to limited availability of kinetic data, the difficulty to handle interfaces, and a lack of model validation. In order to gain confidence in the uses of this kind of models, an intercomparison exercise between two kinetic codes ,"Chemsimul" (Kirkegaard and Bjerbakke,2002) and "Maksima"(Carver et al.1979) has been carried out. Figure 34 shows a comparison of the output data obtained by both codes. The differences in the worst case are lower than 1%.They are linked to the different integration method used for resolving the differential equations, numerical precision used in each code, whether the G-values, kinetics constants have more or less digits.

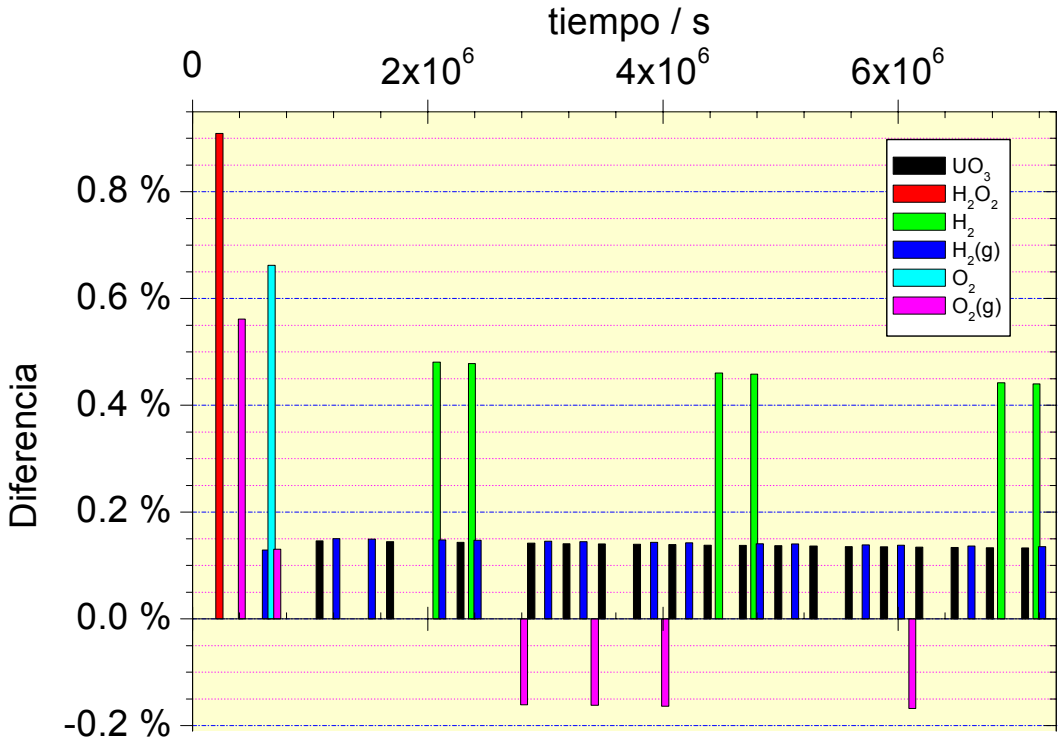

Figure 34: Intercomparison between the two kinetic codes, Chemsimul and Maksima

5.1.3 BOUNDARY CONDITIONS AND PARAMETERS

The boundary conditions as well as the parameters needed for the development of the mathematical and numerical model have been also summarized and discussed in the D12 (Martinez Esparza et al., 2004a)

Boundary conditions include characterization of the spent fuel, groundwater compositions, and canister and cladding characteristics relevant for the MAM, temperature and evaluation time. Parameters of relevance for the model development are the geometry of the system and associated parameters as radiation field, hydraulic parameters for considering a water turnover, and kinetic reactions for considering generation and recombination by radiolysis processes and alteration of the matrix. The main parameters and assumptions are summarized in Table 16.

Table 16: Boundary conditions and parameters used in the base cases

	Granite	Salt
Spent fuel	41.5 MWd/kg U	
Geometry	Fuel pellet surrounded by water	
Water layer	45 μm	40 μm
Surface Area	Specific (70cm^2/g)	Geometric
Alpha dose rate	from Quiñones et al. (2000)	calculated (CEA inventory)
G values	H_2O	5 M NaCl
Water composition	Evolving with time	Fixed with time
pH_2, constant	3 bar	3 bar and 0 (initial)
Canister failure	1,000 y	
Timing	1,000,000 y	
Temperature	25 ºC	
Radiolysis scheme	D4	D4
UO_2 alteration scheme	New scheme (D12)	Christensen scheme

Main discussions were about the calculation of maximum or mean dose rates and depth of the irradiated water layer, that as can be seen in the sensitivity analysis has a great influence in the alteration rate (see section 3.2.3).

5.2 MATHEMATICAL MODEL

The development of the Matrix Alteration Model is summarized in D13 "Mathematical Model Development and Experiments Integration in the MAM"(A. Martínez Esparza et al, 2004b). Processes as well as kinetic data are derived from the mechanistic models developed for non-irradiated UO_2 dissolution experiments with oxygen (de Pablo et al, 2001-2004) as well as from the works performed with hydrogen peroxide by Ekeroth and Jonsson, 2003 and Clarens, 2004).

After the integration of the mechanisms in the radiolytic model, this is calibrated with experimental data and tested with the experiments developed in WP3 with alpha-doped pellets and with real spent fuel.
Finally the model is applied to base case calculations for granite and clay groundwaters.

Oxygen-promoted mechanism for the oxidation of the matrix.

Oxidation of UO_2 surface by oxygen is expressed by Giménez et al. (2001) and de Pablo et al. (2004) as follows:

Eq. 16: $>UO_2 + 1/2O_2 \Leftrightarrow >UO_3$ $k(_{O2exp}) = 0.7\ M^{-1}\cdot s^{-1}$ at 25 ºC (Giménez et al., 2001).

This process has been incorporated into the MAM model based on the mechanism of Schortman and De Sesa (1958) as two elemental processes as follows:

Eq. 17: $>UO_2 + O_2 \Rightarrow >UO_2\text{-}O_2$ K_{O2}

Eq. 18: $>UO_2\text{-}O_2 + >UO_2\text{-}O_2 \Rightarrow 2\ >UO_3$ Fast

where K_{O2}=0,0013 $M^{-1}\cdot s^{-1}$

Hydrogen peroxide promoted mechanism for the oxidation of the matrix.

The proposed mechanism for the oxidation of the spent fuel matrix by hydrogen peroxide is:

Eq. 19: $>UO_2 + H_2O_2 \Rightarrow >UO_2 + 2\cdot OH^\bullet$ K_{H2O2} =2,2 $M^{-1}.s^{-1}$ (calibrated)

Eq. 20: $>UO_2 + \cdot OH^\bullet \Rightarrow >UO_2OH$ KOH= 2.6·104 $M^{-1}\cdot s^{-1}$ (Ekeroth and Jonsson, 2003)

Eq. 21: $>UO_2OH + \cdot OH^\bullet \Rightarrow >UO_3 + H_2O$ Fast

The overall mechanism accounts for the general oxidation reaction by H_2O_2, that is:

Eq. 22: $>UO_2 + H_2O_2 \Rightarrow >UO_3 + H_2O$.

Hydrogen reductant promoted mechanisms

Based on experimental evidence (Sunder et al. 1990, Rollin 2001, Shoesmith 2004) and from the SFS project (K. Spahiu, A. Loida, P. Carbol), there is a clear effect on decreasing the uranium concentration in solution when hydrogen is present in the system.

The mechanism is not well understood (see section 4.2). Today a systematic experimental support for development of reaction mechanisms and constants is necessary in order to take into account the H_2 effect in the model.

However, a scavenging effect of H_2 has been considered in the sensitivity analysis (not including the surface activation effects discussed in Section 4), based on published data of reactions and constants. The decreasing effect is higher in saline than in granite environments, due to the scavenging effect on OH radicals and Cl radicals in saline waters and only on OH radicals in case of granite.

Mechanisms accounting for the dissolution of the oxidised UO_2 co-ordinates sites.

The kinetics constants of the dissolution processes once the surface sites have been oxidized are also derived from the experiments and oxidation/dissolution mechanisms proposed by (de Pablo et al. 2003).

The mechanism is based on two steps:

1. Surface co-ordination of U (VI) by the aqueous ligands (H^+,H_2O or HCO_3)
2. Detachment (dissolution) of the product species.

For H^+ and H_2O the rate-determining step will be the detachment of the product species (de Pablo et al 2003). For bicarbonate, the limiting process will be the surface co-ordination step (de Pablo et al, 1999).

Theses processes have been included in the reaction scheme by means of a simplified mechanism as a function of the rate-determining step (Merino et al 2004). Kinetic constants have been taken from the semi-empirical models developed by de Pablo and co-workers, namely $k_H = 2\ M^{-1}\cdot s^{-1}$, $k_{H2O} = 10^{-5}\ M^{-1}\cdot s^{-1}$ and $k_{HCO3} = 5\cdot 10^{-2}\ M^{-1}\cdot s^{-1}$.

The processes included in the reaction scheme for the dissolution of the oxidized UO_2 are:

Eq. 23: $>UO_3 + H^+ \Rightarrow UO_2(OH)+ \quad k_H$

Eq. 24: $>UO_3 + H_2O \Rightarrow UO_2(OH)_2(aq) \quad k_{H2O}$

Eq. 25: $>UO_3 + HCO_3^- \Rightarrow UO_2CO_3(aq) + OH^- \quad k_{HCO3}$

Eq. 26: $UO_2CO_3(aq) + HCO_3^- \Rightarrow UO_2(CO_3)^{2-} + H^+$ Fast.

5.3 MODEL CALIBRATION

The model calibration with experimental data from tests carried out by using non irradiated UO_2 is presented below.

The computer code used to solve the resulting differential equations from all the kinetic reactions was Chemsimul (Kirkegaard and Bjergbakke, 2002). The results of applying the model to the experiments at different oxygen partial pressures and at variable pH are shown in Figure 35. The calibration process has led to a good fit for pH > 5 and for oxygen partial pressures ranging between 0.05 and 0.21 bar.

The next series of experiments, with carbonate included in the leachant, was modelled by adding the carbonate system in the reaction scheme. The results (Figure 36) show a good agreement between MAM model and the semi-empirical model in the carbonate concentration range of $10^{-4} - 10^{-2}$ M. The divergence of the two models at the low carbonate content is due to the inclusion of the protonation and water molecule complexation in our model. These processes were not included in the semi-empirical model developed by de Pablo et al. (2004) and they are predominant in the dissolution step at low CO_3^- concentration. At high carbonate content, however, the semi-empirical model includes the phenomenon of site saturation, not included in the MAM, a process that should be implemented in future developments of our kinetic model.

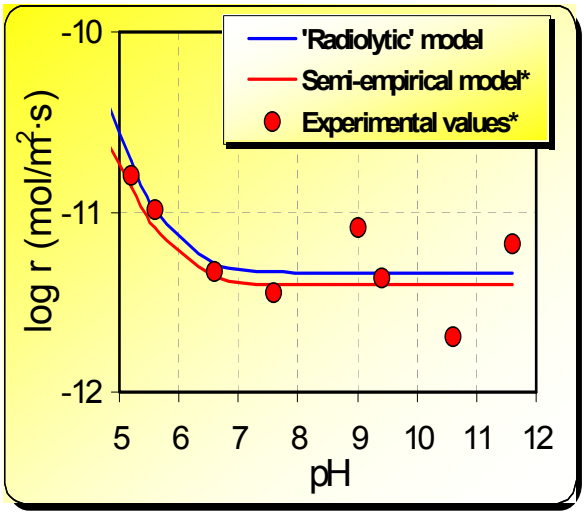

Figure 35: Calibration of the model ('radiolytic') to experiments with 5 % O_2 and comparison with the semi-empirical model of de Pablo (2004)

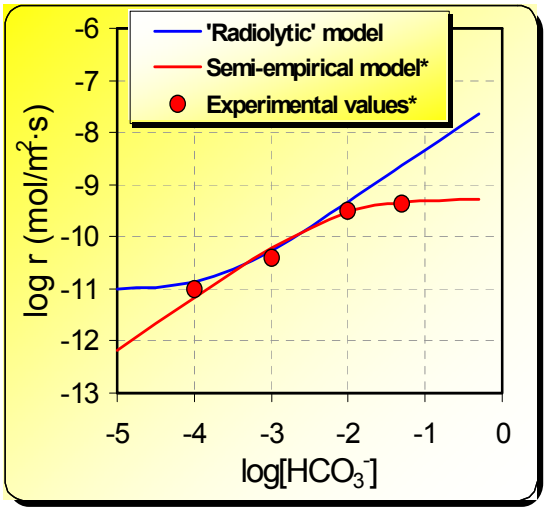

Figure 36: Calibration of the model in presence of carbonate and comparison with the semi-empirical model of de Pablo (2004)

Several experiments were conducted to study the effect of H_2O_2 on the dissolution of unirradiated UO_2. The work focused on studying the effect of hydrogen peroxide concentration as well as the effect of bicarbonates and pH (Figure 37). Hydrogen peroxide was assumed to remain constant in each experiment and only uranium concentration in solution was determined. Different experimental series were carried out. All this work is reported in de Pablo et al. (2003).

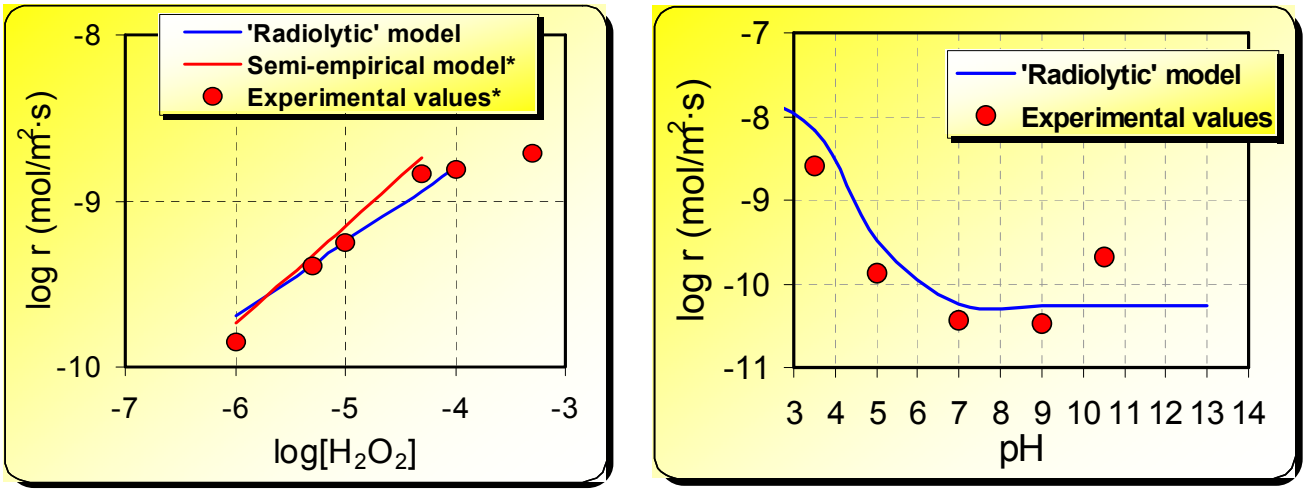

Figure 37: MAM calibration with experimental values, influence of H_2O_2 and pH

The formation of OH radicals by decomposition of H_2O_2 led to introduction of the scheme with recombination reactions when applying the model to non-irradiated UO_2, that is, a system without radiolysis. In this respect, the recombination reactions lead to the formation of O_2, which adds to the overall oxidation of the sample under study. On the other hand, to reproduce the experiments with carbonate in the leachant the carbonate system was also included in the reaction scheme. All these reactions, the radical recombination and carbonate system schemes, have been taken from WP2 and described in D4 for a closed system (Kelm and Bohnert, 2004a). Finally, we obtained a good fit for the experiments with variable pH. The agreement is also good at even lower pH than in the experiments with O_2. At alkaline conditions, the model predicts a constant dissolution rate, as was the case for the experiments with O_2, due to the predominance of the complexation with the water molecule in the dissolution step. This contrasts with the experimental evidence of a higher dissolution rate at high pH. As de Pablo et al. (2003) pointed out, this higher dissolution rate is probably due to the decomposition of H_2O_2 into HO_2^-, a more reactive species not included in our model. The

relevance of this process, however, is not high at the pH conditions expected in the repository, which are less alkaline.

5.4 MODEL VALIDATION

The MAM which was calibrated with unirradiated UO_2 reaction with simulated radiolytic products was applied to the leaching tests of alpha-doped pellets and spent fuel carried out in the scope of SFS project WP3, under the ENRESA-ITU-CIEMAT collaboration agreement. The results shows a very good fitting and the uranium concentration in dissolution is correctly described when steady state is reached. The results of validation with spent fuel 53MWd/t_u dynamic tests in air at hot-cell (25±2ºC) conditions are given in Figure 38. The solution used was a carbonated water containing 1mM Na HCO_3 and 19 mM Na Cl. (see section, 4.1.2 for the description of experiments)

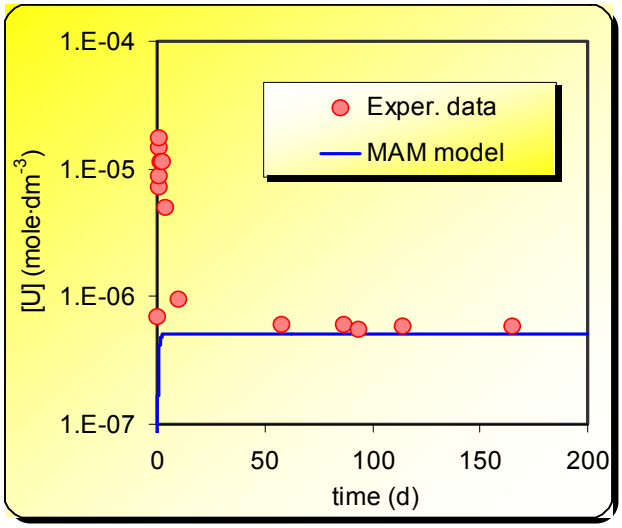

Figure 38: Comparison between the MAM and the SFS experimental results

The dissolution rate calculated from modelled uranium concentrations from spent fuel dissolution experiments is $(4.6 \pm 1.8) \times 10^{-11}$ mol.m^{-2}.s^{-1}. This rate is very close to the one calculated experimentally of $(3.2 \pm 0.2) \times 10^{-11}$ mol.m^{-2}.s^{-1}, which gives confidence in the application of the model to real spent fuel.

5.5 BASE CASE CALCULATIONS

The MAM was applied to the base case in granite (D13, Martinez-Esparza et al., 2004b) and clay host rock (D14, Martinez-Esparza et al., 2004c) by applying the parameters and boundary conditions as agreed in WP4 meeting in Madrid (see Table 16). The saline base case was developed by M. Kelm with the reaction scheme of H. Christensen.

The reference spent fuel for the base case calculation has a burn-up of 41.5 MWd/kg U, with a geometry consisting of a fuel pellet surrounded by a gap full of water. The geochemical conditions vary with the repository concept, but a pH of 7 was considered for the base case calculation. In addition, a constant H_2 pressure of 3 bars coming from the container corrosion was also taken into account. The alpha dose rate calculation is based on the inventory of the reference fuel, the self-absorption of alpha particles in the spent fuel itself and their range in water and the energy deposited in the gap water (Rodríguez-Almazán et al., 1998).

The new scheme developed in the MAM was applied for the granite and clay base cases. The calculated time-dependent concentration of molecular oxidants and reductants and the fuel dissolution rates over the period from 10^3 to 10^6 years are given in Figure 39.

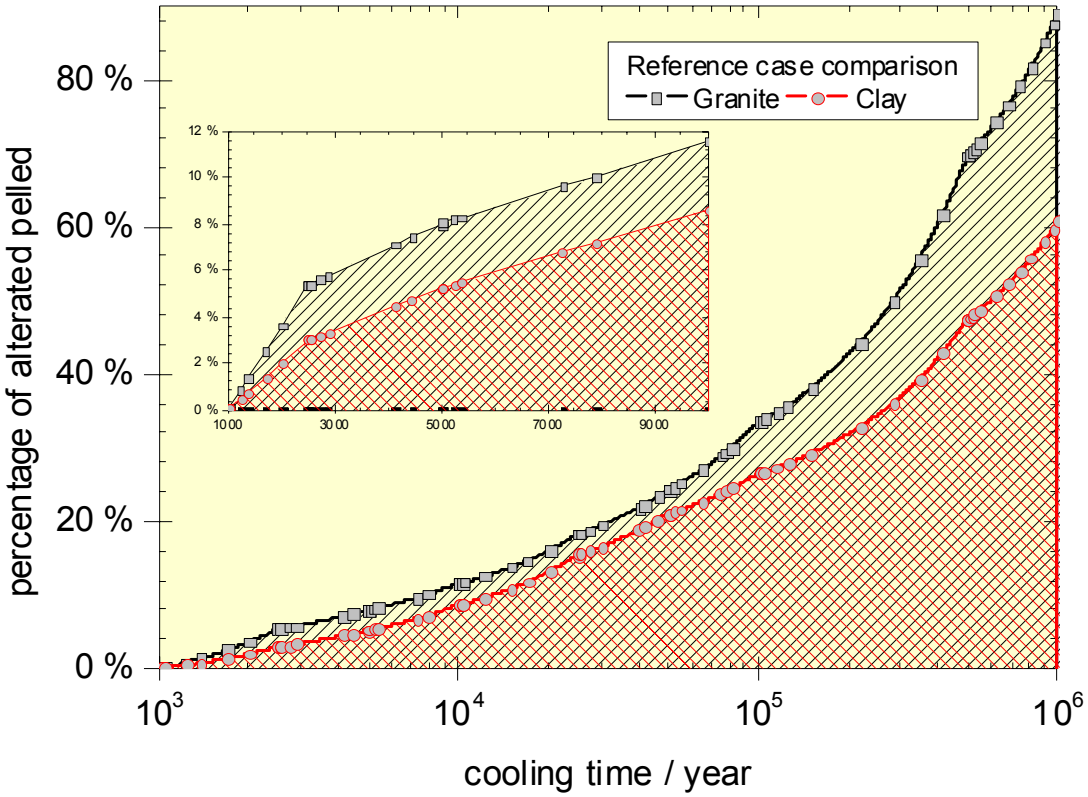

Figure 39: Base case calculations for granite and clay

5.6 SENSITIVITY ANALYSIS

A sensitivity analysis for the granite base case has been developed in order to study the influence of some parameters (specific surface area, burn-up, dose rate, irradiated water thickness, canister lifetime, hydrogen, and carbonate) on the pellet alteration rate with respect to the selected values. A summary of the MAM sensitivity case studies and results are given respectively in Table 17 and in Figure 40.

Table 17: Summary of the MAM sensitivity analysis (Martinez-Esparza et al., 2004c)

Case	Parameter	Value
Specific surface area	Specific surface area	7 $cm^2.s^{-1}$
		1000 $cm^2.s^{-1}$
Carbonate in water	$Pp(CO_{2g})$	10 mbar
		3 mbar
		absence
α LET	Thickness of the irradiated water layer	30 µm
Pellet burnup	UO2 pellet	33 MWd kg^{-1}
		41 MWd kg^{-1}
		47 MWd kg^{-1}
	MOX pellet	41 MWd kg^{-1}
Presence of hydrogen	[H2]aq	1 mM
		160 mM
Canister resistance	Time failure	10,000 y

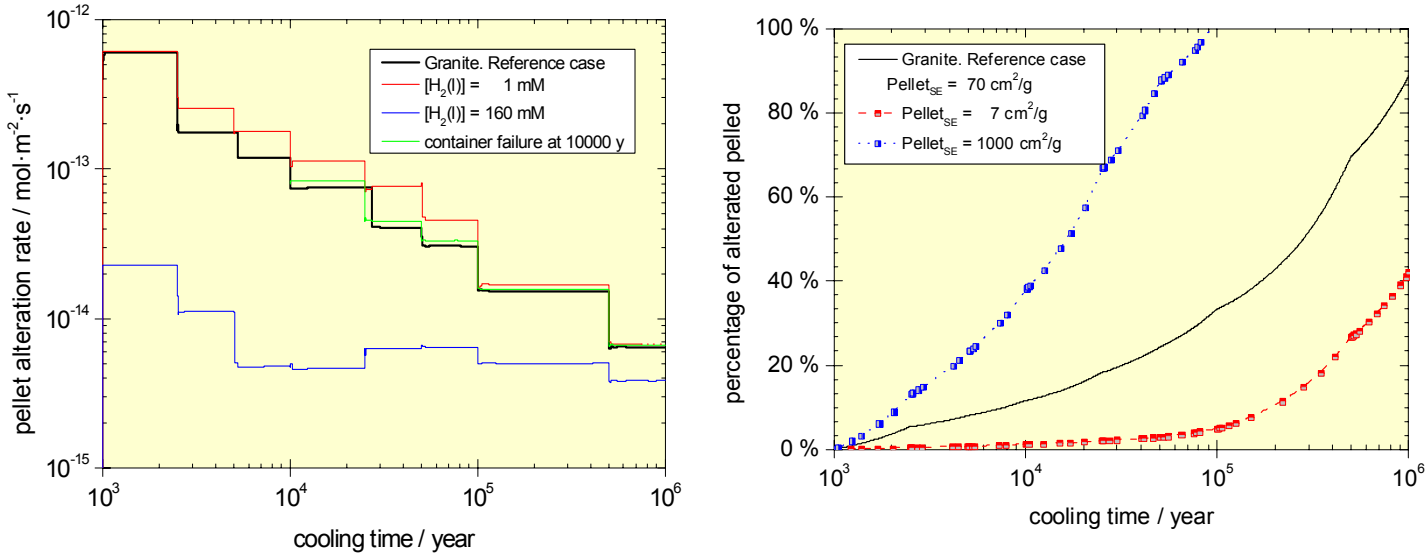

Figure 40: Sensitivity analysis, influence of H_2, container life time (left) and specific surface area (right)

A literature search of rate laws derived from experimental data and reported in several environmental conditions has been done in order to compare these dissolution rates with the ones calculated when applying the MAM. Results are presented in Figure 41 for the granite base case and in Figure 42 for the salt base case.

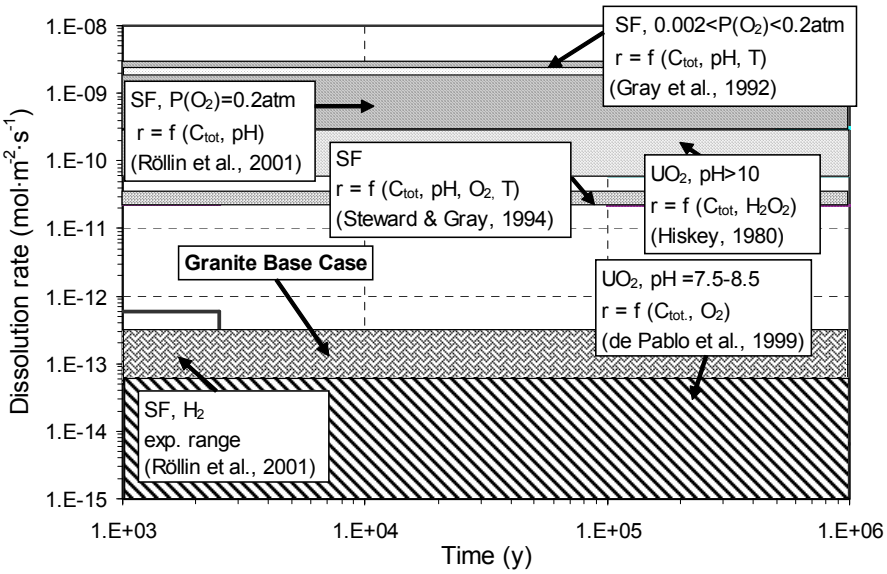

Figure 41: Comparison of the result of the granite base case with published rate laws applied to conditions in the base case (carbonate content, O_2 or H_2O_2 concentration) and experimental rates measured under a hydrogen atmosphere (Martinez-Esparza et al., 2004b)

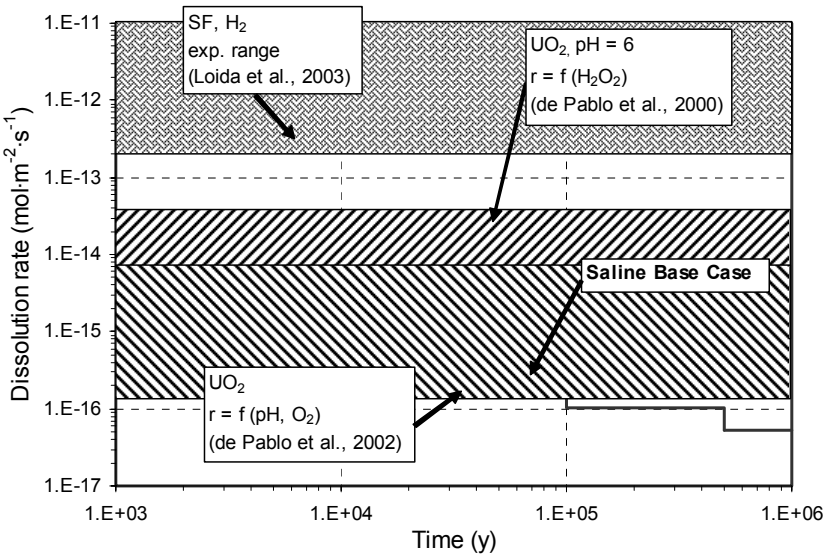

Figure 42: Comparison of the result of the saline base case with published rate laws applied to conditions in the base case (absence of carbonate, O_2 or H_2O_2 concentration) and experimental rates measured under a hydrogen atmosphere (Martinez-Esparza et al., 2004b)

In general, there is a good agreement between the dissolution rates calculated in both media with the range of dissolution rates calculated by using the rate laws elucidated both in presence and in absence of carbonates in the system respectively. The ranges of dissolution rates calculated by using the empirical and semi-empirical models differ in about one order of magnitude depending on the presence or not of carbonate in the studies carried out for deriving such models. This comparative analysis highlights that oxidant compounds as well as carbonate concentration are very important variables of the system when predicting long-term matrix alteration dissolution rates.

5.7 CONCLUSIONS

A new Matrix Alteration Model (MAM) has been proposed in the framework of the SFS project. It is based on the integration of the matrix alteration (oxidation and dissolution) mechanisms in the radiolytic model by means of elemental reactions. Mechanisms have been mainly elucidated from the mechanistic models developed for non-irradiated UO_2 dissolution experiments with oxygen (de Pablo et al., 1999, Giménez et al., 2001, de Pablo et al. 2003, de Pablo et al., 2004) as well as from the work performed by Ekeroth and Jonsson (2003) with hydrogen peroxide.

Model testing was done with data generated within WP3. SCK-CEN and ITU using alpha-doped materials at different environmental conditions, i.e. reducing, anoxic and deaerated. In addition, FZK-INE and ITU performed dissolution experiments with spent fuel in brines and reducing conditions and in carbonated water and oxidising conditions respectively. The presence of humic substances in the experiments carried out by SCK-CEN prevents a straightforward way of testing the model by means of the experimental data generated by this group due to the strongly reductant conditions. Model testing is done with dissolution data generated at ITU with alpha-doped material by taking several hypotheses in agreement in most of the cases with the experimental observations. The model predicts most of the results when considering a pre-oxidation of the surface sample and in some cases the model assumes an initial oxygen concentration in the system. Based on these assumptions, the fitting of the model to the experimental data was possible in most of the studied cases. Dissolution data obtained from spent fuel powdered samples in flow-through tests carried out in the hot cell laboratories at ITU was used as a testing exercise with a quite good result in the modelling work.

The kinetic model was not tested with those experiments where the dissolution data indicate a solubility control, which is the case of the experiments carried out at ITU with alpha-doped and MOX samples at different hydrogen pressures and of the experiments carried out at FzK-INE with spent fuel in brines under reducing conditions. Strong inhibition of the uranium dissolution made difficult to measure and quantify the uranium concentration in solution and therefore matrix dissolution rate.

A preliminary intercomparison case in salt has been performed with MAM and the FzK based Christensen reaction scheme .The results shows a good agreement, but a mechanistic detailed reaction for radiolytic products generated in NaCl needs to be included in the MAM.

MAM has been used for the base case calculations in two different media, granite and clay. The base case considers an initial hydrogen concentration that is kept constant during all the evaluation time corresponding to the expected hydrogen atmosphere generated due to the corrosion of metallic parts in the repository system (3 bars). Modelling results indicate a decrease of the dissolution rates with time in both media. This decrease is related to the decrease of the alpha dose rate. Results indicate quite large spent fuel stability in both media as well as in salt brines.

Experiments performed with alpha- doped materials as well as with spent fuel provide a consistent picture suggesting that H_2 is an active reducing agent, which besides consuming oxygen arising from radiolysis and contamination from air, also reduces traces of any U(VI) present. A possible explanation is an activation of the H_2 by surface catalyst. This process was proposed by Shoesmith (2004) for gamma radiation and seems to be stronger in case of alpha radiolysis.

Future developments of the MAM should be attempted to incorporate such surface processes and mechanism and the influence of the different types of radiation on the role of H_2 as reductant or as fuel /water interface oxidants consumer, incorporating recent developments of SFS project.

6. ANTICIPATED SPENT FUEL PERFORMANCE IN GEOLOGICAL REPOSITORY (WP5)

6.1 SCOPE

The understanding and modelling of processes related to radionuclide release from spent fuel under repository conditions have been brought together in WP 5, which provides two main elements, including:

- a synthesis of findings from the experimental and modelling studies,
- an integrated model, combining the IRF model and the MAM, and including some results of illustrative calculations of the time-dependent release of radionuclides from canisters of spent fuel with different burnup values. These calculations include solubilities of nuclides, as these affect release from a breached canister.

The various aspects serve to illustrate the factors controlling radionuclide release in a spent fuel repository, thus providing an overall performance assessment context.

6.2 FUEL TYPES

The reactor fuels in wide use in Europe include:

- PWR UO_2 fuel, with typical burnups of 35-55 GWd t_{iHM}^{-1} (tons initial heavy metal) and maximum burnups of ~75 GWd t_{iHM}^{-1}
- BWR UO_2 fuel, with typical burnups of 35-50 GWd t_{iHM}^{-1} and maximum burnups of ~60 GWd t_{iHM}^{-1}
- PWR and BWR MOX fuel, with typical burnups of 35-50 GWd t_{iHM}^{-1} and maximum burnups of ~60 GWd t_{iHM}^{-1}

For the SFS project, the reference fuels selected for detailed calculations were PWR UO_2 fuels with burnups of 33, 41, 47.5 and 60 GWd t_{iHM}^{-1}. There was insufficient information on MOX fuels for an integrated assessment, although IRF aspects were assessed (*see* section 2.).

6.3 REFERENCE EBS CONCEPTS AND REPOSITORY ENVIRONMENTS

For calculations of release of radionuclides from a hypothetical container of SF in a repository, two reference EBS (Engineered Barrier System) types are considered in the SFS Project. These are:

1) an EBS for a granite or clay host rock, consisting of a container for spent fuel surrounded by a clay (bentonite) buffer. The container may be carbon steel, stainless steel or a copper shell with a cast iron insert.
2) an EBS for salt host rock, consisting of a steel container surrounded by salt backfill.

Each canister is assumed to contain 1 t_{iHM} of spent fuel (about 4 fuel assemblies), with an internal void volume of 0.5 m^3 (calculations show that the releases are insensitive to the size of the void volume).

Different chemical and mass transport conditions exist in granite, clay and salt host rocks and these are considered in the radionuclide release calculations. The canisters are arbitrarily assumed to have a lifetime of 1000 years for the release calculations, thus temperatures are assumed to be gradually approaching ambient values. The only changes occurring during the containment period are associated with alpha radiation enhanced diffusion of fission products to grain boundaries. After container breaching, leaching of the IRF as well as matrix alteration occur according to the specified IRF and MAM, for the specified mass transfer rates for the different host rocks. These are typically slow, although the effective flow rate of water for crystalline rock is several orders of magnitude greater than for a clay or salt repository (although conditions within a clay buffer are diffusion controlled). Because of slow transport and the moderate corrosion rate of steel (1 μm/a), in most cases, H_2 partial pressures are expected to be 50 to 100 bars and this will be sustained for up to ~100,000 years. The calculations using the MAM have used a conservative value for initial hydrogen pressure of 3 bars and this value is assumed to be sustained for all model calculation times.

6.4 MODEL CALCULATIONS TO ILLUSTRATE VARIOUS PROCESSES

Results of the MAM calculations of the dissolution rate (converted to fractional dissolution rates) are compared in Figure 43 to the estimated range of dissolution rates derived from studies of spent fuel dissolution and alpha-radiolysis effects on UO_2 dissolution in H_2-dominated systems (WP3). The absence of any time-dependence (dose-rate dependence) for H_2-dominated systems may or may not be real, and further work should be done to assess this aspect.

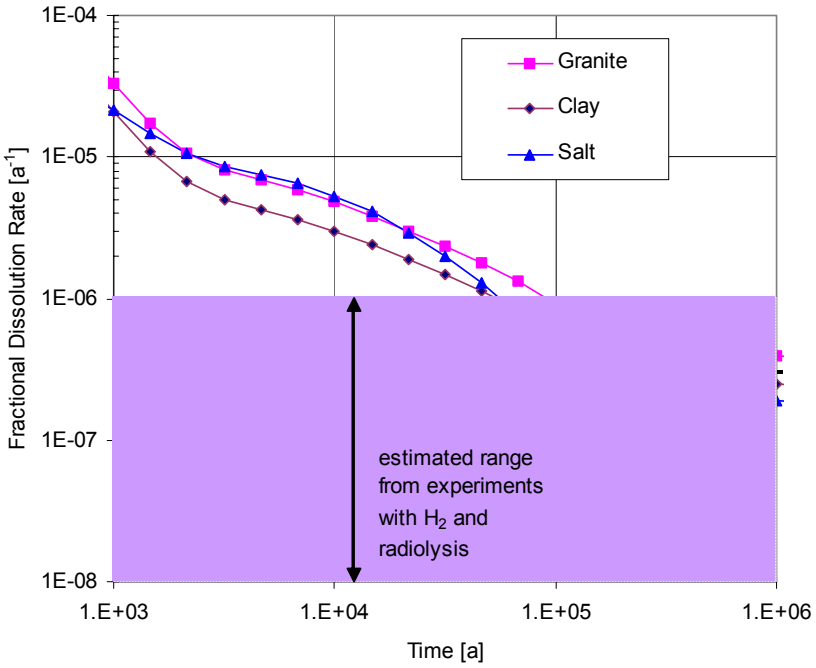

Figure 43: Comparison of fractional dissolution rates calculated using the MAM with the range of values estimated from experimental studies of dissolution of alpha-doped UO_2 and spent fuel in the presence of H_2

Alteration rates calculated with the MAM are, of course, dependent on the dose rate, thus MAM calculations show a difference in time-dependent alteration rate depending on the fuel burnup, in particular at early times. This is illustrated in Figure 44 in terms of integrated fractional dissolution for fuels with burnup values ranging from 33 to 60 GWd t_{iHM}^{-1}. There is a difference in integrated fraction of fuel altered of about 5% at 10^5 years. Such an effect would be even more pronounced with MOX fuel; however, no estimates of the matrix dissolution rate have been made for MOX fuel using the MAM, as little data is available to support the validity of such calculations.

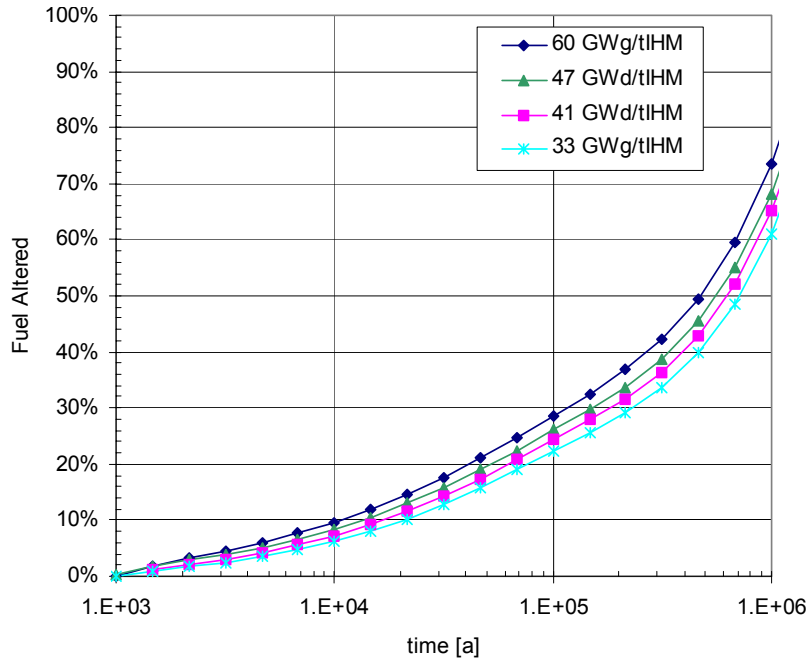

Figure 44: Effect of burnup on fraction of fuel altered over time for granite groundwater

It is interesting to compare the relative contributions of the IRF (i.e. IRF t=0), alpha-enhanced solid state diffusion (i.e. IRF(t)) and matrix dissolution to radionuclide release for different burnup values. (Note that the term IRF(t) used here refers only to the time-dependent portion of the IRF.) This is shown in Figure 45 for spent fuel with a burnup of 41 GWd t_{iHM}^{-1}.

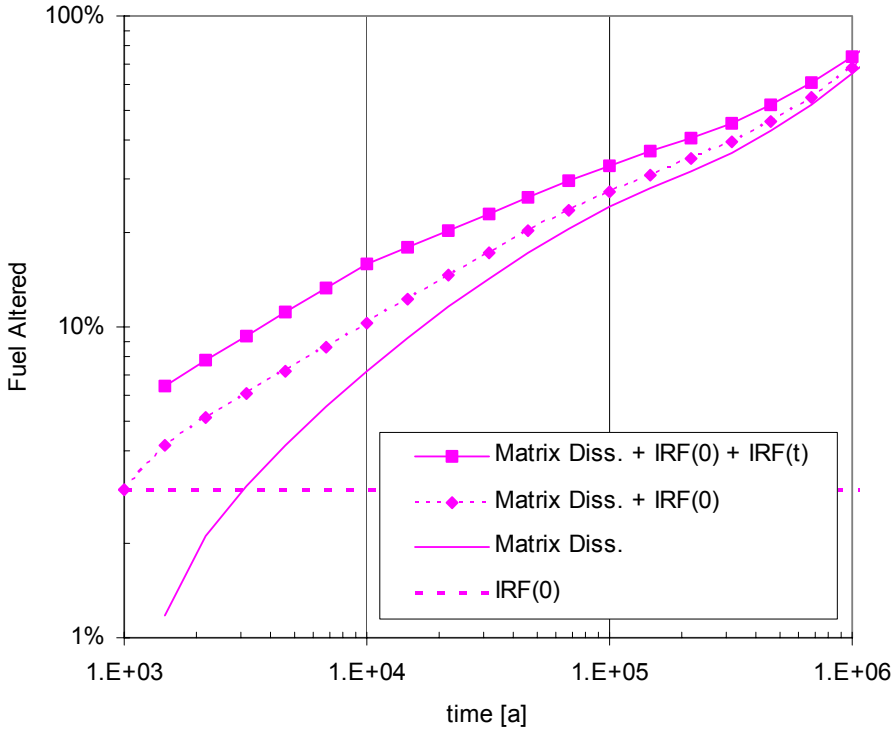

Figure 45: Integrated release of I-129 from spent fuel with a burnup of 41 GWd t_{iHM}^{-1} (granite case) considering matrix dissolution only (lower curve), matrix dissolution plus IRF (t=0) and matrix dissolution plus IRF(t=0) plus IRF(t)

6.5 INTEGRATED MODEL CALCULATIONS

The integrated model combines the IRF model, the MAM, nuclide solubilities and near-field mass transport rates to illustrate the time-dependent release of radionuclides from a reference canister of spent fuel (1 t_{iHM}). The distribution of I-129 in the disposal system as a function of time for fuel with a burnup of 41 GWd t_{iHM}^{-1}, as calculated with the integrated model, is shown in Figure 46 for granite repository porewater chemistry and mass transport conditions. When the container is breached at 1000 years, the IRF is released into the void space within the container and begins to be released into the surrounding rock. After about 500,000 years, the fraction of the total initial inventory that is released from the container is about 50 %. Dissolution and release from the canister is complete after about 1.5 M years. This is in contrast to the case shown in Figure 47 for Np-237, in which a precipitate forms. Here the relatively higher mass transport rate from the container under granite repository (Np solubility = 6×10^{-8} mol/l) conditions leads to less accumulation in the precipitate and to its earlier dissolution, as compared to the clay (Np solubility = 5×10^{-9} mol/l) and salt (Np solubility = 3×10^{-7} mol/l) repository cases. These results illustrate that release from spent fuel and the associated precipitates under disposal conditions is a complex function of matrix alteration rate, nuclide solubility and mass transport conditions.

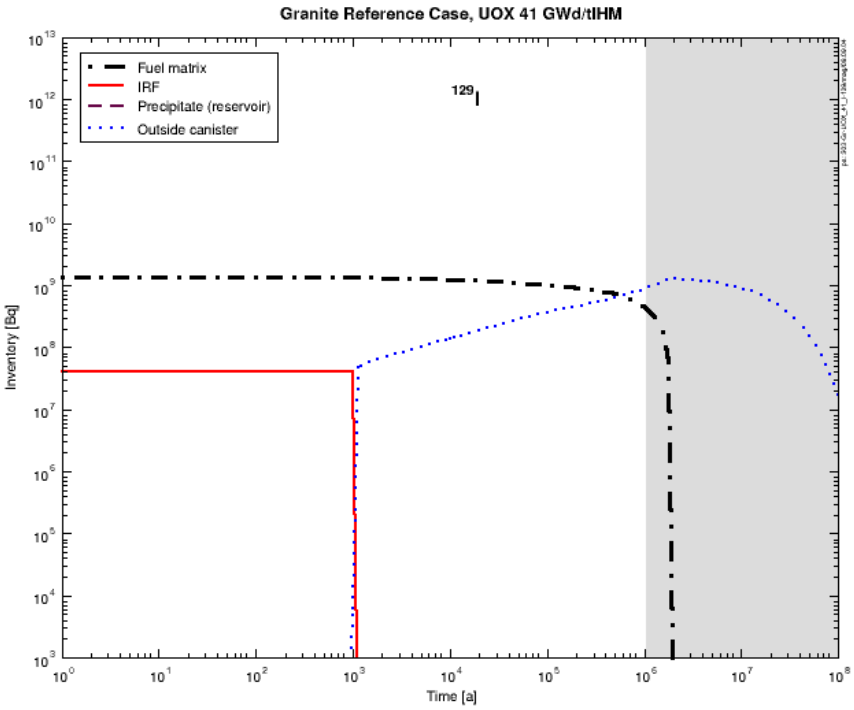

Figure 46: The distribution of I-129 as a function of time, showing the amounts in the fuel matrix, IRF and released from the container, for fuel with a burnup of 41 GWd t_{iHM}^{-1}

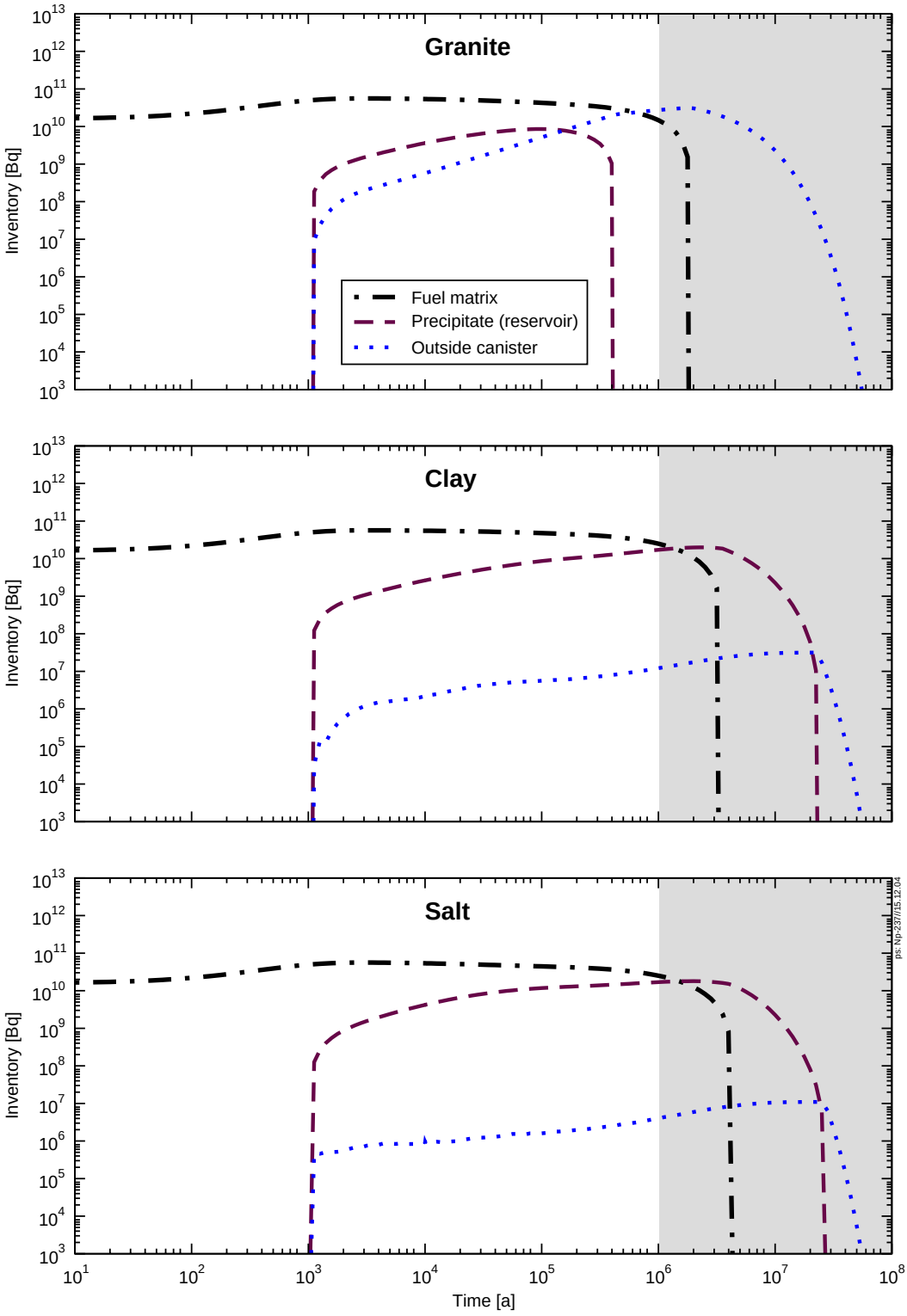

Figure 47: The distribution of Np-237 as a function of time for the case of containers of spent fuel (burnup = 41 GWd t_{iHM}^{-1}) having a breaching time of 1000 years in repositories in granite, clay and salt

6.6 CONCLUSIONS AND PROSPECTIVES

Collectively, the studies have led to valuable insights into the behaviour of spent fuel (UOX and MOX) under disposal conditions relevant in European countries. The RN source term models proposed by the project are based on a few intrinsic parameters of the spent fuel that were selected in order to obtain a relatively sufficient description of the spent fuel behaviour. They are (i) burnup and type of fuel (UOX or

MOX) (specific activities) and (ii) surface area. Concerning the environmental conditions at the spent fuel surface, the main parameters which appear as to be relevant are: pore water chemical composition (pH, carbonate concentration, overpressure/dissolved H_2, Eh, ionic strength…), hydraulic parameters in case of solubility controlled dissolution (porosities, water turn over, volume of water…). The radionuclide source term developed in the frame of the project is divided into two terms: (i) the IRF (Instant Release Fraction) (% of total inventory for each nuclides) and (ii) Fractional matrix dissolution rates (yr^{-1}). For IRF, the main radionuclides quantified are ^{129}I, ^{137}Cs, ^{135}Cs, ^{36}Cl, ^{79}Se, ^{126}Sn ,^{14}C. and ^{99}Tc, ^{107}Pd. The radionuclides embedded in the matrix are assumed to be released congruently with the dissolution of the matrix.

The evaluation of the radionuclides release is based on the state of understanding acquired for different processes which occur before and during the water ingress, and how the model translates this understanding. For example, the kinetic radiolysis model depends on the kind of radiation ($\alpha\beta\gamma$), the chemical reactions and kinetics parameters retained to describe the chemical solution evolution . These reactions may be different according to salt environment, high enriched environment with corrosion products and the chemical composition of the clay/granite. Furthermore, because only very few data are available about high temperature kinetics, it was assumed that data obtained at low temperature (25°C) are applicable at higher temperature.

The main important findings and significant uncertainties important for future R&D are:

Concerning IRF values:

1. IRF values for some radionuclides may be very high (15-25%) at burnups of 60-70 GWd t_{iHM}^{-1}. This is largely due to the rim restructuring, which leads to accumulation of volatile fission products in pores in the rim. There is very little information on the leaching behaviour of higher burnup fuels and on the leachability of the rim, thus the IRF model pessimistically assumes rapid release of the fission products in pores. Similarly, the microstructure of MOX fuel suggests that very high IRF values (~50 %) may be possible. Future leaching studies should focus on examining these pessimistic assumptions.
2. The uncertainties in α radiation enhanced diffusion are large, covering several orders of magnitude. Although the contribution of this process to the IRF and to overall radionuclide release from spent fuel is not large, it would be useful to further refine the understanding to reduce the uncertainty in model predictions.
3. The effects of He buildup may be a significant issue for high burnup and MOX fuels. These aspects were not explored in the SFS Project, but should be looked at in future because build-up of high gas pressures in pores might destabilise grain boundaries, possibly leading to cracking.

Concerning matrix dissolution:

4. For brine solutions (case of salt repository), radiolytic models for gamma and alpha radiolysis have been tested and shown to have good agreement with experiments for a wide range of conditions. Nonetheless, these experiments have not dealt with production of radiolysis products at surfaces, thus more work is required in this area.
5. Studies of the effect of H_2 on the dissolution of spent fuel and on α-doped UO_2 show significant reductions in the dissolution rate relative to oxidising conditions, in addition to reductions in the concentrations of molecular radiolytic oxidants in solution, suggesting that surface reactions involving H_2 may be important in suppressing surface oxidation. How this occurs is not understood and should be focused on in future studies.
6. Experimental studies of the effects of alpha radiolysis of water on UO_2 dissolution under anoxic conditions using α-doped UO_2 suggest that there is a threshold below which the effects on dissolution rate are undetectable. This aspect is not taken into account in the proposed MAM model. The range of this threshold value has to be evaluated according to environmental characteristics.

7. A matrix alteration model (MAM) that has a strong mechanistic basis has been developed and tested. The model uses radiolytic rate equations to calculate oxidant concentrations in solution as a function of time, for reference groundwater conditions for granite, clay and salt repositories, including an H_2 pressure of 3 bars and considering the decline of the dose rate as the fuel decays. The time-dependent concentrations are then used to calculate matrix dissolution rates as a function of time. Uncertainties in the reactive fuel surface area, radiolytic yields and evolution of solution chemistry (including corrosion products, clay and H_2 concentrations) should be further explored in order to improve this model.

Concerning spent fuel performance:

8. For the rapid release of activity, a synthesized table gives the evolution of the RN inventories in the various microstructure (gap, rim grains, rim pores, grain boundaries) as a function of time so that every end-users can decide which is to be associated to the IRF.
9. Fractional matrix dissolution rates calculated with the MAM are in the range of 3×10^{-5} yr^{-1} at the presumed time of container breaching (1000 years), gradually decreasing to 1×10^{-6} yr^{-1} at 10^5 years. Experimental data from various studies using spent fuel and α-doped UO_2 with H_2 overpressures suggest that the dissolution rates may be in the range of 10^{-6} yr^{-1} to 10^{-8} yr^{-1}, and it is not possible at present to comment on time-dependence of the rate.
10. An integrated model of spent fuel dissolution combining the IRF model and the MAM has been used to illustrate the time-dependent release of radionuclides from a container of spent fuel. The model illustrates the relative importance of various fuel-related processes involved in dissolution and retention of radionuclides.
11. Overall, the potential for spent fuel to confine radionuclides is good for low to moderate burnup fuels, in particular, work on hydrogen effects has good potential to confirm the good performance of this material as a waste form. For high burnup and MOX fuels, much work remains to be done to further examine the pessimistic assumptions of the IRF model.

7. List of Deliverables

Fifteen deliverables were planned within the SFS project and these correspond to all the reports describing the major achievements of the project. The content and status of the deliverables are summarised here below (status July 2005):

Deliverable No[1]	Deliverable title	Scientific Content	planned date / delivery date	Reference	Nature [2] and dissemination [3]
D1	Report on the statistical evaluated data set predicting the Instant Release Fraction at the initial time IRF(t=0)	synthesises all the available data on the anticipated initial instant release fraction based on the leaching data and the post irradiation examination	Jul.03 / Nov.04	Nagra report NTB 04-08, Johnson et al. (2004)	Re,Da PU
D2	Synthesis report on the relevant diffusion coefficients.	Synthesises the existing data on the Fickian diffusion within spent nuclear fuel and proposes some theoretical development on the so-called alpha self irradiation enhanced diffusion in order to estimate the potential range of magnitude of this process along time	Oct.02 / oct.03	CEA report CEA-R-6039, Lovera et al. (2003)	Re,Da, Th PU
D3	Model predicting the evolution of the IRF as a function of time.	describes the general model of instant release fraction developed within SFS with the various options and give some quantitative assessment for UOX and MOX fuels.	Jul.04 / mid-05	paper *in press*, Journal of Nuclear Materials, Johnson et al. (2005)	Re,Si PU
D4	Report on radiolysis products in brines : Data and model with key parameters.	gathers the experimental data obtained within the SFS/WP2 on the radiolysis of brines and presents the kinetic model developed from these data	Oct.03 / April04	FZK report FZKA 6977, Kelm & Bohnert (2004)	Re,Da,Si PU
D5	Report on radiolysis products in CO_2 rich solutions, Data and Model	synthesised all the experimental data obtained on the radiolysis of carbonate-rich solutions	Oct.03 / mid-2005	SUBATECH report under publication	Re,Da,Si PU

[1] Deliverable numbers in order of delivery dates: D1 – Dn

** Additional deliverables not included in this list are semi-annual, annual and final project reports. Deliverables denoted in work package description denote both deliverables of this list (D1-5) and progress reports

[2] Please indicate the nature of the deliverable using one of the following codes:

Re = Report **Da** = Data set **Eq** = Equipment
Pr = Prototype **Si** = Simulation **Th** = Theory
De = Demonstrator **Me** = Methodology **O** = other (describe in annex)

[3] Please indicate the dissemination level using one of the following codes:

PU = Public
RE = Restricted to a group specified by the consortium (including the Commission Services).
CO = Confidential, only for members of the consortium (including the Commission Services).

D6	Report on the solid and solution alteration induced by He^{2+} (alpha) beam radiolysis at UO_2/H_2O interface	Paper describing and comparing the results obtained by external irradiation of UO_2 and addition of H_2O_2.	Oct.03 /	Paper under review, J. Nucl. Mater., Corbel et al. (2005)	Re PU
D7	Report on the radiolytic species important for the UO_2 oxidation in chloride and in carbonate containing solution including best estimates of rate constants obtained from fitting experiments and model.	Report on the radiolytic species important for the UO_2 oxidation in chloride containing solution including best estimates of rate constants obtained from fitting experiments and model.	Feb.04	Studsvik report Studsvik/N-04/14, Christensen et al (2004a)	Re,Si PU
		Calculation of corrosion rates of α-doped UO_2	Jun.04	Studsvik report Studsvik/N-04/91, Christensen et al (2004b)	Re,Si PU
D8	Report about modelling of heterogeneous systems.		June 04 / oct.03	Studsvik report Studsvik/N-03/027, Christensen et al. (2003)	Re,Si PU
D9	Report on the relation between the irradiation field and the corrosion rate	Synthesises the interpretation of the experimental data acquired within the project and published in the literature in terms of relation between the residual alpha activity and the alteration rate	Oct.03 / mid-05	Cachoir et al. (2005), JRC-ITU-SCA-2005/01 technical report.	Re PU
D10	Report on the effect of hydrogen on fuel corrosion rates	Synthesises the experimental data acquired on the H2 competing effect on fuel alteration and assess the potential origin of this strong influence.	Oct.03 / mid-05	Carbol et al. (2005) SKB technical report TR-05-09,	Re PU
D11	Synthesis of radiolysis and competing hydrogen effects	*Report cancelled at the mid-term meeting*			
D12	Report on the conceptual model for matrix alteration	Describes the phenomenology of fuel alteration in geological repository and the approach followed to model it in the matrix alteration model. Details are given on relevant boundary conditions and parameters to consider	May.03 / Jan.04	ENRESA unpublished report, Martinez-Esparza et al. (2004a)	Re PU
	Report on environmental boundary conditions	Describes the boundaries conditions, relevant for European countries, for identification of the processes involved in SNF radionuclides release	Aug. 03 / Aug.05	Andriambololona Z. & Johnson Andra report C NTASCM 05-0008	Re PU

D13	Report on the integrated matrix alteration model including radiolysis, competing effects of hydrogen, electrochemical dissolution and solubility control	Describes the development of the matrix alteration model focusing in particular on the calibration of the parameters based on the available experimental data. Base case calculations in granite, salt and clay case are also presented.	May 04 / Aug.04	ENRESA unpublished report, Martinez-Esparza et al. (2004b)	Re PU
D14	Report on the applicability of the model to experimental data	Describes the sensitivity analyses of the matrix alteration model and the comparison with the available experimental data.	Sept.04 / Nov.04	ENRESA unpublished report, Martinez-Esparza et al. (2004c)	Re PU
D15	Synthesis report on the spent fuel stability in a geological repository	Assess the spent fuel performance in repository based on the models developed within the SFS project for clay, granite and salt environment.	Oct.04 / April 05	NAGRA report, NTB 04-09 (2005)	Re PU

In addition to these contract deliverables, other reports have been prepared and issued during the project and are available to any SFS partners:

- **WP4**: The results and conclusions of the literature review on modelling has been published as Modelling spent Fuel and HLW Behaviour in Repository Conditions. A review of the State of the art. ENRESA Technical Publication08/2002 (A.Martínez-Esparza et al, 2002)
- **WP4**: AVILA.Workshop Proceedings (April 2003) ENRESA-CIEMAT. CIEMAT. Proceedings collections. ISBN. 84-7834-440-3(J.Quiñones/A.Martinez-Esparza)
- **WP4**: Boundary conditions presented by ANDRA/NAGRA (Andriambolona and Johnson) were given in a draft technical note entitled: *"The environmental boundary conditions for the evaluation of the spent fuel matrix dissolution"*. The results of the discussion on this draft on boundary conditions are included as reference case boundary conditions in ENRESA Public report TEPUB N° 1.2005.
- **WP4**: an ENRESA technical report synthesising the D12, D13 and D14 was published as ENRESA Publicacion tecnica 01/2005.(Martinez-Esparza et al, March 2005)

8. Dissemination and Use of the Results

8.1 DISSEMINATION DURING THE FIRST YEAR OF THE PROJECT (2002)

Several presentations have been given in workshops or conferences during the first year of the project :

- The Coordinator gave an overview presentation of the status of the project at the Spent Fuel Workshop organized by the CEA in Avignon, 24th-25th September 2002. The presentation has been integrated in the workshop proceedings.
- The coordinator gave also an overview of the SFS status at the annual meeting of the In Can Processes project in Gothenburg, 2nd September.
- Several technical presentations have been made at the Spent Fuel Workshop on dedicated aspects of the SFS project:
    - V.V. Rondinella, J. Cobos-Sabate, α–doped UO_2 studies;
    - D.H. Wegen, T. Gouder, M. Eckle, Fuel corrosion investigation by electrochemical techniques;
    - C. Poinssot, P. Lovera, L. Johnson, Definition of a modelling approach able to define the IRF as a function of time;
    - A. Loida, Overview on high burnup spent fuel dissolution studies at FZK/INE;
    - K. Spahiu, Results on the influence of hydrogen on spent fuel leaching;
    - K. Lemmens, Preliminary results of static and dynamic dissolution tests with α doped UO_2 in Boom Clay conditions;
    - C. Corbel, E. Mendès, Studies of the behavior of UO_2 / water interfaces under He^{2+} beam;
    - M. Kelm, Behavior of Pu-doped pellets in brines;
    - T. Lundstrom, UO_2 dissolution and the effect of radiolysis;
    - J. Mérino, E. Cera, J. Bruno, Radiolytic modelling of short term spent fuel dissolution experiments;
- Some presentations have been presented at the Scientific Basis for Nuclear Waste Management MRS meeting in December 2002 in Boston and will be published in the MRS proceedings:
    - D. Cui, J. Devoy, Surface precipitation during the leaching of spent fuel;
    - Influence of plutonium on the dissolution behaviour of the spent fuel matrix. J. Cobos, T. Wiss, T. Gouder, V. Rondinella.
    - J. Mérino, E. Cera, J. Bruno, Building confidence in radiolytic modelling: application to spent fuel dissolution experiments.
    - C. Poinssot, P.Lovera, P. Toulhoat, JP. Piron, JM. Gras, Anticipated long term evolution of spent nuclear fuel: consequences on the release rate of radionuclides in long term storage and geological disposal.

8.2 DISSEMINATION DURING THE SECOND YEAR OF THE PROJECT (2003)

- Several papers have been prepared and presented at the MRS conference "Scientific basis for nuclear waste management" XXVI held in Kalmar (Sweden) in June 2003:
    - C. Ferry, P. Lovera, C. Poinssot, L. Johnson (2003), Quantitative assessment of instant release fraction (IRF) for fission gases and volatile elements as a function of burnup and time under geological disposal conditions. Scientific Basis for Nuclear Waste

Management XXVII, vol. 807, Mat. Res. Soc. Symp. Proc., V. M. Oversby y L. O. Werme, Eds.: Materials Research Society, 2004, pages 35-40

- J. de Pablo I. Casas, J. Giménez, F. Clarens, L. Duro and J. Bruno (2003), The oxidative dissolution mechanism of uranium dioxide.the effect of pH and oxygen partial pressure. Scientific Basis for Nuclear Waste Management XXVII, vol. 807, Mat. Res. Soc. Symp. Proc., V. M. Oversby y L. O. Werme, Eds.: Materials Research Society, 2004, pages 83-88.
- J. Merino, E. Cera, J. Bruno and A. Martínez-Esparza, Modelling the release of radionuclides from the spent fuel and their transport in the near field: a coupled approach. Scientific Basis for Nuclear Waste Management XXVII, vol. 807, Mat. Res. Soc. Symp. Proc., V. M. Oversby y L. O. Werme, Eds.: Materials Research Society, 2004, pages 785-790.
- J. Quiñones, J. Cobos, P. P. Díaz Arocas y V. V. Rondinella, modelling of the $(U_{(1\ y)}{}^{238}Pu_y)O_{2+x}$ leaching behaviour in deionised water under anoxic conditions, Scientific Basis for Nuclear Waste Management XXVII, vol. 807, Mat. Res. Soc. Symp. Proc., V. M. Oversby y L. O. Werme, Eds.: Materials Research Society, 2004, pp. 409-414.

- Conference ICEM 2003, Oxford, Sept.2003:
  - J. Quiñones, J. Merino, E. Cera, J. Bruno, A. Martinez-Esparza (2003), A radiolytic modelling intercomparison exercise: influence of alpha radiation on spent fuel alteration process.
  - V. Rondinella, T.Wiss, J.P. Hiernaut (2003), Studies on Spent Fuel Alteration During Storage and Radiolysis effects on Corrosion behaviour Using alpha doped UO_2.

- Conference MIGRATION 2003, Gyeongju, Sept.2003:
  - B. Grambow, T. Mennecart, M. Fattahi, G. Blondiaux (2003), Electrochemical aspects of radiolytically enhanced UO_2 dissolution.
  - K. Spahiu, J. Devoy, D. Cui, M. Lundstrom (2003) The reduction of U(VI) by near-field hydrogen in the presence of UO_2(s)
  - T. Mennecart, M. Fattahi, B. Grambow, Z. Andriambololona (2003), Effect of alpha radiolysis on doped UO_2 dissolution under reducing conditions.

- Conference PLUTONIUM SCIENCES 2003:
  - J. Cobos, T. Wiss, T. Gouder, V.V. Rondinella. (2003), influence of plutonium on the dissolution behaviour of the spent fuel matrix

8.3 DISSEMINATION FROM THE THIRD YEAR OF THE PROJECT (2004)

- Spent Fuel Workshop 2004, Lake Forrest, April.2004:
  - Major Outcomes of the European Union Project on Spent Fuel Stability in Repository Conditions, C. Poinssot
  - Dissolution tests with α-doped UO_2 in Boom Clay conditions: Results from static and dynamic tests, K.Lemmens.
  - Estimate of Self-Irradiation Enhanced Diffusion Coefficients in Spent Nuclear Fuel, C. Ferry.
  - Evaluation of the IRF as a Function of Burnup for PWR and BWR UO2 and MOX Fuel, L. Johnson.
  - The Fate of Radiolytic Oxidants During Spent Fuel Leaching in the Presence of Hydrogen, K. Spahiu.
  - Gamma Radiolysis of Chloride Brine under Pressure with No Gas Phase Allowed, M. Kelm.

- Calibration and Validation of a Radiolytic Model to Describe the Oxidative Dissolution of the Spent Fuel, J. Merino.

- Several papers have been prepared and presented at the MRS conference "Scientific basis for nuclear waste management" XXVIII held in San Francisco (USA) in April 2004:
  - J. Quiñones, J. M. Cobo, A. González de la Huebra y A. Martínez Esparza, experimental study about the influence of the γ dose on the spent fuel dissolution in presence of H_2 atmosphere, Scientific Basis for Nuclear Waste Management XXVIII, vol. 824, Mat. Res. Soc. Symp. Proc., S. Stroes-Gascoyne, J. Hanchar y L. Browning, Eds. San Francisco. USA: Material Research Society, 2004, pp. 153-158.
  - J. Quiñones, A. GONZÁLEZ DE LA HUEBRA Y A. MARTÍNEZ ESPARZA, "Coprecipitation experiments of simulated spent fuel solution in presence of metallic iron in synthetic bentonitic-granitic water under oxidising conditions,", pp. 425-430.
  - M. Kelm, E. Bohnert, radiolytic corrosion of 238Pu doped UO2 pellets in 5M NaCl solution
  - V. Rondinella, J. Cobos, T. Wiss, leaching behaviour of low activity alpha-doped UO_2.

- Several papers presenting some findings of the SFS project are published or in press in high-quality scientific journals:
  - J. Quiñones, A. González de la Huebra y A. Martínez Esparza, "Effect of corroded engineering barrier on the alteration process of the spent fuel matrix under repository conditions," *Geochimica et Cosmochimica Acta*, vol. 68, pp. 113, 2004.
  - J.Merino, E.Cera, J.Bruno, J. De Pablo, J. Quinones, A. Martinez (2005), radiolytic modelling of spent fuel oxidative dissolution mechanism. Calibration with UO_2 dynamic leaching experiments, J. Nucl. Mat., *in press*.
  - L. Johnson, C. Ferry, C. Poinssot, P. Lovera (2005), Spent fuel radionuclides source term model for assessing spent fuel performance in geological disposal. Part I: Assessment of the Instant Release Fraction, J. Nucl. Mat., *in press*.
  - M. Kelm, E. Bohnert, (2005), gamma radiolysis of brines: effect of dissolved hydrogen radiolytic gases on the radiolytic yield of long lived products, J. Nucl. Mat., *in press*.
  - Corbel, C., Sattonnay G., Guilbert, S., Garrido, F. , Barthe, M.F. ,Jegou, C. (2005). Addition versus radiolytic production effects of hydrogen peroxide on aqueous corrosion of UO_2. J. Nucl. Mat., *in press.*

- Finally, several papers will be presented at the MRS conference "Scientific basis for nuclear waste management" XXIX which will be held in Ghent (Belgium) in September 2005:
  - C.Poinssot, C. Ferry, B. Grambow, M. Kelm, K. Spahiu, A. Martinez, L. Johnson, E. Cera, J. de Pablo, J. Quinones, D. Wegen, K. Lemmens, T. McMenamin, Mechanisms governing the release of radionuclides from spent nuclear fuel in geological repository: major outcomes of the European Project SFS.
  - Quiñones J., Iglesias E., Martínez-Esparza A., Merino J., Cera E., Bruno J., de Pablo J., Casas I., Giménez J., Clarens F., Rovira M., (2005), Mat. Res. Soc. Symp. Proc, Scientific Basis for Nuclear Waste Management XXIX, in press (this issue).
  - A. POulesquen, C. Jégou, Influence of alpha radiolysis of water on UO2 matrix alteration, Chemical/Transport Model.
  - C. Cachoir, S. Salah, K. Lemmens and N. Maes, Static dissolution tests of alpha-doped UO2 under repository relevant conditions: Influence of Boom Clay and alpha-activity on fuel dissolution rates.
  - de Pablo J., Clarens F., Casas I., Giménez J., Rovira M., Role of hydroxyl radicals during oxidative dissolution of UO2 by hydrogen peroxide.
  - Poulesquen A., Jégou C., Determination of alpha dose rate profile at the UO2/water interface.
  - Metz V., Loida A., Kienzler B., Reaction path modelling of spent fuel corrosion in Brines: comparison with experimental results

With more that 25 oral presentations in international conferences, more than 15 oral presentations in international workshops and already 5 papers published, the dissemination of the results of the SFS project

was quite successful. Most of the results and findings have already been transferred to the concerned scientific community and the new EU project (in particular 6th FWP NFPRO). Dissemination of results will last well beyond the formal timeframe of the project since several papers are still in preparation. This view is therefore obviously partial.

9. Management and Co-ordination Aspects

The SFS project was headed by the CEA projects leader of the "high level waste conditioning, storage and disposal" domain: prof. Pierre TOULHOAT was therefore the project official coordinator from Nov.01 up to Sept.02. Dr. Jean-Marc CAVEDON replaced him and act as project official coordinator up to the end of the project. The day-to-day management and scientific coordination was ensured by Dr. Christophe POINSSOT with the support of a Management Committee consisting of Jean-Marc CAVEDON, Christophe POINSSOT and Bernd GRAMBOW (ENSTIMN and ARMINES). Each individual Work Package had a Technical Manager who was responsible for all scientific aspects of the work and reports to the Coordinator.

9.1 PROJECT MEETINGS

The project was managed with the aim of minimizing the meetings which are always time and money consuming. Therefore, the number of general meetings was restricted to the annual meeting and the mid-term meeting was merged with the allowance of the European Commission with the second year annual meeting. The following sections detail the specific SFS meetings held during the 3 years of the project. Nevertheless, one has to mention that all the partners agree that the success of such a project relies on the actual synergies, exchanges and collaborative works implemented between the partners, which require anyhow regular and frequent contacts. In that sense, the partners regret that financial consideration restrict their possibility to go deeper in the collaboration between partners from different countries, although most of the partners decided to spend much more for travel expenses on their own funding.

9.1.1 FIRST YEAR OF THE PROJECT: NOV01 – OCT02.

The following meetings were held between November 2001 and 2002:

- **Coordination meeting**: 16th and 17th May 2002, Madrid, attended by WP leaders and coordination team.
- **Annual meeting**: 7th-8th October 2002, Karlsruhe (Germany), attended by all participants and EC coordinator.
- **WP1 meetings**: 23rd May 2002 in Wettingen (Switzerland) and 7th November 2002 in Saclay (France), attended by CEA and NAGRA.
- **WP2 meetings**: 22nd March 2002 in Karlsruhe (Germany), attended by CEA, SUBATECH and KFZ-INE.
- **WP3 meeting**: 4th-5th February 2002 in Karlsruhe (Germany), attended by SKB, ITU, SUBATECH, ENRESA, ENVIROS, CIEMAT, UPC, INE, SCK-CEN.
- **WP4 meetings**: 5th February 2002 in Karlsruhe (Germany), attended by ENVIROS, ENRESA, CIEMAT, ITU, SUBATECH, SKB, ANDRA and FZK and Avila workshop (Spain) attended by all participants.

9.1.2 SECOND YEAR OF THE PROJECT: NOV02 – OCT03.

- **WP4 meeting**: 4th February in Madrid (Spain), attended by ENRESA, UPC, ENVIROS, CEA, SUBATECH, ANDRA, KFZ-INE, ITU.

- **Mid term meeting**: 20th – 21th May in Paris (France), attended by all partners;

- **Annual meeting**: 15th – 17th October in Cambrils (Spain), attended by all partners and the EC coordinator (T. McMenamin);

9.1.3 THIRD YEAR OF THE PROJECT: NOV03 – OCT04.

- **WP4 meeting**: 11th February in Madrid (Spain), attended by CEA, SUBATECH, ANDRA, FZK, ITU, SKB, SCK-CEN, ENVIROS, UPC, CIEMAT.

- **Annual and final meeting**: 8th – 10th September in Wettingen (Swizerland), attended by every partners;

9.2 5TH FRAMEWORK CLUSTERING

The 5th Framework Program "Rates and mechanisms of radioactive release and retention inside a waste disposal canister" (In Can Processes), with 9 Partners and coordinated by AEA Technology plc., was also working on the spent fuel alteration in geological disposal conditions up to Sept.03. This project has 6 work packages aiming to

(i) measure the actual rate of UO_2 dissolution in oxidizing and reducing conditions,
(ii) measure the effect of α radiolysis on the actual dissolution rate in oxidizing and reducing conditions by the mean of α doped material,
(iii) measure the actual rate of spent fuel dissolution in oxidizing and reducing conditions,
(iv) determine whether U^{VI} can be reduced to U^{IV} in repository conditions,
(v) determine whether Np^{V} can be reduced lower oxidation state in repository conditions,
(vi) model the previous results and reevaluate thermodynamic data used for spent fuel PA studies.

In Can Processes and SFS were closely related and representatives from each program have attended the progress meetings of the other program. Therefore, M. Cowper attended the SFS kick-off meeting in Paris (15th January 2002), the 1st annual meeting in Karlsruhe (7th-8th October 2002). K Spahiu represented the SFS project at the In Can Processes Mid-Term Meeting in Stockholm (March 2002) and final meeting in Kalmar (June 2003) while C. Poinssot attended the 2nd annual meeting in Gothenburg (2nd September 2002). We have also to mention that K. Ollila attended the Avila workshop as a In Can Processes representative.
Finally, SFS and ICP submits a common paper at the next EURADWASTE 2004 conference on the general outputs of both projects in the field of spent fuel long term alteration in geological disposal and related radionuclides releases.

9.3 TIP

The TIP is completed and given to the Commission independently of this report.

9.4 STATUS OF THE BUDGETS

A synthetic view of yearly and cumulative budget overall the project is given in Table 14. Overall, the cumulative budget spent in Year 3 by all the partners was 1 079 140 € against an original yearly budget of 885,652 €, i.e. a significant increase of roughly 22%. Most of this increase is related to a larger implication of the partners than initially planned in order to reach the objectives and therefore a larger personal and overhead costs. Hence, CEA, ENSTIMN, ITU, NAGRA, SCK-CEN CIEMAT and UPC overspent their personnel costs. This situation has to be related overall to the complexity of the technical problems addressed by the project which were probably underestimated and that required from the partners a significant effort at the end of the project to derive from the results obtained reliable conclusions. In addition, several unplanned tasks were included within the project during its course on the partner's own funding in order again to successfully reach the objectives. That's the case for example of the additional work performed by CIEMAT with alpha doped material and modelling exercise with the three reference geological medium.

The significance of the conclusions driven at the end of the project and their obvious influence both on future R&D and spent fuel performance assessment in geological repository confirm a posteriori the relevance of this supplementary effort.

The cumulative budget since the beginning represents 3 217 737 €, i.e. 118% of the initial total budget of the project.

Partner	COST CATEGORY	ORIGINAL BUDGET (Euros)	ACTUAL COSTS (Euros) Year 1	Year 2	Year 3	Total	TOTAL PERCENTAGE SPEND Year 1	Year 2	Year 3	Difference planned/realised (Euros)
CEA	Labour	195156	72530,92	69864	91853	234247,9	37%	73%	120%	-39091,92
	Overheads	193837	67474,22	71973	98489	237936,2	35%	72%	123%	-44099,22
	Labour + Overheads	388993	140005,1	141837	190342	472184,1	36%	72%	121%	-83191,14
	Travel	16100	8139,16	9868	1840	19847,16	51%	112%	123%	-3747,16
	Durable Equipment	0	0	0	0	0	0%	0%	0%	0
	Consumables	0	0	0	0	0	0%	0%	0%	0
	Subcontracts	0	0	0	0	0	0%	0%	0%	0
	Other	0	0	0	0	0	0%	0%	0%	0
	Total	405093	148144,3	151705	192182	492031,3	37%	74%	121%	-86938,3
ARMINES	Labour	54829	0	27455,48	0	27455,48	0%	50%	50%	27373,52
	Overheads	43863	0	21963,57	0	21963,57	0%	50%	50%	21899,43
	Labour + Overheads	98692	0	49419,05	0	49419,05	0%	50%	50%	49272,95
	Travel	10000	0	2669,96	3036	5705,96	0%	27%	57%	4294,04
	Durable Equipment	0	0	0	0	0	0%	0%	0%	0
	Consumables	0	3158,38	0	0	3158,38	0%	0%	0%	-3158,38
	Subcontracts	0	0	0	0	0	0%	0%	0%	0
	Other	0	0	0	0	0	0%	0%	0%	0
	Total	108692	3158,38	52089,01	3036	58283,39	3%	51%	54%	50408,61
ENSTIMN	Labour	28826	27455,48	27455,48	32390	87300,96	95%	190%	303%	-58474,96
	Overheads	23060	21963,57	21963,57	25914	69841,14	95%	190%	303%	-46781,14
	Labour + Overheads	51886	49419,05	49419,05	58304	157142,1	95%	190%	303%	-105256,1
	Travel	2500	4356,1	1436,34	3036	8828,44	174%	232%	353%	-6328,44
	Durable Equipment	0	0	0	0	0	0%	0%	0%	0
	Consumables	10000	6867,03	0	0	6867,03	69%	69%	69%	3132,97
	Subcontracts	0	0	0	0	0	0%	0%	0%	0
	Other	0	0	0	0	0	0%	0%	0%	0
	Total	64386	60642,18	50855,39	61340	172837,6	94%	173%	268%	-108451,57
ANDRA	Labour	90636	30560,6	35441	33233,2	99234,8	34%	73%	109%	-8598,8
	Overheads	106704	35978,4	41724	39124,8	116827,2	34%	73%	109%	-10123,2
	Labour + Overheads	197340	66539	77165	72358	216062	34%	73%	109%	-18722
	Travel	24700	4936,3	1343,73	6521,21	12801,24	20%	25%	52%	11898,76
	Durable Equipment	0	0	0	0	0	0%	0%	0%	0
	Consumables	0	0	0	0	0	0%	0%	0%	0
	Subcontracts	0	0	0	0	0	0%	0%	0%	0
	Other	0	0	0	0	0	0%	0%	0%	0
	Total	222040	71475,3	78508,73	78879,21	228863,2	32%	68%	103%	-6823,24
ENRESA	Labour	56071	19358	14026	22688	56072	35%	60%	100%	-1
	Overheads	81162	28014	20304	32845	81163	35%	60%	100%	-1
	Labour + Overheads	137233	47372	34330	55533	137235	35%	60%	100%	-2
	Travel	11232	6399	2083	5046	13528	57%	76%	120%	-2296
	Durable Equipment	0	0	0	0	0	0%	0%	0%	0
	Consumables	0	0	0	0	0	0%	0%	0%	0
	Subcontracts	0	0	0	0	0	0%	0%	0%	0
	Other	0	0	0	0	0	0%	0%	0%	0
	Total	148465	53771	36413	60579	150763	36%	61%	102%	-2298
FZK	Labour	230521	68163,03	87848	77567	233578	30%	68%	101%	-3057,03
	Overheads	165263	49831,9	62444	51129	163404,9	30%	68%	99%	1858,1
	Labour + Overheads	395784	117994,9	150292	128696	396982,9	30%	68%	100%	-1198,93
	Travel	4196	4284,81	0	0	4284,81	102%	102%	102%	-88,81
	Durable Equipment	0	0	0	0	0	0%	0%	0%	0
	Consumables	0	0	0	0	0	0%	0%	0%	0
	Subcontracts	0	0	0	0	0	0%	0%	0%	0
	Other	0	0	0	0	0	0%	0%	0%	0
	Total	399980	122279,7	150292	128696	401267,7	31%	68%	100%	-1287,74
ITU	Labour	296410	89613,59	172424,5	113177	375215,1	30%	88%	127%	-78805,13
	Overheads	275594	80275,7	159832,3	93015	333123	29%	87%	121%	-57529
	Labour + Overheads	572004	169889,3	332256,8	206192	708338,1	30%	88%	124%	-136334,13
	Travel	11500	4499,68	5190,63	579	10269,31	39%	84%	89%	1230,69
	Durable Equipment	49974	13571,94	19233,5	27726	60531,44	27%	66%	121%	-10557,44
	Consumables	36122	8662,31	23298,5	0	31960,81	24%	88%	88%	4161,19
	Subcontracts	0	0	0	0	0	0%	0%	0%	0
	Other	0	0	0	7626	7626	0%	0%	0%	-7626
	Total	669600	196623,2	379979,5	242123	818725,7	29%	86%	122%	-149125,69

SKB	Labour	37397	9349,2	11619,72	15582	36550,92	25%	56%	98%	846,08
	Overheads	29918	7480	9295,76	12467	29242,76	25%	56%	98%	675,24
	Labour + Overheads	67315	16829,2	20915,48	28049	65793,68	25%	56%	98%	1521,32
	Travel	7500	2500	4007	2747	9254	33%	87%	123%	-1754
	Durable Equipment	0	0	0	0	0	0%	0%	0%	0
	Consumables	0	0	0	0	0	0%	0%	0%	0
	Subcontracts	0	0	0	0	0	0%	0%	0%	0
	Other	0	0	0	0	0	0%	0%	0%	0
	Total	74815	19329,2	24922,48	30796	75047,68	26%	59%	100%	-232,68
NAGRA	Labour	44982	14263	14307,86	24190	52760,86	32%	64%	117%	-7778,86
	Overheads	35985	11312	11446,4	19270	42028,4	31%	63%	117%	-6043,4
	Labour + Overheads	80967	25575	25754,26	43460	94789,26	32%	63%	117%	-13822,26
	Travel	10000	2405	2335,46	2200	6940,46	24%	47%	69%	3059,54
	Durable Equipment	0	0	0	0	0	0%	0%	0%	0
	Consumables	0	0	0	0	0	0%	0%	0%	0
	Subcontracts	16000	0	0	15050	15050	0%	0%	94%	950
	Other	0	0	0	0	0	0%	0%	0%	0
	Total	106967	27980	28089,72	60710	116779,7	26%	52%	109%	-9812,72
SCK	Labour	91591	25243,23	40131,18	50333	115707,4	28%	71%	126%	-24116,41
	Overheads	73272	20193,21	32104,54	39266	91563,75	28%	71%	125%	-18291,75
	Labour + Overheads	164863	45436,44	72235,72	89599	207271,2	28%	71%	126%	-42408,16
	Travel	5000	984,48	1229,41	1229	3442,89	20%	44%	69%	1557,11
	Durable Equipment	0	0	0	0	0	0%	0%	0%	0
	Consumables	29706	5141,74	5803,43	8490	19435,17	17%	37%	65%	10270,83
	Subcontracts	0	0	0	0	0	0%	0%	0%	0
	Other	0	0	0	0	0	0%	0%	0%	0
	Total	199569	51562,66	79268,56	99318	230149,2	26%	66%	115%	-30580,22
CIEMAT	Labour	66014	52785,06	54683,45	29970	137438,5	80%	163%	208%	-71424,51
	Overheads	76545	61218,72	58283,52	31167	150669,2	80%	156%	197%	-74124,24
	Labour + Overheads	142559	114003,8	112967	61137	288107,8	80%	159%	202%	-145548,75
	Travel	12780	3300,34	3186,74	4697	11184,08	26%	51%	88%	1595,92
	Durable Equipment	0	0	0	0	0	0%	0%	0%	0
	Consumables	0	0	0	0	0	0%	0%	0%	0
	Subcontracts	0	0	0	0	0	0%	0%	0%	0
	Other	0	0	0	0	0	0%	0%	0%	0
	Total	155339	117304,1	116153,7	65834	299291,8	76%	150%	193%	-143952,83
UPC	Labour	17801	7477,57	7157,2	5228	19862,77	42%	82%	112%	-2061,77
	Overheads	14241	5981,43	5724,6	4183	15889,03	42%	82%	112%	-1648,03
	Labour + Overheads	32042	13459	12881,8	9411	35751,8	42%	82%	112%	-3709,8
	Travel	6000	2753,32	1651,17	1388	5792,49	46%	73%	97%	207,51
	Durable Equipment	0	0	0	0	0	0%	0%	0%	0
	Consumables	0	0	0	0	0	0%	0%	0%	0
	Subcontracts	0	0	0	0	0	0%	0%	0%	0
	Other	0	0	0	0	0	0%	0%	0%	0
	Total	38042	16212,32	14532,97	10799	41544,29	43%	81%	109%	-3502,29
ENVIROS	Labour	60826	21900,15	16858,53	22013	60771,68	36%	64%	100%	54,32
	Overheads	9787	3525,48	2677,53	3575	9778,01	36%	63%	100%	8,99
	Labour + Overheads	70613	25425,63	19536,06	25588	70549,69	36%	64%	100%	63,31
	Travel	12450	4150	4150	4150	12450	33%	67%	100%	0
	Durable Equipment	0	0	0	0	0	0%	0%	0%	0
	Consumables	0	0	0	0	0	0%	0%	0%	0
	Subcontracts	0	0	0	0	0	0%	0%	0%	0
	Other	0	0	0	0	0	0%	0%	0%	0
	Total	83063	29575,63	23686,06	29738	82999,69	36%	64%	100%	63,31
STUDSVIK	Labour	24930	7737	9441	7736	24914	31%	69%	100%	16
	Overheads	20622	6409	7820,4	6409	20638,4	31%	69%	100%	-16,4
	Labour + Overheads	45552	14146	17261,4	14145	45552,4	31%	69%	100%	-0,4
	Travel	3600	1318	1317,19	965	3600,19	37%	73%	100%	-0,19
	Durable Equipment	0	0	0	0	0	0%	0%	0%	0
	Consumables	0	0	0	0	0	0%	0%	0%	0
	Subcontracts	0	0	0	0	0	0%	0%	0%	0
	Other	0	0	0	0	0	0%	0%	0%	0
	Total	49152	15464	18578,59	15110	49152,59	31%	69%	100%	-0,59
TOTAL	**Labour**	**1295990**	**446436,8**	**588713,4**	**525960,2**	**1561110**	34%	80%	120%	-265120,47
	Overheads	**1149853**	**399657,6**	**527557,2**	**456853,8**	**1384069**	35%	81%	120%	-234215,62
	Labour + Overheads	**2445843**	**846094,5**	**1116271**	**982814**	**2945179**	35%	80%	120%	-499336,09
	Travel	**137558**	**50026,19**	**40468,63**	**37434,21**	**127929**	36%	66%	93%	9628,97
	Durable Equipment	**49974**	**13571,94**	**19233,5**	**27726**	**60531,44**	27%	66%	121%	-10557,44
	Consumables	**75828**	**23829,46**	**29101,93**	**8490**	**61421,39**	31%	70%	81%	14406,61
	Subcontracts	**16000**	**0**	**0**	**15050**	**15050**	0%	0%	94%	950
	Other	**0**	**0**	**0**	**7626**	**7626**	#DIV/0!	#DIV/0!	#DIV/0!	-7626
	Total	**2725203**	**933522,1**	**1205075**	**1079140**	**3217737**	34%	78%	118%	-492533,95

Table 3: synthesis of the budget status for each partner of the SFS project.

10. References

ALLEN A.O., HOCHANADEL C.J.,. GHORMLEY, J.A, DAVIS T.W (1956)., J. Phys. Chem., 56, 575.

ALLEN G.C. AND TYLER J.W., (1986), Surface Characterisation of α-U_3O_7 using X-ray photoelectron spectroscopy. J. Chem. Soc., Faraday Trans. 1, 82, 1367-1379.

ALTMAIER, M., METZ, V., NECK, V., MÜLLER, R., FANGHÄNEL, T. (2003). Solid-liquid equilibria of $Mg(OH)_2$(cr) and $Mg(OH)_3Cl{:}4H_2O$(cr) in the system Mg-Na-OH-Cl-H_2O at 25°C. Geochimica et Cosmochimica Acta 67, 3595-3601.

ANDRIAMBOLOLONA Z. AND JOHNSON, (2003). The environmental boundary conditions for the evaluation of spent fuel matrix dissolution. Technical Note for WP4 in the framework of the EU project SFS, *Andra C NT ASCM 05-008*.

BRUNO J., CERA E., DURO L., ERIKSEN T.E. AND WERME L.O., (1996). A Kinetic Model for the Stability of Spent Nuclear Matrix under Oxic Conditions. J. of Nuclear Materials Vol. 238, 110-120.

BRUNO J., CERA E., DURO L., PON J. DE PABLO J. AND ERIKSEN T.E., (1998). Development of a kinetic model for the dissolution of UO_2 spent nuclear fuel. Application of the model to the minor radionuclides. SKB Technical Report. TR-98-22.

CACHOIR C., LEMMENS K (2004).: "Static dissolution of α-doped UO_2 in Boom Clay conditions: Preliminary results", Mat. Res. Soc. Symp. Proc., 807, 59-64.

CACHOIR, C., GLATZ, J.P., GRAMBOW, B., LEMMENS, K., MARTINEZ-ESPARZA A., MENNECART, T., RONDINELLA, V., SPAHIU, K., WEGEN, D. (2005). Effect of alpha irradiation field on long-term corrosion rates of spent fuel. European commission framework program 1998-2002. Spent fuel stability under repository conditions. (***Deliverable D9)***

CACHOIR, C., SALAH, S., LEMMENS, K. AND MAES, N (2005). Static dissolution tests of alpha-doped UO_2 under repository relevant conditions: Influence of Boom Clay and alpha-activity on fuel dissolution rates. Scientific Basis for Nuclear Waste Management XXIX, Ghent, Belgium

CARBOL, P. SOLATIE, D. BETTI M. (2000) , Analysis of $^{233}U_3O_8$ by radiometric methods, Technical Report JRC-ITU-TN-2000/01.

CARBOL, P., COBOS-SABATE, J., SOLATIE, WEGEN, D., WISS, T., VAN WINCKEL, S., NASYROW,R., BIRCK, S. (2003) Characterisation of ^{233}U-doped UO_2 pellet. Report JRC-ITU-TPW-2003/16. European Commission, DG JRC, Institute for Transuranium Elements, Karlsruhe, Germany. *In print*.

CARBOL, P., COBOS-SABATE, J., GLATZ, J-P, RONCHI, C., RONDINELLA, V., WEGEN, D-H, WISS, T., LOIDA,A., METZ, V., KIENZLER, B., SPAHIU, K., GRAMBOW, B., QUINONES, J., MARTINEZ ESPARZA, A. (2005). The effect of dissolved hydrogen on the dissolution of 233U doped UO2(s), high bur-up fuel and MOX fuel. SKB Technical Report, TR-05-09 (***Deliverable D10***).

CARVER M. B., HANLEY D. V., AND CHAPLIN K. R., (1979). Maksima Chemist. A program for mass action kinetics simulation by automatic chemical equation manipulation and integration by using Stiff techniques, AECL, Chalk River, Ontario AECL-6413, 1979.

CASAS I., GIMÉNEZ J., MARTÍ V., TORRERO M.E., DE PABLO J (1994)., Radiochim. Acta, 66/67, 23.

CERA E., MERINO J. AND BRUNO J., (2000). Liberación de los radionucleidos e isótopos estables contenidos en la matriz del combustible. Modelo conceptual y modelo matemático del comportamiento del residuo. ENRESA Publicación Técnica 03/2000.

CHRISTENSEN H., SUNDER S. AND SHOESMITH D.W (1994)., J. All. Comp., 213/214, 93.

CHRISTENSEN, H. (2003). Oxidation of UO_2 fuel by water radiolysis products. The effect of secondary phases. Studsvik Nuclear AB, Studsvik/N(K)-03/027. (***Deliverable D8***)

CHRISTENSEN, H. (2004a). Oxidation of UO2 fuel by water radiolysis products. Oxidation in 5 M Na Cl solutions. Studsvik Nuclear AB, Studsvik/N-04/014 (***Deliverable D7a***)

CHRISTENSEN, H. (2004b). Calculation of corrosion rates of alpha-doped UO_2. Studsvik Nuclear AB, Studsvik/N-04/091 ***(Deliverable D7b***)

CHRISTENSEN, H., LUNDSTRÖM, T. (2004). Oxidation of UO_2 fuel by water radiolysis products. Oxidation in 5 M NaCl solutions. Studsvik Nuclear AB, Studsvik/N-04/014

CLARENS F., DE PABLO J., DÍEZ I., CASAS I., GIMÉNEZ J. AND ROVIRA M., (2003). The formation of studtite during the oxidative dissolution of UO_2(s) by hydrogen peroxide: An AFM study. Enviado a Chemical Geology.

CLARENS F. (2004) Efecto de la radiólisis y de los productos radiolíticos en la disolución del UO2: Aplicación al modelo de alteración de la matriz del combustible nuclear gastado. Science, Universidad Politécnica de Cataluña.

J. COBOS, V.V. RONDINELLA, HJ. MATZKE, A. MARTINEZ-ESPARZA, AND T. WISS (1999): "The effect of α-radiolysis on the dissolution behaviour of UO_2", Proc. Int. Conf. on Future Nuclear Systems GLOBAL '99, Aug. 29- Sept. 3, 1999, Jackson Hole, WY, USA, American Nuclear Society (CD-ROM).

J. COBOS, J.A. SERRANO, J.P. GLATZ, J. DE PABLO, B. SÄTMARK (2001): "The kinetic of dissolution of irradiated UO_2 fuel under oxidising conditions in flow experiments". Proc. Int. Conf. on Environmental Remediation and Radioactive Waste Management, ICEM 2001. Sept 30th Oct. 4th Brugge, Belgium.

COBOS, J., HAVELA, L., RONDINELLA, V., DE PABLO J., GLATZ, J.P., CARBOL, P., MATZKE, H.. (2002). Corrosion and dissolution of UO_2 containing alpha emitters. Radiochim.Acta 90 (2002) 597-602

J. COBOS, T. WISS, T. GOUDER, V.V. RONDINELLA (2003): "XPS and SEM study of unirradiated MOX fuel corrosion in demineralized and in carbonated granitic water", Mat. Res. Soc. Symp. Proc., 757, 365-375.

CORBEL, C., SATTONNAY G., GUILBERT, S., GARRIDO, F. , BARTHE, M.F. ,JEGOU, C. (2005). Addition versus radiolytic production effects of hydrogen peroxide on aqueous corrosion of UO_2. J. Nucl. Mater., *in press* ***(Deliverable D6)***

DE PABLO J., CASAS I., GIMÉNEZ J., MOLERA M., ROVIRA M., DURO L. AND BRUNO J., (1999). The oxidative dissolution mechanism of uranium dioxide. I. The effect of temperatura in hydrogen carbonate medium. Geochim. et Cosmochim. Acta, 63 (19/20), 3097-3103.

DE PABLO J., CASAS I., CLARENS F., EL AAMRANI F. AND ROVIRA M., (2001). The effect of hydrogen peroxide on the oxidative dissolution of unirradiated uranium dioxide. Mater. Res. Soc. Symp. Proc. 663, pp 409-416.

DE PABLO J., CASAS I., GIMÉNEZ J., CLARENS F., DURO L. AND BRUNO J., (2003). The oxidative dissolution mechanism of uranium dioxide. The effect of pH and oxygen. Materials Research Society Symposium de Kalmar, Sweden 2003

DE PABLO J., CASAS I., GIMÉNEZ J., CLARENS F., DURO L., AND BRUNO J. (2004) The oxidative dissolution mechanism of uranium dioxide. The effect of pH and oxygen. In Scientific Basis for Nuclear Waste Management XXVII, Vol. 807 (ed. V. M. Oversby and L. O. Werme), pp. 83-88. Materials Research Society.

DE PABLO J., CLARENS F., CASAS I., GIMÉNEZ J., ROVIRA M., (2005) Role of hydroxyl radicals during oxidative dissolution of UO2 by hydrogen peroxide. Scientific Basis for Nuclear Waste Management XXIX, Ghent, Belgium

DEVOY, J., HASCHKE, J., CUI, D., SPAHIU, K. (2003), Behaviour of spent fuel: chemistry and catalysis in the UO_2-water system, Mat. Res. Soc. Symp. Series, 807 pp. 41-46.

EKEROTH E. AND JONSSON M. (2003) Oxidation of UO2 by radiolytic oxidants. J. Nucl. Mater. 322, 242-248.

FERNANDEZ, A., RICHTER, K. , FOURCAUDOT, S., CLOSSET, J.C., C. FUCHS, C., BABELOT, F., VOET, R., SOMERS, J. (1999), Adv. in Science and Technology, 24 539-546.

FERRY, C., LOVERA, P., POINSSOT, C., JOHNSON, L. (2004). Quantitative assessment of the Instant Release Fractio, (IRF) for fission gases and volatile elements as a function of burnup and time under geological disposal conditions. Mat. Res. Symp. Proc. Vol. 807, 35-40.

FERRY, C., LOVERA, P., POINSSOT, C., GARCIA, P. (2005). Enhanced diffusion under alpha self-irradiation in spent nuclear fuel: Theoretical approaches. J. Nucl. Mat. (in press)

FISCHER, U., W. WIESE, W. (1983), Verbesserte konsistente Berechnung des nuklearen Inventars abgebrannter DWR-Brennstoffe auf der Basis von Zell-Abbrand-Verfahren mit KORIGEN. KfK-3014.

GIMÉNEZ J., CLARENS F., CASAS I., ROVIRA M., DE PABLO J. AND BRUNO J., (2001). Oxygen consumption in uranium dioxide dissolution experiments inbicarbonate medium. Migration'01.

GRAMBOW, B., LOIDA, A., DRESSLER, P., GECKEIS, H., GAGO, J., CASAS, I., IJ.DE PABLO, J., GIMENEZ, J., TORRERO, M.E (1996)., Long-term safety of radioactive waste disposal: Chemical reaction of fabricated and high burnup spent fuel with saline brines, Forschungszentrum Karlsruhe, Wissenschaftliche Berichte FZKA 5702.

GRAMBOW, B., MÜLLER, R (1990)., Chemistry of glass corrosion in high saline brines Mater. Res. Soc. Symp.Proc. 176 229-241.

GRAMBOW, B., LOIDA, A., MARTINEZ-ESPARZA, A., DIAZ-AROCAS, P., DE PABLO, J., PAUL, J.L. ,MARX, G., GLATZ, J.P., LEMMENS, K., OLLILA, K., CHRISTENSEN, H. (2000), Source term for performance assessment of spent fuel as a waste form, European Commission, Nuclear Science and Technology, EUR 19140 EN 2000.

GRAMBOW B., MENNECART T., FATTAHI M., BLONDIAUX G (2004)., Radiochimica acta

W.J. GRAY, C.N, WILSON (1995): "Spent fuel dissolution studies: FY 1991 to 1994", Report PNL-10540.

W.J. GRAY: (1998) "Spent fuel dissolution rates as a function of burn-up and water chemistry." Report PNL-11895.

GUILLAMONT, R., FANGHÄNEL, T., GRENTHE, I., NECK, V., PALMER, D., RAND, M.H. (2003), Update on the chemical thermodynamics of uranium, neptunium, plutonium americium and technetium, OECD-NEA, Chemical Thermodynamics Vol. 5, pp. 182-187, Elsevier 2003.

JEGOU C., BROUDIC V., POULESQUEN A., BART J.M (2004).: "Effects of α and γ radiolysis of water on alteration of the spent UO_2 nuclear fuel matrix", Mat. Res. Soc. Symp. Proc., 807, 391-396.

JENSEN, A.Ö., ALBINSSON, Y. (2004). Preliminary results on oxygen production from alpha radiolysis (^{238}Pu) under Ar/H_2-pressure without any solid phase in high-pressure vessels. NR-PRO progress meeting, Gothenburg, May 2004.

JOHNSON, L.J, POINSSOT, C., FERRY, C., LOVERA, P. (2004). Estimates of the Instant Release Fraction for UO2 and MOX fuel at t=0, NAGRA Technical Report 04-08 (***Deliverable D1***)

JOHNSON, L.J., FERRY, C., POINSSOT,C., LOVERA,P. (2005a), Part I: Assessment of the Instant Release Fraction, J. Nucl. Mat. (*in press*) (***Deliverable D3***)

JOHNSON ET AL. (2005b). Spent fuel evolution under disposal conditions. Synthesis of results from the EU Spent Fuel Stability (SFS) Project. NAGRA Technical Report NTB 04-09, Nagra Wettingen, Switzerland (***Deliverable D15)***

JONSSON, M., NIELSEN, F., EKEROTH, E., ERIKSEN, T. (2003),. Modelling of the effects of radiolysis on UO_2 dissolution employing recent experimental data, Mat. Res. Soc. Symp. Series, vol. 807 (Oversby, V. M. and Werme, L.O. eds.), pp. 385-390, 2003**.**

J. M. HASCHKE, V. M. OVERSBY (2002), Journal of Nuclear Materials 305, 187-201.

KELM, M., BOHNERT, E. (2004a). A kinetic model for the radiolysis of chloride brine, ist sensitivity against model parameters and a comparison with experiments. Forschungszentrum Karlsruhe, FZKA 6977.(***Deliverable D4***)

KELM, M., BOHNERT, E.(2004b). Radiolytic corrosion of 238Pu- doped UO_2 pellets in 5 M NaCl solution. Mat. Res. Symp. Proc. Vol. 824, 159-166

KELM, M., BOHNERT, E.(2005). Gamma radiolysis of brnes: Effect of dissolved hydrogen radiolytic gases on the radiolytic of long lived products, J. Nucl. Mat. (*in press*)

KING, F., M. J. QUINN, M.J., MILLER, H.H. (2004), The effect of hydrogen and gamma radiation on the oxidation of UO_2 in 0.1 $mol \cdot dm^{-3}$ NaCl solution, SKB Technical Report TR-99-27, 1999.

KING, F., SHOESMITH, D. (2004). Electrochemical studies of the effect of H_2 on UO_2 dissolution, SKB Technical Report TR-04-20.

KIRKEGAARD P. AND BJERGBAKKE E., (2002). CHEMSIMUL: A Simulator for Chemical Kinetics. Roskilde, Denmark: Riso National Laboratory, Riso-R-1085(EN), 2002.

LELOUS K.(1997): "Etude de la lixiviation du combustible usé en présence de matériaux d'environnement". Thèse de doctorat de l'Université Paris Sud (France).

LIU, L., NERETNIKS, I. (2002), The effect of hydrogen on the oxidative dissolution of spent fuel, Nucear Technology, 138, pp. 69-77**.**

LOIDA A., GRAMBOW B., GECKEIS H. (1996), Journal of Nuclear Materials, 238, 11.

LOIDA, A., GRAMBOW, B., GECKEIS, H (2001)., Spent fuel corrosion behavior in salt solution in the presence of hydrogen overpressure, Proc. of ICEM'01: The 8th Internat. Conf. on Radioactive Waste Management and Environmental Remediation, Bruges, B, September 30-October 4, 2001 (CD-ROM).

LOVERA, P., FERRY, C., POINSSOT, C., JOHNSON, L.J. (2003). Synthesis report on the relevant diffusion coefficients of fission products and helium in spent nuclear fuels, CEA Report , CEA-R-6039, ISSN 0429-3460 (***Deliverable D2)***

LUNDSTRÖM, T. (2003). Radiation Chemistry of Aqueous Solutions Related to Nuclear Reactor Systems and Spent Fuel Management, Dissertation No 840, Linköping University, Sweden.

MC NAMARA B., BUCK E. AND HANSON B. (2003), Mat. Res. Symp. Proc. Vol 757, *in press.*

MARIMBEAU ET AL. (1998). The DARWIN Fuel Cycle Package. Procedures for Material Balance Calculation and Qualification. ENC'98, Nice, France, October 25-28, 1998.

MARTÍNEZ ESPARZA A., ESTEBAN J. A., QUIÑONES J., DE PABLO J., CASAS I., GIMÉNEZ J., CLARENS F., ROVIRA M., MERINO J., CERA E., AND BRUNO J. (2002) Modelling Spent Fuel and HLW Behaviour in Repository Conditions. A review of the stat of the art. In ENRESA Publicaciones técnicas, Vol. 08/2002.

MARTÍNEZ ESPARZA A., CERA E., ANDRIAMBOLOLONA Z., BRUNO J., CASAS I., CLARENS F., DE PABLO J., GAGO J. A., GONZÁLEZ DE LA HUEBRA A., GRAMBOW B., JEGOU C., KIENZLER B., MERINO J., METZ V., MISERQUE F., POINSSOT C., QUIÑONES J., AND SPAHIU K. (2004a) D12. Conceptual model of the Matrix Alteration Model (MAM). WP4: Matrix Model Construction. Contract Nº FIKW-CT-2001-20192 SFS. In European Commission. 5th Euratom Framework Programme 1998-2002. Key Action: Nuclear Fission (ed. A. Martínez Esparza and E. Cera), ***(Deliverable D12)***

MARTÍNEZ ESPARZA A., CERA E., ANDRIAMBOLOLONA Z., BRUNO J., CÁCERES J., CACHOIR C., CARBOL P., CASAS I., CAVEDON J. M., CLARENS F., COBOS J., DE PABLO J., GAGO J. A., GIMÉNEZ J., GLATZ J. P., GONZÁLEZ DE LA HUEBRA A., GRAMBOW B., IGLESIAS E., JEGOU C., KELM M., KIENZLER B., LEMMENS K., LOIDA A., MERINO J., METZ V., MISERQUE F., POINSSOT C., POULESQUEN A., QUIÑONES J., RONDINELLA V. V., ROVIRA M., SERRANO D., SPAHIU K., WEGEN D., AND WISS T. (2004b) D13. Mathematical Model Development and Experiments Integration in the MAM. WP4: Matrix Model Construction. Contract Nº FIKW-CT-2001-20192 SFS. In European Commission. 5th Euratom Framework Programme 1998-2002. Key Action: Nuclear Fission (ed. A. Martínez Esparza and E. Cera), (***Deliverable D13***)

MARTÍNEZ ESPARZA A.,QUINONES, J., GAGO, J., CACERES, J., IGLESIAS, E., GONZALEZ DE LA HUEBRA, A., DE PABLO, J., CASAS,I., CLARENS, F., GIMENEZ, J., ROVIRA, M., CERA, E., MERINO, J., BRUNO, J., GRAMBOW, B. (2004 c) D14. MAM Sensitivity Analysis and Applicability. WP4: Matrix Model Construction. Contract Nº FIKW-CT-2001-20192 SFS. In European Commission. 5th Euratom Framework Programme 1998-2002. Key Action: Nuclear Fission (ed. A. Martínez Esparza and J. Quinones) (***Deliverable D14***)

MARTÍNEZ ESPARZA A., GAGO, J., QUINONES, J., GONZALEZ DE LA HUEBRA, A., (2004d). Models used in PA to describe the waste forms durability under repository. Different approaches and results. En Informe tecnico, vol. DFN/RR-07/SP-04, Madrid, Ciemat.

MARTINEZ ESPARZA, A., CUNADO, M.A., GAGO, J.A., QUINONES, J. , IGLESIAS, E., COBOS, J., GONZALEZ DE LA HUEBRA, A., CERA, E., MERINO, J., BRUNO, J., DE PABLO, J., CASAS, I., CLARENS, F., GIMENEZ, J. (2005). Development of a Matrix Alteration Model (MAM). ENRESA report 01/2005.

MARX G. (2000) in B.Grambow et al. EUR 19140- Source term for performance assessment of spent fuel as a waste form, Luxembourg 2000.

MENNECART T., GRAMBOW B., FATTAHI M., BLONDIAUX G., ANDRIAMBOLOLONA Z. (2004), Mat. Res. Soc. Symp. Proc., 807, 403-408.

J. MERINO, E. CERA, J. BRUNO AND A. MARTÍNEZ-ESPARZA, Modelling the release of radionuclides from the spent fuel and their transport in the near field: a coupled approach. Scientific Basis for Nuclear Waste Management XXVII, vol. 807, Mat. Res. Soc. Symp. Proc., V. M. Oversby y L. O. Werme, Eds.: Materials Research Society, 2004, pages 785-790.

MERINO J., CERA E., BRUNO J., DE PABLO J., QUIÑONES J., AND MARTÍNEZ ESPARZA A. (2004) Radiolytic modelling of spent fuel oxidative dissolution mechanism. Calibration with UO2 dynamic leaching experiments. J. Nucl. Mater. (in press)

METZ V., LOIDA A., KIENZLER B. (2005). Reaction path modelling of spent fuel corrosion in Brines: comparison with experimental results. Scientific basis for Nuclear Waste Management XXIX, Ghent, Belgium.

NECK, V., KIM, J.I. (2001) Solubility and hydrolysis of tetravalent actinides. Radiochimica Acta 89, 1-16, 2001.

NECK, V., ALTMAIER, M., MÜLLER, R., SCHLIEKER, M., FANGHÄNEL ,T. (2003), Solubility of U(VI) in NaCl and $MgCl_2$ solutions. 9th International Conference on Chemistry and Migration Behaviour of Actinides and Fission Products in the Geosphere, Migration '03, 47, 2003.

OLLILA, K., ALBINSSON, Y., OVERSBY, V., COWPER, M. (2003), Dissolution rates of unirradiated UO_2, UO_2 doped with ^{233}U, and spent fuel under normal atmospheric conditions and under reducing conditions using an isotope dilution method, SKB Technical Report TR-03-13, October 2003.

V. OVERSBY (1999): "Uranium dioxide, SIMFUEL, and spent fuel dissolution rates – a review of published data.", *SKB report* TR-99-22, October 1999

PARKS, G.A., POHL, D.C. (1988), Hydrothermal solubility of uraninite, Geochim. Cosmochim. Acta 52, 863-875, 1988.

PASTINA B., LAVERNE,. B. AND J. A. (2001), Effect of molecular hydrogen on hydrogen peroxide in water radiolysis, J. Phys. Chem. A 105, 9316-9322 (2001).

PETRIK, N.G., ALEXANDROV, A.B., VALL, A.I. (2001), Interfacial energy transfer during gamma radiolysis of water on the surface of ZrO_2 and some other oxides, J. Phys. Chem. B, 105, pp. 5935-5944, 2001.

POINSSOT C., LOVERA P., FAURÉ M.H. (2001), Material Research Society, Scientific Basis for Nuclear Waste Management symposium.

POINSSOT C., LOVERA P., FERRY C., GRAS J.M. (2002), Material Research Society, Scientific Basis for Nuclear Waste Management symposium.

POINSSOT, C. (ED.) ET AL. (2004). Contract N° FIKW-CT-2001-00192 SFS. Second annual Progress report of the SFS project '1st November-31st October 2003.

POINSSOT, C., FERRY, C., GRAMBOW, B., KELM, M., SPAHIU, K., MARTINEZ ESPARZA A., JOHSON,L., CERA, E., DE PABLO, J., QUINONES, J., WEGEN, D., LEMMENS, K., MCMENAMIN, T. (2005). Mechanisms governing the release of radionuclides from spent nuclear fuel in geological repository: Major outcomes of the European project SFS., Scientific basis for Nuclear Waste Management XXIX, Ghent, Belgium.

POULESQUEN, A., JÉGOU, C. (2005), Influence of alpha radiolysis of water on UO2 matrix alteration, Chemical/Transport Model. Scientific basis for Nuclear Waste Management XXIX, Ghent, Belgium

POULESQUEN A., JÉGOU C (2005)., Determination of alpha dose rate profile at the UO2/water interface. Scientific basis for Nuclear Waste Management XXIX, Ghent, Belgium

QUIÑONES J., GARCÍA-SERRANO J., SERRANO J.A., DÍAZ-AROCAS P., ALMAZAN J.L.R (1998).: "SIMFUEL and UO_2 solubility and leaching behaviour under anoxic conditions", Mat. Res. Soc. Symp. Proc., 506, 247-252.

J. QUIÑONES, J. MERINO, E. CERA, J. BRUNO, J. COBOS Y A. MARTÍNEZ ESPARZA, *A radiolytic modelling intercomparison exercise: Influence of alpha radiation on spent fuel alteration process*. Oxford, England: American Society of Mechanical Engineers (ASME), 2003.

J. QUIÑONES, J. COBOS, P. P. DÍAZ AROCAS Y V. V. RONDINELLA, "Modelling of the $(U_{1-y}{}^{238}Pu_y)O_{2+x}$ leaching behaviour in deionised water under anoxic conditions," en *Scientific Basis for Nuclear Waste Management XXVII*, vol. 807, *Mat. Res. Soc. Symp. Proc.*, V. M. Oversby y L. O. Werme, Eds.: Materials Research Society, 2004, pp. 409-414.

QUIÑONES, J., COBOS, J.M., GONZÁLEZ DE LA HUEBRA, A., MARTÍNEZ ESPARZA A. (2004). Experimental study about the influence of the γ dose on the spent fuel dissolution in presence of H_2 atmosphere, Mat. Res. Soc. Symp. Proc., vol.824, S. Stroes-Gascoyne, J. Hanchar y L. Browning, Eds. , pp. 153-158.

J. QUIÑONES, A. GONZÁLEZ DE LA HUEBRA Y A. MARTÍNEZ ESPARZA, "Coprecipitation experiments of simulated spent fuel solution in presence of metallic iron in synthetic bentonitic-granitic water under oxidising conditions," en Scientific Basis for Nuclear Waste Management XXVIII, vol. 824, Mat. Res. Soc. Symp. Proc., S. Stroes-Gascoyne, J. Hanchar y L. Browning, Eds. San Francisco. USA: Material Research Society, 2004, pp. 425-430.

QUIÑONES J., Iglesias E., Martínez-Esparza A., Merino J., Cera E., Bruno J., de Pablo J., Casas I., Giménez J., Clarens F., Rovira M., (2005), Mat. Res. Soc. Symp. Proc, Scientific Basis for Nuclear Waste Management XXIX, Ghent, Belgium

RODRÍGUEZ ALMAZÁN J.L., DÍAZ P., SERRANO J., COBOS J., QUIÑONES J., CUÑADO M.A. AND ESTEBAN J.A., (1998). Estimación de la generación de gases y otros productos radiolíticos en el agua del campo próximo en un almacén geológico profundo, a partir del cálculo de la tasa de dosis alfa (□) y gamma (□). Ciemat DFN/RA01/SP98.

RÖLLIN, S., SPAHIU, K., EKLUND U-B (2001), Determination of dissolution rates of spent fuel in carbonate solutions under different redox conditions with a flow-through experiment, J. Nucl. Mater., 297, pp. 231-243.

V.V. RONDINELLA, HJ. MATZKE, J. COBOS, AND T. WISS (1999): "α-radiolysis and α-radiation damage effects on UO_2 dissolution under spent fuel storage conditions", Mat. Res. Soc. Symp. Proc., 556, 447-454.

V.V. RONDINELLA, HJ. MATZKE, J. COBOS, AND T. WISS (2000): "Leaching behaviour of UO_2 containing α-emitting actinides", Radiochim. Acta, 88, 527-531.

RONDINELLA, V., COBOS, J., MATZKE, HJ., WISS,T., CARBOL, P., SOLATIE, D. (2001), Leaching behaviour and α-decay damage accumulation of UO_2 containing short-lived actinides, Mat. Res. Soc. Symp. Proc, 663 pp. 392-399.

RONDINELLA, V., COBOS, J., WISS, T. HIERNAUT, J.P. (2003), Studies on spent fuel alterations during storage and radiolysis effects on corrosion behaviour using alpha-doped UO_2, proc. ICEM '03, Oxford, UK, Sept 21-25, 2003, ASME 2003, (CD-ROM).

RONDINELLA, V., Cobos, J., Wiss, T. (2004). Leaching behaviour of low activity alpha doped UO_2, Mat. Res. Soc. Symp. Proc. Vol.824, 167-173

ROQUE B. ET AL. (2002). Experimental validation of the code system DARWIN for spent fuel isotopic predictions in fuel cycle applications. Proceedings on International Conference PHYSOR 2002, Séoul, Korea, October 7-10, 2002.

ROUSSEAU G. (2002) *Thesis*, University of Nantes, France

W. RUNDE, S. D. CONRADSON, D. W. EFURD, N. LU, C. E. VANPELT, C. D. TAIT, (2002), Applied Geochemistry 17, 837-853.

SATTONAY, G., ARDOIS, C., CORBEL,C., LUCCHINI, JF., BARTHE, M.F., GARRIDO, F., GOSSET, D. (2001). Alpha radiolysis effects on UO_2 alteration in water. J.Nucl.Mater. 288 (2001) 11-

J.A. SERRANO, J.P. GLATZ, E.H. TOSCANO, D. PAPAIOANNOU, J. BARRERO, M. COQUERELLE (1998), Journal of Alloys and Compounds 271-273, 573-576.

J.A. SERRANO, J.P. GLATZ, E.H. TOSCANO, J. BARRERO, D. PAPAIOANNOU (2001), Journal of Nuclear Materials 294, 339-343.

J. SOMERS, R. VOET, C. FUCHS, H. HEIN, C. BOSHOVEN,S. FOURCAUDOT, N. MODERY, M. MURRAY-FARTHING (2001): "Fabrication of UO_2 pellets doped with ^{233}U for α–radiolysis investigations", *Technical Report* JRC-ITU-TPW-2001/12

SPAHIU, K., WERME, L., EKLUND, U.B. (2000), The influence of near field hydrogen on actinide solubilities and spent fuel leaching, Radiochim Acta, 88 pp. 507-511.

SPAHIU, K., EKLUND, U.B., CUI, D., LUNDSTRÖM, M. (2002),. The influence of near field redox conditions on spent fuel leaching, In: Scientific Basis for Nuclear waste management XXV, Mat. Res. Soc. Symp. Series, 713, pp. 633-638.

SPAHIU, K., DEVOY, J., CUI, D., LUNDSTRÖM, D. (2004), The reduction of U(VI) by near field hydrogen in the presence of UO_2(s), Radiochim Acta 92. *In print*.

STROES-GASCOYNE S., KING F., BETTERIDGE J.S., GARISTO F (2002).: "The effects of alpha-radiolysis on UO_2 dissolution determined from electrochemical experiments with ^{238}Pu-doped UO_2", Radioch. Acta, 90, 603-609.

STROES-GASCOYNE S., BETTERIDGE J.S.(2004): "The effects of alpha-radiolysis on UO_2 dissolution determined from batch experiments with ^{238}Pu-doped UO_2", Presented at the *MRS 2004 Symposium on the Scientific Basis for Nuclear Waste Management*, San Francisco, 2004

SUNDER, S., BOYER, G.D., MILLER, N H, (1990). XPS studies of UO_2 oxidation by alpha radiolysis of water at 100 ºC, J. Nucl. Mater., 175, p. 163-169, 1990.

STULTZ, J., PAFFET, M.T., JOYCE, S.A. (2004), Thermal evolution of hydrogen following water adsorption on UO_2(100), J. Phys. Chem. B, 108, 2362-2364.

SUNDER, S., SHOESMITH, D., MILEER, N.H. (1997). Oxidation and dissolution of nuclear fuel (UO2) by the products of the alpha radiolysis of water. J.Nucl.Mater. 244, 66

SUZUKI, T., ABDELOUAS, A., GRAMBOW, B. (2005). Report on radiolysis products in CO_2 rich solutions, paper submitted to MIGRATION'05, Avignon, France. ***(Deliverable D5)***

THOMAS G.F., TILL G (1984).: "The dissolution of unirradiated UO_2 fuel pellets under simulated disposal conditions", Nucl. Chem. Waste Manag., 5, 141-147.

11. Annex I: radiolytic kinetic scheme developed in SFS

11.1.1 REACTION SCHEME FOR WATER SYSTEM

Tableau 4: reaction scheme used in WP2 modelling for the radiolytic reactions in pure water systems.

Eq.No	Reaction					Rate Constant[a]
1	OH	+OH	$=H_2O_2$			k(1) = 5.500E+09[b]
2[c]	OH	$+E^-$	$=OH^-$			k(2) = 3.000E+10
3	OH	+H	$=H_2O$			k(3) = 7.000E+09
4	OH	$+HO_2$	$=H_2O$	$+O_2$		k(4) = 6.600E+09
5	OH	$+O_2^-$	$=O_2$	$+OH^-$		k(5) = 1.000E+10
6	OH	$+H_2O_2$	$=HO_2$	$+H_2O$		k(6) = 2.700E+07
7	OH	$+H_2$	=H	$+H_2O$		k(7) = 3.400E+07
8	OH	$+OH^-$	$=H_2O$	$+O^-$		k(8) = 1.300E+10
9	OH	$+HO_2^-$	$=HO_2$	$+OH^-$		k(9) = 7.500E+09
10	O^-	$+H_2O$	=OH	$+OH^-$		k(10) = 1.800E+06
11	E^-	$+E^-$	$=H_2$	$+OH^-$	$+OH^-$	k(11) = 5.500E+09
12	E^-	+H	$=H_2$	$+OH^-$		k(12) = 2.500E+10
13	E^-	$+O_2^-$	$=HO_2^-$	$+OH^-$		k(13) = 1.300E+10
14	E^-	$+HO_2$	$=HO_2^-$			k(14) = 2.000E+10
15	E^-	$+H_2O_2$	=OH	$+OH^-$		k(15) = 1.100E+10
16	E^-	$+O_2$	$=O_2^-$			k(16) = 1.900E+10
17	E^-	$+H^+$	=H			k(17) = 2.300E+10
18	E^-	$+H_2O$	=H	$+OH^-$		k(18) = 1.900E+01
19	E^-	$+HO_2^-$	$=O^-$	$+OH^-$		k(19) = 3.500E+09
20[d]	O_2^-	$+O_2^-$	$=HO_2^-$	$+O_2$	$-H^+$	k(20) = 1.800E+09
21	H	+H	$=H_2$			k(21) = 7.800E+09
22	H	$+O_2^-$	$=HO_2^-$			k(22) = 2.000E+10
23	H	$+HO_2$	$=H_2O_2$			k(23) = 1.000E+10
24	H	$+H_2O_2$	$=H_2O$	+OH		k(24) = 9.000E+07
25	H	$+O_2$	$=HO_2$			k(25) = 2.100E+10
26	H	$+OH^-$	$=E^-$	$+H_2O$		k(26) = 2.200E+07
27	HO_2	$+HO_2$	$=H_2O_2$	$+O_2$		k(27) = 8.400E+05
28	HO_2	$+O_2^-$	$=O_2$	$+HO_2^-$		k(28) = 9.600E+07
29	HO_2		$=H^+$	$+O_2^-$		k(29) = 8.000E+05
30	H^+	$+O_2^-$	$=HO_2$			k(30) = 5.000E+10
31	H_2O_2		$=H^+$	$+HO_2^-$		k(31) = 3.560E-02
32	H^+	$+HO_2^-$	$=H_2O_2$			k(32) = 2.000E+10
33	H_2O		$=H^+$	$+OH^-$		k(33) = 2.599E-05
34	H^+	$+OH^-$	$=H_2O$			k(34) = 1.430E+11
35[e]	O_2		$=O_2D$			k(36) = 1.000E+06
36[e]	H_2		$=H_2D$			k(37) = 1.000E+06

[a] Constants given for room temperature (for 1st order reactions in s^{-1}, for true and pseudo 2nd order reactions in L/(mol*s), for reaction 20 (third order reaction) in $L^2/(mol^2*s)$).

[b] Read this and the following constants as $5.5 * 10^9$.

[c] E^- symbolizes the solvated electron

[d] As the kinetic code accepts only a maximum of 2 reactants, a third specie can be introduced as a catalyst which is written with a negative sign on the right hand side of the equation. But only eq. 20 and 165 are true third order.

[e] O_2D and H_2D represent O_2 and H_2 which have desorbed from the solution and do not further participate in radiation chemical reactions.

[f] ClR-- is the radical anion ClO_3^{2-}

[g] UO2D and UO3D represent U compounds which do not further participate in radiation chemical reactions

11.1.2 SCHEME EXTENSION FOR CHLORIDE SYSTEM

Tableau 5: reaction scheme extension used in the WP2 modelling for the radiolytic reactions within the chloride system.

Eq.No	Reaction	Rate Constant[a]
37	$OH + Cl^- = ClOH^-$	k(37) = 4.300E+09
38	$OH + HClO = ClO + H_2O$	k(38) = 9.000E+09
39[d]	$OH + ClO_2^- = ClO_2 + H_2O - H^+$	k(39) = 6.300E+09
40	$E^- + Cl = Cl^- + H_2O$	k(40) = 1.000E+10
41	$E^- + Cl_2^- = Cl^- + Cl^- + H_2O$	k(41) = 1.000E+10
42	$E^- + ClOH^- = Cl^- + OH^- + H_2O$	k(42) = 1.000E+10
43	$E^- + HClO = ClOH^-$	k(43) = 5.300E+10
44	$E^- + Cl_2 = Cl_2^-$	k(44) = 1.000E+10
45	$E^- + Cl_3^- = Cl_2^- + Cl^-$	k(45) = 1.000E+10
46[d]	$E^- + ClO_2^- = ClO + OH^- - H^+$	k(46) = 4.500E+10
47[d]	$E^- + ClO_3^- = ClO_2 + OH^- - H^+$	k(47) = 0.000E+00
48	$H + Cl = Cl^- + H^+$	k(48) = 1.000E+10
49	$H + Cl_2^- = Cl^- + Cl^- + H^+$	k(49) = 8.000E+09
50	$H + ClOH^- = Cl^- + H_2O$	k(50) = 1.000E+10
51	$H + Cl_2 = Cl_2^- + H^+$	k(51) = 7.000E+09
52	$H + HClO = ClOH^- + H^+$	k(52) = 1.000E+10
53	$H + Cl_3^- = Cl_2^- + Cl^- + H^+$	k(53) = 1.000E+10
54	$HO_2 + Cl_2^- = Cl^- + HCl + O_2$	k(54) = 4.000E+09
55	$HCl = Cl^- + H^+$	k(55) = 5.000E+05
56	$HO_2 + Cl_2 = Cl_2^- + H^+ + O_2$	k(56) = 1.000E+09
57	$HO_2 + Cl_3^- = Cl_2^- + HCl + O_2$	k(57) = 1.000E+09
58	$O_2^- + Cl_2^- = Cl^- + Cl^- + O_2$	k(58) = 1.200E+10
59	$O_2^- + HClO = ClOH^- + O_2$	k(59) = 7.500E+06
60	$H_2O_2 + Cl_2^- = HCl + HCl + O_2^-$	k(60) = 1.400E+05
61	$H_2O_2 + Cl_2 = HO_2 + Cl_2^- + H^+$	k(61) = 1.900E+02
62	$H_2O_2 + HClO = HCl + H_2O + O_2$	k(62) = 1.700E+05
63	$OH^- + Cl_2^- = ClOH^- + Cl^-$	k(63) = 7.300E+06
64	$OH^- + Cl_2 = HClO + Cl^-$	k(64) = 1.000E+10
65	$H^+ + ClOH^- = Cl + H_2O$	k(65) = 2.100E+10
66	$H_2O + Cl_2O_2 = HClO + ClO_2^- + H^+$	k(66) = 2.000E+02
67	$H_2O + Cl_2O_2 = O_2 + HClO + HCl$	k(67) = 0.000E+00
68	$H_2O + Cl_2O = HClO + HClO$	k(68) = 1.000E+02
69	$H_2O + Cl_2O_4 = ClO_2^- + ClO_3^- + H^+ + H^+$	k(69) = 1.000E+02
70	$H_2O + Cl_2O_4 = HClO + HCl + O_4$	k(70) = 1.000E+02
71	$O_4 = O_2 + O_2$	k(71) = 1.000E+05
72	$Cl^- + Cl = Cl_2^-$	k(72) = 2.100E+10
73	$Cl^- + ClOH^- = Cl_2^- + OH^-$	k(73) = 9.000E+04
74	$Cl^- + HClO = Cl_2 + OH^-$	k(74) = 6.000E-02
75	$Cl^- + Cl_2 = Cl_3^-$	k(75) = 1.000E+04
76	$ClOH^- = OH + Cl^-$	k(76) = 6.100E+09
77	$Cl_2^- = Cl + Cl^-$	k(77) = 1.100E+05
78	$Cl_2^- + Cl_2^- = Cl_3^- + Cl^-$	k(78) = 7.000E+09
79	$Cl_3^- = Cl_2 + Cl^-$	k(79) = 5.000E+04
80	$ClO + ClO = Cl_2O_2$	k(80) = 1.500E+10
81	$ClO_2 + ClO_2 = Cl_2O_4$	k(81) = 1.000E+02
82	$Cl_2O_2 + ClO_2^- = ClO_3^- + Cl_2O$	k(82) = 1.000E+02

Table 6: Additional equations for the chloride system.

Eq.No	Reaction						Rate Constant[a]
83[f]	E^-	$+ClO_3^-$	$= ClR^{--}$				k(83) = 1.600E+05
84[f]	ClR^{--}	$+OH$	$=OH^-$	$+ClO_3^-$			k(84) = 1.000E+10
85[f]	ClR^{--}	$+O^-$	$=OH^-$	$+ ClO_3^-$	$-H^+$		k(85) = 1.200E+09
86	HClO	+HClO	$=Cl^-$	$+ ClO_2^-$	$+H^+$	$+H^+$	k(86) = 6.000E-09
87	ClO_2^-	+HClO	$=Cl^-$	$+ClO_3^-$	$+H^+$		k(87) = 9.000E-07
88	HClO	+HClO	$=O_2$	+HCl	+HCl		k(88) = 3.000E-10

[f] Equations 83 - 85 are based on pulse radiolysis experiments,
equations 86 - 88 describe the natural uncatalysed decay of HClO. Eqs. 86-88 depend on ionic strength. For 5M NaCl the rate constants are: 3.43E-08 , 4.10E-06 and 2.10E-09 .

11.1.3 RADIOLYTIC SCHEME EXTENSION FOR THE U-SYSTEM.

Table 7: Scheme extension for the U system, including the reactions with the chlorine species (modifications according to Grambow,B. et al., FZKA 6420 (2000))

Eq.No	Reaction						Rate Constant[a]
89	UO_2	+OH	$=UO_3H$				k(89) = 4.000E+08
90	UO_2	$+H_2O_2$	$=UO_3H$	+OH			k(90) = 2.000E-02
91[d]	UO_2	$+HO_2$	$=UO_3H$	$+H_2O_2$		$-H_2O$	k(91) = 2.000E+08
92[d]	UO_2	$+O_2^-$	$=UO_3H$	$+HO_2^-$		$-H_2O$	k(92) = 2.000E+08
93	UO_3H	$+UO_3H$	$=UO_3$	$+UO_2$		$+H_2O$	k(93) = 3.000E+00
94	UO_3H	+OH	$=UO_3$	$+H_2O$			k(94) = 8.000E+08
95	UO_3H	$+E^-$	$=UO_2$	$+OH^-$			k(95) = 5.000E+08
96	UO_3H	$+H_2O_2$	$=UO_3$	$+H_2O$		+OH	k(96) = 2.000E-02
97	UO_3H	$+O_2^-$	$=UO_3$	$+HO_2^-$			k(97) = 2.000E+08
98	UO_3H	$+O_2^-$	$=UO_2$	$+OH^-$		$+O_2$	k(98) = 4.000E+08
99	UO_3H	$+HO_2$	$=UO_3$	$+H_2O_2$			k(99) = 4.000E+08
100[d]	UO_3	$+E^-$	$=UO_3H$	$+OH^-$		$-H_2O$	k(100) = 5.000E+07
101	UO_3	$+O_2^-$	$=UO_3^-$	$+O_2$			k(101) = 4.000E+06
102	UO_3^-	$+H_2O$	$=UO_3H$	$+OH^-$			k(102) = 1.000E+01
103	UO_3H	+H	$=UO_2$	$+H_2O$			k(103) = 4.500E+06
104	UO_3	+H	$=UO_3H$				k(104) = 4.500E+05
105	UO_3	$+HO_2$	$=UO_3H$	$+O_2$			k(105) = 4.000E+06
106[g]	UO_3		$=UO_3D$				k(106) = 4.000E-05
107[d]	UO_2	$+O_2$	$=UO_3H$	$+HO_2$		$-H_2O$	k(107) = 1.000E-04
108	UO_3H	$+O_2$	$=UO_3$	$+HO_2$			k(108) = 1.000E-04
109[g]	UO_2		$=UO_2D$				k(109) = 7.000E-02
110[g]	UO_2D		$=UO_2$				k(110) = 7.000E-09
111[d]	UO_2	$+Cl_2^-$	$=UO_3H$	+HCl	$+Cl^-$	$-H_2O$	k(111)= 4.000E+08
112	UO_2	+HClO	$=UO_3H$	+Cl			k(112)= 4.000E-03
113	UO_3H	$+Cl_2^-$	$=UO_3$	+HCl		$+Cl^-$	k(113)= 8.000E+08
114	UO_3H	+HClO	$=UO_3$	+Cl		$+H_2O$	k(114)= 4.000E-03

11.1.4 RADIOLYTIC SCHEME EXTENSION FOR GAS SORPTION

Table 8: Scheme extension for gas sorption (together with eqs. 35 and 36) and additional equations of water radiolysis.

Eq.No	Reaction	Rate Constant[a]
115	H_2D =H_2	k(115) = A
116	O_2D =O_2	k(116) = B
117	OH +O- =HO_2^-	k(117) = 1.800E+10
118	H_2O_2 =H_2O +O	k(118) = 1.000E-03
119	O +O =O_2	k(119) = 1.000E+09

The desorption rate constants k(35) and k(36) are assumed to be 10^{+6} s^{-1} so that the equilibrium between liquid and gas phase is quickly established. From Henry's constants (KH) for the solubility of the gases, the volume of the liquid ($V_{Lq.}$) and the free gas volume (V_{Gas})the rate constants k(115) and k(116) are calculated:

$$A = 10^6 * \frac{KH_{H2} * V_{Lq.}}{0.4036 * V_{Gas}}$$

$$B = 10^6 * \frac{KH_{O2} * V_{Lq.}}{0.4036 * V_{Gas}}$$

Table 9: Henry's constants and the molarity of water in relevant solutions.

Solution	KH_{H2} (Mol/(L*MPa))	KH_{O2} (Mol/(L*MPa))	Water molarity (Mol/L)
Water	0.007	0.0116	55.5
5 M NaCl	0.00268	0.00221	49.5

11.1.5 SCHEME EXTENSION FOR NI CONTAINING SOLUTIONS

Table 10: radiolytic scheme extension used in WP2 modelling for Ni-containing solutions.

Eq. No.	Reaction	Rate constant[a]
120	Ni++ +E- =Ni+	k(120)= 2.900E+10
121	Ni+ +OH =Ni++ +OH-	k(121)= 2.200E+10
122	Ni+ +H2O2 =Ni++ +OH +OH-	k(122)= 4.300E+07
123	Ni+ +Cl2- =Ni++ +Cl- +Cl-	k(123)= 3.000E+09
124	Ni+ +O2 =NiO2+	k(124)= 1.700E+09
125	NiO2+ =Ni++ +O2-	k(125)= 7.800E+02

11.1.6 SCHEME EXTENSION FOR FE CONTAINING SOLUTIONS

Table 11: radiolytic scheme extension used in WP2 modelling for Fe-containing solutions.

Eq. No.	Reaction	Rate constant[a]
126	Fe+2 +OH =Fe+3 +OH-	k(126)=4.300E+08
127	Fe+2 +HO2 =H2O2 +Fe+3 -H+	k(127)=1.200E+06
128	Fe+2 +O- =Fe+3 +OH- -H+	k(128)=3.800E+09
129	Fe+2 +O2- =H2O2 +Fe+3 -H+ -H+	k(129)=1.000E+07
130	Fe+2 +Cl =Fe+3 +Cl-	k(130)=1.300E+10
131	Fe+2 +Cl2- =Fe+3 +Cl- +Cl-	k(131)=3.100E+07
132	Fe+2 +ClO2 =ClO2- +Fe+3	k(132)=3.000E+03
133	Fe+3 +HO2 =Fe+2 +H+ +O2	k(133)=3.100E+05
134	Fe+3 +E- =Fe+2	k(134)=6.000E+10
135	Fe+3 +H =Fe+2 +H+	k(135)=1.200E+09
136	Fe+2 +H2O2 =Fe+3 +OH +OH-	k(136)=7.000E+01

11.1.7 SCHEME EXTENSION FOR CARBONATE SYSTEM

Tableau 12: radiolytic scheme extension used in WP2 modelling for carbonate systems.

Eq. No.	Reaction	Rate constant
137	H+ +CO3-2 =HCO3-	k(137)=5.000E10
138	CO2 +H2O =H+ +HCO3-	k(138)=2.000E04
139	H+ +HCO3- =CO2 +H2O	k(139)=5.000E10
140	HCO3- +H+ =CO3-2	k(140)=2.000E00
141	CO2 +E- =CO2-	k(141)=7.700E09
142	HCO3- +OH =CO3- +H2O	k(142)=8.500E06
143	CO3-2 +OH =CO3- +OH-	k(143)=3.900E08
144	HCO3- +H =H2 +CO3-	k(144)=4.400E04
145	CO3-2 +E- =CO2- +OH- +OH- -H2O	k(145)=3.900E05
146	CO3- +CO3- =C2O6-2	k(146)=1.400E07
147	CO3- +H2O2 =CO3-2 + O2- +H+ +H+	k(147)=9.800E05
148	CO3- +HO2- =CO3-2 +O2 +H+	k(148)=1.000E07
149	CO3- +O2- =CO3-2 +O2	k(149)=4.000E08
150	CO3- +CO2- =CO3-2 +CO2	k(150)=3.000E08
151	CO2- +E- =HCOO- +OH- -H2O	k(151)=1.000E09
152	CO2- +CO2- =C2O4-2	k(152)=6.500E08
153	CO2- +O2 =CO2 +O2-	k(153)=2.000E09
154	CO2- +H2O2 =CO2 +OH- +OH	k(154)=7.300E05
155	CO2- +HCO3- =HCOO- +CO3-	k(155)=1.000E03
156	C2O6-2 = C2O4-2 +O2	k(156)=1.000E00
157	C2O6-2 =HO2- +OH- +CO2 +CO2 -H2O	k(157)=2.000E02
158	CO3- +C2O4-2 =C2O4- +CO3-2	k(158)=3.000E03
159	C2O4-2+E- =C2O4-3	k(159)=3.100E07
160	C2O4-2+OH =C2O4- +OH-	k(160)=7.700E06
161	CO3- +HCOO- =HCO3- +CO2-	k(161)=1.500E05
162	HCOO-+OH =H2O +CO2-	k(162)=3.200E09
163	HCOO-+H =H2 +CO2-	k(163)=2.100E08
164	HCOO-+E- =H2 +CO2- -H+	k(164)=8.000E08

11.1.8 SCHEME EXTENSION FOR CHLORINE HYDROLYSIS

Table 13: radiolytic scheme extension used for WP2 modelling for chlorine hydolysis.

Eq. No.	Reaction	Rate constant
165[d]	HClO +Cl- =Cl2 +H2O -H+	k(165)=9.000E03
166	Cl2 =HClO +Cl- +H+ -H2O	k(166)=1.500E01

11.1.9 RADIATION CHEMICAL PRIMARY YIELDS

Table 14: radiation chemical primary yield (molecules/100eV)

	Gamma		Alpha	
Specie	Water	5 M NaCl	Water	5 M NaCl
H_2O_2	0.70	0.09	0.98	0.23
HO_2	0	0	0.22	0.05
H_2	0.45	0.60	1.30	1.52
H	0.55	0.03	0.21	0.26
e^-_{aq}	2.65	3.89	0.06	0.06
OH	2.70	0.09	0.25	0.06
OH^-	0.00	0	0	1.01
H^+	2.65	0.44	0.06	0
Cl^-	0.00	-6.26	0	-1.62
Cl_2^-	0.00	2.43	0	0
ClOH-	0.00	0.38	0	0.55
HClO	0.00	1.02	0	1.07
H_2O	-4.10	-1.67	-2.65	-3.25

The yield $(100\ eV)^{-1}$ is equivalent to 104 $10^{-9}Mol.L^{-1}.Gy^{-1}$ in water or 123 $10^{-9}Mol.L^{-1}.Gy^{-1}$ in 5 M NaCl.

Comments:

- Only reactions 20 and 165 are of true third order, all others of first, second or pseudo second order.
- The U system is applicable for the 'active' layer. To keep the UO_2 concentration in the layer constant the equilibrium according to eq. 109 and eq. 110 is established. With starting concentrations [UO2]= 5 10^{-4} mol/L and [UO2D]= 1000 mol/L a steady state concentration of [UO2]= 1 10^{-4} is achieved.
- The pH is kept fixed (at least for chloride system as long as no further data are available).
- The concentration of Cl^- is kept fixed (at least for chloride system as long as no diffusion data in/out of the 'active' layer are introduced).